



**IFM-GEOMAR**

Leibniz-Institut für Meereswissenschaften  
an der Universität Kiel

## **FS SONNE Fahrtbericht / Cruise Report SO-210 ChiFlux**

- **Identification and investigation of fluid flux, mass wasting and sediments in the forearc of the central Chilean subduction zone –**

Valparaiso - Valparaiso  
23.09. – 01.11.2010



Berichte aus dem Leibniz-Institut  
für Meereswissenschaften an der  
Christian-Albrechts-Universität zu Kiel

**Nr. 44**  
Mai 2011





**IFM-GEOMAR**

Leibniz-Institut für Meereswissenschaften  
an der Universität Kiel

# **FS SONNE Fahrtbericht / Cruise Report SO-210 ChiFlux**

**- Identification and investigation of fluid flux, mass wasting  
and sediments in the forearc of the  
central Chilean subduction zone –**

Valparaiso - Valparaiso  
23.09. – 01.11.2010



Berichte aus dem Leibniz-Institut  
für Meereswissenschaften an der  
Christian-Albrechts-Universität zu Kiel

**Nr. 44**

Mai 2011

ISSN Nr.: 1614-6298

Das Leibniz-Institut für Meereswissenschaften  
ist ein Institut der Wissenschaftsgemeinschaft  
Gottfried Wilhelm Leibniz (WGL)

The Leibniz-Institute of Marine Sciences is a  
member of the Leibniz Association  
(Wissenschaftsgemeinschaft Gottfried  
Wilhelm Leibniz).

**Herausgeber / Editor:**  
Peter Linke

**IFM-GEOMAR Report**  
ISSN Nr.: 1614-6298

**Leibniz-Institut für Meereswissenschaften / Leibniz Institute of Marine Sciences**  
IFM-GEOMAR  
Dienstgebäude Westufer / West Shore Building  
Düsternbrooker Weg 20  
D-24105 Kiel  
Germany

**Leibniz-Institut für Meereswissenschaften / Leibniz Institute of Marine Sciences**  
IFM-GEOMAR  
Dienstgebäude Ostufer / East Shore Building  
Wischhofstr. 1-3  
D-24148 Kiel  
Germany

Tel.: ++49 431 600-0  
Fax: ++49 431 600-2805  
[www.ifm-geomar.de](http://www.ifm-geomar.de)



**Table of Content:**

1	Summary / Zusammenfassung.....	3
2	Introduction.....	5
2.1	Objectives .....	5
2.2	Geological Setting of the Study Area and Maps.....	6
3	Participants .....	10
3.1	Scientific Crew.....	10
3.2	Ship's Crew.....	11
4	Cruise Narrative.....	13
5	Scientific Equipment .....	19
5.1	Shipboard Equipment.....	19
5.1.1	Parasound .....	19
5.1.2	Kongsberg EM120 Multibeam Bathymetry System .....	19
5.2	Water Column Measurements.....	21
5.3	Seafloor Observations by OFOS.....	22
5.4	ROV Operations.....	23
5.5	Lander Operations.....	25
5.6	TV-Grab Operations .....	29
5.7	Sediment Sampling and Sedimentology .....	30
5.8	Zoology .....	31
5.9	Microbiological Studies .....	32
5.10	Pore Water Geochemistry .....	33
5.11	Volcanology .....	34
6	Work Completed and First Results.....	35
6.1	Hydroacoustic Work .....	35
6.1.1	Parasound .....	35
6.1.2	EM120 .....	39
6.2	Water Column Studies .....	42
6.3	Seafloor Observations (OFOS, ROV).....	45
6.4	ROV Deployment and Sampling .....	50
6.5	Lander Deployments .....	54
6.6	TV-Grab Deployments.....	57
6.7	Sediment Sampling and Sedimentology .....	58
6.8	Zoological Studies .....	61
6.9	Microbiological Studies .....	66

6.10	Pore Water Geochemistry .....	69
7	Acknowledgements.....	75
8	Data and Sample Storage and Availability .....	75
9	References.....	75
	Annex I: List of Stations .....	78
	Annex II: Carbonate Sample Description .....	84
	Annex III: List of Core Stations.....	90
	Annex IV: Zoological Sample Collection.....	91
	Annex V: Core Descriptions .....	95

## 1 Summary / Zusammenfassung

(P. Linke)

Leg 1 and 2 of cruise SO210 with RV SONNE to the active continental margin off Chile were conducted by shiptime exchange with RV METEOR. Funds for mobilizing the research team were provided by the German Science Foundation (DFG) in conjunction with the Collaborative Research Centre (SFB) 574 of the University of Kiel. In the first years, the SFB 574 investigated the pathways and fluxes of volatiles through the erosive subduction zone off Central America. For comparison, the studies were extended to the accretionary margin off Central Chile. Cruise SO210 is the last cruise conducted in the framework of SFB 574 and based on bathymetric investigations of previous SFB-cruises on the RVs VIDAL GORMAZ and JAMES COOK. The first leg of cruise SO210 was dedicated to long gravity coring for volcanic ash layers from the eruptive Southern Volcanic Zone (SVZ) of the Andes that were either deposited as fallouts onto the incoming Nazca Plate or transported down the slope and across the Chile Trench. Eight gravity cores of 12 m length were retrieved seaward of the Chile Channel on the outer rise of the Nazca Plate. The second goal for coring was the description and dating of previously mapped submarine landslides as well as retrieval of slide-related material for geo-technical experiments. As the deployment frame for long coring had to be removed on the second leg we continued coring for mass-wasting and geochemistry with short cores. Ten gravity cores of 3 or 6 m barrel length were retrieved upslope of slides, the glide plane and redeposited material downslope of the slide evacuation area. This sampling activity was supported by detailed acoustic surveys with Parasound and multibeam to remap critical areas for mass wasting in search for events, e.g. triggered by the recent Mw 8.8 Maule Earthquake, such as flanks of submarine canyons or previously detected submarine slides and to fill data gaps in the existing bathymetric data. The major activity of the entire cruise was dedicated to the search and detailed sampling of manifestations of fluid discharge activity on the Chilean forearc. A total of 11 deployments with the video sled OFOS and 12 dives by the ROV KIEL 6000 were conducted for ground-truthing of information from detailed side scan sonar surveys and methane measurements which indicated possible seep activity and has been obtained during previous cruises to the Chilean forearc. In 5 working areas we found manifestations of fluid discharge. In these areas the survey was followed by an intense sampling of bottom water, sediments, carbonates, mega and meiofauna and the deployment of instrumentation on the seafloor. The goal of these deployments was to measure in situ seabed methane emission rates and associated fluxes of sulfide and major electron acceptors such as oxygen at seep sites along the Chilean margin and to understand its controls. This was accompanied by CTD casts to trace oxygen and the fate of methane discharge in the water column. Sediment cores obtained by multicorer or ROV were used for the geochemical characterization of the pore water and microbiological studies which included turnover rate measurements, molecular studies, flow through experiments and sampling of active sediments. Authigenic carbonates obtained by TV-Grab or ROV were sampled for fauna, biomarker studies and investigations to reconstruct the growth structures, calcification processes and fluid-pathway systematic. The sampling of sediments and carbonates recovered a unique fauna with 79 different taxa, several of them appear to be species new to science.

Die Expedition SO210 (Leg 1 und 2) mit FS SONNE zum aktiven Kontinentalrand vor Chile wurde im Rahmen des Schiffszeittausches mit FS SONNE durchgeführt. Die Finanzierung zur

Mobilisierung des wissenschaftlichen Teams wurde durch die Deutsche Forschungsgemeinschaft (DFG) in Verbindung mit dem Sonderforschungsbereich (SFB) 574 bereitgestellt. In den ersten Jahren untersuchte der SFB 574 die Wegsamkeiten und Flüsse von Volatilen durch die erosive Subduktionszone vor Zentralamerika. Die Studien wurden zum Vergleich auf den akkretionären Kontinentalrand vor Zentral Chile ausgeweitet. Die Expedition SO210 ist die letzte Schiffsreise, die im Rahmen des SFB 574 durchgeführt wurde und baute auf den bathymetrischen Untersuchungen vorangegangener SFB-Ausfahrten auf den Forschungsschiffen VIDAL GORMAZ und JAMES COOK auf. Der erste Fahrtabschnitt der Reise SO210 war der Gewinnung von langen Schwerlotkernen zur Beprobung vulkanischer Aschelagen aus der eruptiven Südlichen Vulkanzone (SVZ) der Anden gewidmet, die entweder als fallout auf der einfallenden Nazca Platte abgelagert wurden oder den Kontinentalhang herunter und über den Chile Graben hinaus transportiert wurden. Acht Schwerlotkerne mit 12 m Länge wurden seewärts des Chile Kanals auf dem ansteigenden Teil der Nazca Platte abgeteuft. Das zweite Ziel des Kernprogrammes war die Beschreibung und Datierung von zuvor kartierten untermeerischen Rutschungen als auch die Gewinnung von Rutschungsmaterial für geo-technische Experimente. Da das Kernabsatzgestell auf dem 2. Fahrtabschnitt abgebaut werden mußte, wurde das Kernprogramm nur mit kurzen Kernen für Rutschungen und Geochemie weitergeführt. Zehn Schwerelote mit 3 oder 6 m Länge wurden hangaufwärts der Rutschungen, auf der Rutschungsbahn und an wiederabgelagerten Material hangabwärts der Rutschungsebene gewonnen. Dieses Beprobungsprogramm wurde unterstützt durch detaillierte akustische Kartierungen mit Parasound und Multibeam, um kritische Zonen erneut zu kartieren auf der Suche nach Ereignissen, wie dem rezenten 8,8 Mw Maule Erdbeben, an Flanken von untermeerischen Canyons oder zuvor erfassten Hangrutschungen, und um Datenlücken in dem existierenden bathymetrischen Datensatz zu füllen. Die Hauptaktivität der gesamten Expedition war der Suche und detaillierten Beprobung der Manifestationen von Fluidaustritten am Chilenischen Kontinentalrand gewidmet. Insgesamt wurden 11 Einsätze mit dem Videoschlitten OFOS und 12 Tauchgänge mit dem ROV KIEL 6000 durchgeführt, um bereits vorliegende Hinweise auf mögliche seep Aktivitäten zu überprüfen, die mittels detaillierter side scan Sonaruntersuchungen und Methanmessungen während vorangegangenen Ausfahrten zum Chilenischen Kontinentalrand gewonnen wurden. In 5 Arbeitsgebieten konnten wir diese Manifestationen von Fluidaustritten nachweisen. In diesen Gebieten folgte den Vorerkundungen eine intensive Beprobung des Bodenwassers, der Sedimente, Karbonate, Mega- und Meiofauna sowie der Einsatz von Instrumenten am Meeresboden. Das Ziel dieser Einsätze war die in situ Messung von benthischen Methanfreisetzungsraten und damit assoziierten Flüssen von Sulfid und anderen wichtigen Elektronenakzeptoren wie Sauerstoff an Austrittsstellen entlang des Chilenischen Kontinentalrandes sowie das Verständnis seiner Steuerparameter. Diese Untersuchungen wurden durch CTD-Profile begleitet, um Sauerstoff und das Schicksal der Methanfreisetzung in der Wassersäule zu erfassen. Sedimentkerne, die mittels Multicorer und ROV gewonnen wurden, wurden zur geochemischen Charakterisierung des Porenwassers und mikrobiologischen Studien herangezogen, die Messungen der Umsatzraten, molekulare Studien, Durchflußexperimente und die Beprobung aktiver Sedimente umfassten. Authigene Karbonate wurden mit dem TV-Greifer und dem ROV gewonnen und für Fauna und Biomarker-Untersuchungen sowie für Studien zur Rekonstruktion von Wachstumsstrukturen, Kalzifizierungsprozessen und Fluidkanalsystematiken beprobt. Die Beprobung der Sedimente und Karbonate barg eine einmalige Fauna mit 79 verschiedenen Taxa, von denen einige vollkommen unbekannte Arten darstellen.

## 2 Introduction

(P. Linke)

The expedition SO-210 to the continental margin of Chile (ChiFlux) was the last cruise in the framework of the Collaborative Research Centre (SFB) 574. The overarching goal of SFB 574 is to understand the role and fate of volatiles and fluids in the entire subduction system. Volatiles and fluids have a major influence on, e.g., short- and long-term climate change, the geochemical evolution of the hydrosphere and atmosphere, as well as subduction-related natural hazards, such as earthquakes, volcanic eruptions and tsunamis, because they are cycled through the entire subduction system. During the first six years of the SFB 574, our investigations concentrated on the erosive Central American subduction system. One of the major results of the SFBs forearc investigations was the development of a new model for the hydrogeological system of an erosional convergent margin and the effect of forearc dewatering on earthquake activity in Central America. To determine whether this model is also applicable to accretionary margins, and if not how it needs to be modified, is a major goal for the remainder of the SFB.

The Chilean margin, which switched from erosion to accretion within the last several million years, has been chosen for this study. The extensive work off Costa Rica and Nicaragua has shown that fluid venting - mainly occurring at mounds, along faults and at submarine land-slip scarps in the mid-slope area of the continental margin - is controlled by the dewatering of subducted sediments. Morphological, geochemical, biological, geophysical and volcanological investigations of the forearc of the Chilean subduction system between 33-37°S were the main focus of the SO-210 expedition to test the model of the subduction hydrogeological system.

### 2.1 Objectives

(P. Linke)

Major goals of the expedition were:

- 1) to investigate the dewatering processes in the forearc of the central Chilean subduction zone, in particular the origin and output flux of vent fluids and volatiles,
- 2) to study biological processes fuelled by the discharge of fluids and volatiles (e.g. methane),
- 3) to use cold seep carbonates as a geochemical archive of cold seep activity,
- 4) to evaluate the role of forearc fluids in triggering mass wasting events that could generate tsunamis,
- 5) to characterize geochemically the subducting sediments, in order to determine the input flux of climate-relevant volatiles (CO<sub>2</sub>, sulphur and halogens) and a variety of trace elements, necessary for determining the mass balance of chemical fluxes through the subduction system, and
- 6) to investigate the distribution of volcanic ashes to improve estimates on the volume of material emitted by volcanic eruptions and to date distinct events within the sedimentary sequence. An additional goal was to detect recent changes in the morphology of the sea floor and the discharge activity of fluids and gases, which are related with the earthquake on February 27 and the associated tsunamis.

Preliminary investigations by Chilean colleagues as well as sampling during cruise M67/1 revealed definite indications of fluid venting which together with detailed, recent geophysical

and bathymetric investigations on the RVs VIDAL GORMAZ and JAMES COOK (3-4/2008) were basis for the present cruise.

## 2.2 Geological Setting of the Study Area and Maps

(D. Völker, J. Geersen)

The South Chilean forearc is formed by the subduction of the Nazca Plate under the South American Plate at a present rate of 6.6 cm/yr and a convergence azimuth of about 80° (Fig. 2.2.1) (Angermann et al., 1999). The oblique subduction results in a northward increase in plate age at the trench of about 1 Ma/100km (Tebbens and Cande, 1997).

Since about 4 – 6 Ma the part of the margin between 33°S, where the Juan-Fernandez Ridge collides with the lower forearc, and the Chile Triple Junction at 46.5°S is in an accretionary state (Kukowski and Oncken, 2006; Melnick and Echtler, 2006). Before 4 – 6Ma, the marine forearc has experienced subduction erosion. The change from subduction erosion to sediment accretion is supposed to have occurred during the onset of glaciation in the Patagonian Andes about 6 Ma ago, resulting in increased sediment flux to the trench (e.g. Bangs and Cande, 1997; Melnick and Echtler, 2006). Today, the trench fill thickness in the study area varies between 1500 m in the South and 2000 m in the North (Diaz-Naveas, 1999; Ranero et al., 2006; Völker et al., 2006). In the trench between 33°S – 42°S, sediment is being transported northward guided by a trench-parallel axial channel that cuts 100 - 200 m into the sedimentary trench fill (e.g. Völker et al., 2006).

In the region of the cruise, the most prominent morphologic features on the oceanic Nazca Plate are the Mocha and the Valdivia Fracture Zones (Fig. 2.2.1). The Mocha Fracture Zone intersects the trench around 38°S and the Valdivia Fracture Zone around 40.5°S. These fracture zones separate young (0 - 25 Ma) oceanic lithosphere at the south from old (30 – 35 Ma) oceanic lithosphere at the north. The morphology of the lower continental slope appears complex with a rough seafloor and a series of margin-parallel accretionary ridges at the lowermost slope. In contrast the seafloor at the upper continental slope appears quite smooth and undisturbed (Bangs and Cande, 1997; Geersen et al., 2011-A). The smooth morphology of the upper slope is interrupted by north-south trending ridges and escarpments that displace the seafloor up to 500 m (Fig. 2.2.2). These morphologic features represent surface expressions of deep-seated thrust and normal faults (Geersen et al., 2011-A).

The continental slope is deeply incised by a number of prominent submarine canyon systems that feed terrigenous material of Andean origin to the trench (Fig. 2.2.2). Where swath bathymetric data is available, it can be shown that the canyons directly connect to major river systems that drain both the Andean and the Coastal Cordillera. The activity of individual canyons is evident from their sheer size as they cut up to 1000 m deep into the continental slope as well as by canyon fan systems that have formed where the canyons end in the Chile Trench.

### 2.2.1. Seismotectonic segmentation of the South Chilean margin

The Chilean continental margin is affected by recurring great subduction earthquakes. Earthquakes occur in distinct seismotectonic segments that break every 150 – 200 years (e.g. Lomnitz, 1970, 2004). Two seismotectonic segments are located in the working area of cruise SO210 (Fig. 2.2.1), the Valdivia Segment to the south and the Concepción-Constitución Segment to the north of the Arauco Peninsula. The Valdivia Segment was last ruptured by the

Mw 9.5 Valdivia (or great Chile) Earthquake on 22 May 1960. This earthquake ruptured about 1000 km of the Nazca – South America plate boundary between the Arauco Peninsula and the Chile Triple Junction and resulted in a vertical coastal uplift of up to 5.7 m. The last earthquake in the Concepción-Constitución Segment was the Maule Earthquake on the 27 February 2010 with Mw 8.8. The hypocenter of the Maule earthquake lies at 35.9°S, 72.7°W in about 35 km depth, and the rupture area extends along the marine forearc between 33°S - 38.5°S (Fig. 2.2.1) (e.g. Moreno et al., 2010). Here, coastal uplift of up to 2.5 m was observed (Farías et al., 2010).

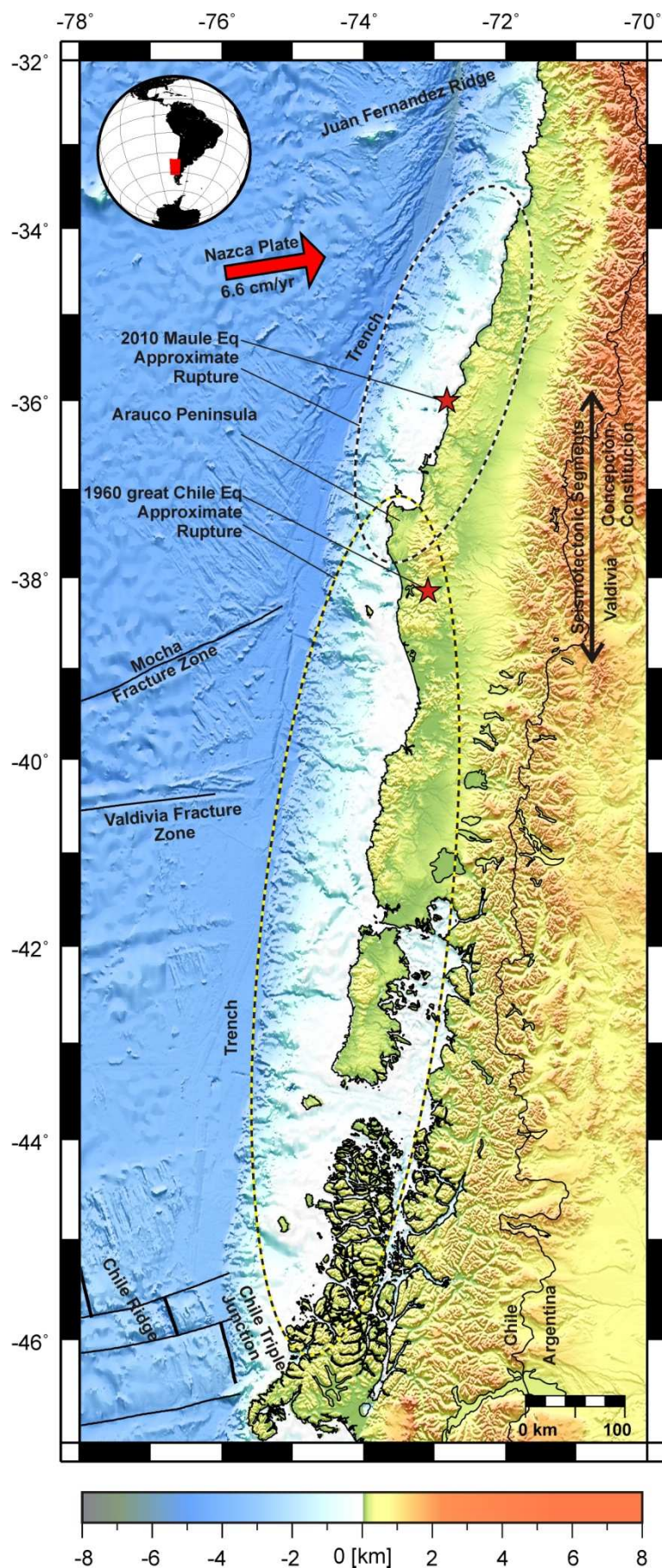


Fig. 2.2-1: Morphologic and tectonic features of Southern Central Chile between 33°S, where the Juan Fernandez Ridge is subducting and the Chile Triple Junction at 46°30'S. Epicentres and rupture areas of the 1960 and 2010 megathrust earthquakes are indicated. The rupture areas define the seismotectonic Valdivia and Concepción-Constitución segments that overlap at Arauco Peninsula.



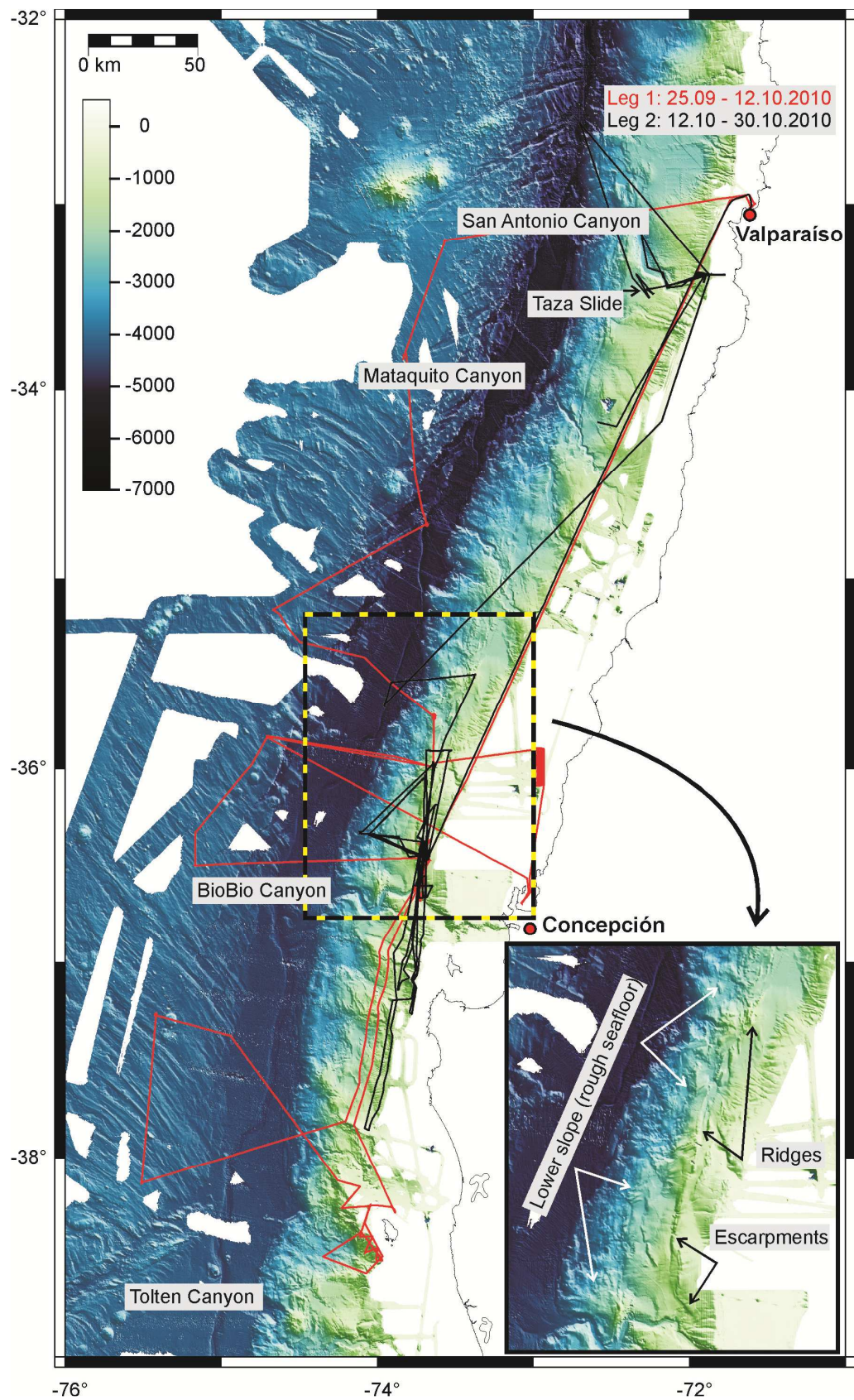


Fig. 2.2-2: Bathymetry of the working area and cruise tracks of both legs of SO210. One can distinguish a rough lower continental slope that is part of the accretionary wedge from a relatively smooth upper continental slope that is interrupted by few elongate, trench-parallel ridges and escarpments. The major submarine canyon systems of the working area are indicated.

### 3 Participants

#### 3.1 Scientific Crew

Leg 1	Participant	Working area	Institution
1	Linke, Peter	Chief scientist	IFM-GEOMAR
2	Völker, David	Hydrosweep/Parasound/Sediments	SFB574
3	Geersen, Jacob	Hydrosweep/Parasound/Sediments	SFB574
4	Bodenbinder, Andrea	Methane / Oxygen	IFM-GEOMAR
5	Treude, Tina	Microbiology	IFM-GEOMAR
6	Steeb, Philip	Microbiology, PhD	SFB574
7	Rovelli, Lorenzo	CTD, Eddy Correlation	IFM-GEOMAR
8	Wefers, Peggy	Methane	SFB574
9	Scholz, Florian	Porewater Geochemistry	IFM-GEOMAR
10	Domeyer, Bettina	Porewater Geochemistry	IFM-GEOMAR
11	Surberg, Regina	Porewater Geochemistry	IFM-GEOMAR
12	Lomnitz, Ulrike	Porewater Geochemistry	IFM-GEOMAR
13	Liebetrau, Volker	Carbonates/Isotope geochemistry	IFM-GEOMAR
14	Kutterolf, Steffen	Volcanic Ashes	SFB574
15	Freundt, Armin	Volcanic Ashes	SFB574
16	Bannert, Bernhard	Video-technician, TV grab	Oktopus
17	Cherednichenko, Sergiy	Lander-Electronics	IFM-GEOMAR
18	Valdés, Francisco	Seep Macrofauna/Chilean Observer	UCV
19	Petersen, Asmus	Coring	IFM-GEOMAR
20	Queisser, Wolfgang	TV-MUC/ROV-Winch	IFM-GEOMAR
21	Abegg, Fritz	ROV-Coordinator/Pilot	IFM-GEOMAR
22	Pieper, Martin	ROV-Mechanics/Pilot	IFM-GEOMAR
23	Hussmann, Hannes	ROV-Electronics/Pilot	IFM-GEOMAR
24	Cuno, Patrik	ROV-Programming/Pilot	IFM-GEOMAR
25	Meier, Arne	ROV-Winch/Pilot	IFM-GEOMAR
26	Suck, Inken	ROV-Pilot	IFM-GEOMAR
27	Foster, Andrew	ROV-Pilot	Schilling Robotics

Leg 2	Participant	Working area	Institution
1	Linke, Peter	Chief scientist	IFM-GEOMAR
2	Völker, David	Hydrosweep/Parasound/Sediments	SFB574
3	Geersen, Jacob	Hydrosweep/Parasound/Sediments	SFB574
4	Bodenbinder, Andrea	Methane / Oxygen	IFM-GEOMAR
5	Treude, Tina	Microbiology	IFM-GEOMAR
6	Steeb, Philip	Microbiology, PhD	SFB574
7	Bryant, Lee	CTD, Eddy Correlation	Duke Univ.
8	Wefers, Peggy	Methane	SFB574
9	Scholz, Florian	Porewater Geochemistry	IFM-GEOMAR
10	Domeyer, Bettina	Porewater Geochemistry	IFM-GEOMAR
11	Surberg, Regina	Porewater Geochemistry	IFM-GEOMAR
12	Lomnitz, Ulrike	Porewater Geochemistry	IFM-GEOMAR
13	Liebetrau, Volker	Carbonates/Isotope geochemistry	IFM-GEOMAR

14	Kriwanek, Sonja	Lander/Benthic Fluxes	IFM-GEOMAR
15	Grundmann, Bernd	Photographer	freelancer
16	Türk, Matthias	Video-technian, TV grab	IFM-GEOMAR
17	Cherednichenko, Sergiy	Lander-Electronics	IFM-GEOMAR
18	Valdés, Francisco	Seep Macrofauna/Chilean Observer	UCV
19	Petersen, Asmus	Coring	IFM-GEOMAR
20	Queisser, Wolfgang	TV-MUC/ROV-Winch	IFM-GEOMAR
21	Abegg, Fritz	ROV-Coordinator/Pilot	IFM-GEOMAR
22	Pieper, Martin	ROV-Mechanics/Pilot	IFM-GEOMAR
23	Hussmann, Hannes	ROV-Electronics/Pilot	IFM-GEOMAR
24	Cuno, Patrik	ROV-Programming/Pilot	IFM-GEOMAR
25	Grossmann, Tibor	ROV-Pilot	freelancer
26	Suck, Inken	ROV-Pilot	IFM-GEOMAR
27	Engemann, Greg	ROV-Pilot	Schilling Robotics

### 3.2 Ship's Crew

No.	Name	Given Name	Rank
1	Mallon	Lutz	Master
2	Korte	Detlef	Chief Mate / 1. Officer
3	Göbel	Jens	2. Officer
4	Aden	Nils	1. Officer
5	Dr. Heuser	Sabine	Ship's Doctor / Surgeon
6	Leppin	Jörg	Electronic Engineer
7	Grossmann	Matthias	System Manager
8	Ehmer	Andreas	System Manager
9	Rex	Andreas	Chief Engineer
10	Klinder	Klaus-Dieter	2. Engineer
11	Thomsen	Sascha	2. Engineer
12	Zebrowski	Dariusz	Electrician
13	Blohm	Volker	Fitter
14	Krawazcak	Ryszard	Motorman
15	Freiwald	Petra	Motorman
16	Wieden	Wilhelm	Chief Cook
17	Garnitz	Andre	2. Cook
18	Schmandke	Harald	Chief Steward
19	Royo	Luis	2. Steward
20	Schrapel	Andreas	Boatswain
21	Bierstedt	Torsten	A.B.
22	Kraft	Jürgen	A.B.
23	Stängl	Günther	A.B.
24	Dolief	Joachim	A.B.
25	Ross	Reno	A.B.
26	Dehne	Dirk	A.B.
27	Altendorf	Denis	S.M. / Apprentice
28	Ide	Steven	S.M. / Apprentice





Fig. 3.2.1: Composite picture of all participants and crew members

*Addresses:*

Duke University , Civil and Environmental Engineering Department, , 121 Hudson Hall, Duke University, Durham NC, 27708 USA

IFM-GEOMAR, Leibniz-Institut für Meereswissenschaften, Wischhofstr. 1-3, 24148 Kiel, Germany

Oktopus, Wischhofstr. 1-3, 24148 Kiel, Germany

Schilling Robotics, 260 Cousteau Place, Davis, CA 95618 U.S.A.

UCV: Dpto. de Biología Marina, Facultad de Ciencias del Mar, Universidad Católica del Norte. Larrondo 1281, Coquimbo, Chile

## 4 Cruise Narrative

(P. Linke)

At 10:30 a.m. on September 22, a group of 12 scientists and technicians embarked RV SONNE in Valparaíso (Chile). Immediately after embarkation the unpacking and loading of 11 containers with scientific equipment was started together with the ship's crew and a group of harbor workers. At the same time divers were engaged to treat the dense colonization of the ship's hull, which occupied already 1/3 of the multibeam array and hampered the hydroacoustic measurements and the ship's speed significantly. On board the vessel a cooling container was stored in the lower hold as well as 3 of 5 ROV containers and 1 container with coring equipment on deck. Loading was completed on September 23 at 16:00 and rigging of the major sampling gear was started. On the crowded deck beside the gravity corer and ROV Kiel 6000, a TV grab, multicorer, a video sled and 4 landers of IFM-GEOMAR are tied, which can be deployed video-guided. On September 24 at 13:00 the main group of 14 scientists and technicians embarked and started with the unpacking of the numerous boxes to equip the laboratories.

On the morning of September 25 our Chilean partner and observer arrived, completing the boarding of the scientific crew and allowing RV SONNE to leave the harbor at 15:00. Outside the harbor we successfully completed the first technical dive to test the function and handling of the ROV on the aft deck and steamed with 12 knots towards the first coring station. We arrived at 06:00 on the first coring station on incoming the plate (GC-1), the weather was getting rough (Bft 7), but we sampled GC-2 and GC-3 during the night.

On September 27, a winch test with the new 11 mm cable for the CTD was performed, at 14:45 we did the first deployment of the new CTD-rosette on the new cable. After this, we recovered the 4th gravity corer on the incoming plate. Gravity coring on the toe of the Reloca slide during the next morning failed, but the Posidonia calibration and first OFOS deployment in Box 3 (CSMA\_N) was conducted with first visual finding of cold seep communities followed by a CTD in the early morning of the 29<sup>th</sup> of September.

Afterwards we headed towards the 5th gravity corer position on the incoming plate. Unfortunately, we had to abandon the station as we had to drop of an ill crew member at the hospital of Talcahuano. After successful „delivery“ we used the wind shelter of the Concepcion peninsula for further mapping of the shelf area (Box 5), where our Chilean colleagues suspect a massive slide after the last earth quake – which, however, we were not able to verify. Instead we spent a rather calm night despite some strong wind and continued OFOS-mapping in Box 3 and gravity coring by repetition of abandoned core position 5 and new position 6 on the incoming plate during the 1<sup>st</sup> of October. In the night between 1st and 2nd of October, we conducted two further OFOS transects in Box 2 until the early morning. Here, black and white spots colonized by sulfide-oxidizing bacteria were found on the sediment surface. We were able to sample these spots with the first video-guided multicorer. The first analyses of the water samples obtained by the CTD rosette showed elevated methane concentrations at these sites.

OFOS surveys in Box 1 and Box 4 during the night resulted in finding, beside the carbonates, biological indicators of cold seeps. Here, we found large numbers of large tube worms (Vestimentifera) and white clams (Vesicomidae) which live in symbiosis with sulfide-oxidizing bacteria.

On the 3<sup>rd</sup> of October the weather calmed down and we were able to deploy the ROV for the first time in Box 1. The images obtained during this first dive largely compensated everybody for waiting so long for this moment. At the sea surface we were accompanied by sea lions, while at the bottom, huge Humboldt squids were frequent visitors. We entered a new and foreign world flying amongst large carbonate blocks with Gorgonians and soft corals growing on them, hosting tube worms within their crevasses and overhangs indicating passage-ways of seeping fluids. The highlight of the first dive was the discovery of a whale skeleton, the tissue of which had probably offered substrate for a fauna similar to those found at hot and cold seeps. This whale, however, had by now been reduced to its bones of which the ROV pilots were able to retrieve two vertebrae and close-by sediment samples for microbiological analyses. The first deployment of the TV-Grab on the 4<sup>th</sup> of October failed due to problems with the hydraulics.

The 2<sup>nd</sup> ROV dive aimed towards an area with extended clam fields and bacterial mats, which were sampled with push cores for microbiological and geochemical analyses. In the following nights measurements and sampling was conducted by the CTD rosette, the microstructure CTD and the gravity corer. The 3<sup>rd</sup> dive was conducted in the working area of the first dive (Box 1) and was dedicated to the sampling of authigenic carbonates. For this purpose the ROV was equipped with a hydraulic chain saw which was used with the ORION manipulator. The ROV was positioned in front of a carbonate block, its side above a crevasse was covered by white bacteria. The first sawing attempts under water were started with excitement. They were set in full length showing the methodological potential and the ability of the several components. Even horizontal cuts were performed by the well-coordinated ROV pilots. The following cut was made to obtain a smaller sample segment at the front of the carbonate block. Finally, the sample had to be retrieved from the block by using a chisel. During this manoeuvre, the hydraulics of the 2<sup>nd</sup> manipulator, the Riggmaster, here used to keep the ROV away from the rock, failed and we had to abandon the dive. The following deployment of the new TV-grab was abandoned as well due to problems with the hydraulics and without samples.

In the morning of the 6<sup>th</sup> October the new elevator lander of IFM-GEOMAR equipped with two eddy correlation (EC) modules as well as the POZ-lander equipped for the measurement of the current regime and physical parameters were deployed video-guided at the sea floor. During the following ROV dive the two EC modules were taken from the elevator and deployed in the vicinity of bacterial mats to conduct non-invasive oxygen measurements combined with high resolution turbulence measurements. Furthermore, we found a big bacterial mat in the vicinity suitable for the combined sampling by pore water sampler (PWS), push cores and the INSINC-modules for in situ incubation. During the 5<sup>th</sup> dive these instruments were positioned on the bacterial mat and the samples recovered. While the PWS conducted a preprogrammed sampling of the pore water by rhizones, both EC modules were carried back to the elevator. The very successful dive was completed by the transport of the PWS after its sampling was done back to the elevator.

In the early morning of October 7, profiles with the microstructure CTD were repeated in Box 2 at the deployment site. After a gravity corer in Box 4 (clam site, ROV dive 2) the ROV started its 5<sup>th</sup> dive to deploy the pore water sampler together with the Insinc modules and push cores at a bacterial mat in Box 2. The dive ended with the recovery of the 2 eddy correlation modules and the pore water samples on the elevator. The wind had peaked up again during the day when the ROV began to surface in the afternoon at 16:00. The manoeuvre went smooth until the first floats on the cable were recovered when a sudden crash was noticed on the fan

tail and the holder of the recovered Insinc modules were floated on the sea surface. The ROV was hit by the propeller and dove down immediately. The recovery procedure was completed and the damage of the vehicle was visible. The ROV was hit by the ship's propeller in the right open front of the floatation unit, the Orion was hit and the porch was disrupted. However, the electronics, telemetry and hydraulics were still operational and the ROV team decided to repair the ROV on board. Due to the weather conditions it was decided not to retrieve the landers. The program was continued with the last missing gravity corer at the Bio Bio slide and with a multibeam track heading south in parallel to the coast line.

After leaving the station a slide in the Bio Bio Canyon and during the following day the last two stations on the incoming Nazca plate were sampled with the gravity corer and sediment cores like from a text book were recovered. After this, we steamed towards our working area at Isla Mocha and mapped the fault in the south of the island during stormy seas to search for gas flares in the water column until the morning of October 10. After the second CTD we stopped station work until 19:00 and sought for some shelter in the wind shade of the island to enable the delicate repair of the ROV. In the late afternoon we headed north performing a bathymetric survey and stopped in the early morning at the abandoned lander station and recovered the POZ-lander. As the swell was still high we decided to continue the transit to Valparaiso and leave the elevator on the sea floor.

After a 6 hour stay at the harbor of Valparaiso, with an exchange of personal and expedition goods (TV-grab), demobilization of the Core Launch and Recovery System (LARS), taking on of provisions and a tour for 10 Chilean students around the vessel, SONNE left the harbor under full speed to reach the position of the left-behind elevator to be able to recover it prior to another prognosed change of the weather to the worse. While the small POZ-Lander had been already recovered during the transit to Valparaiso, the larger landers are more easily and safely recovered without the Core LARS on deck. We were able to get the elevator back on board during perfectly flat seas without any difficulties, and thus the two Eddy Correlation Modules and the Pore Water Sampler were recovered safely and laden with large amounts of data. Afterwards, another gravity core and two night-time OFOS-surveys (east to west) were conducted on a profile on which high heat flow anomalies had given first hints to the existence of an advection of deep fluids.

On the 14<sup>th</sup> of October, the video-guided Profiler Lander was placed on a bacterial mat. The Lander was equipped with an optode as well as pH and sulfide sensors and completed 27 profiles in micrometer steps. Subsequently, 2 additional gravity cores were taken, both indicating active de-gassing. Due to increasing wind speeds, the following two days were dedicated to the sampling of carbonates using the TV grab. Thus, several large carbonate samples could be retrieved in Box 1.

On the 17<sup>th</sup> of October, the wind had calmed down enough such that, after successful recovery of the Profiler Lander, the ROV was able to dive again. The first dive after the accident at Mound Felix showed that the ROV is entirely back in business, and that the team effort to repair it on board had been a great success. Already on the next day, the second dive was used to employ the hydraulic chain saw for the more detailed sampling of carbonates in Box 1. After carefully choosing the cutting level, this new in-situ tool was able to show its capabilities and several pieces of carbonates were retrieved. Even the sample we were not able to retrieve during the first use of the chain saw, due to a failure of the hydraulics, could be retrieved now. Heavily laden with carbonate samples, the ROV returned to the surface. In the following, the

Profiler Lander was deployed once again in Box 2. After intense night-time sampling of the accretionary prism with the gravity corer the engagement of the pore-water team was finally rewarded with first indications of deep fluids and chloride anomalies.

After recovery of the BIGO-Lander, the elevator was deployed on the 18<sup>th</sup> of October, again equipped with two Eddy Correlation Modules, the Pore Water Sampler and for the first time a Benthic Chamber in Box 4. During the subsequent ROV dive, all of the modules were taken out of the elevator and deployed in a previously chosen site. The POZ-lander was deployed in the vicinity to record the current regime and tidal impact. The work was hampered by a large swell with hardly any winds sent to us by a large low pressure system from Antarctica. Launch and recovery of the ROV reminded of a surfer waiting for the right wave in order to deploy the central tool of our cruise without any damage. The ninth dive was used to collect the tools deployed the previous day sent down by the Ocean Elevator Lander. On the way, we inspected the surface morphology and fauna of the hill-top which showed a characteristic sequence of plate-like depressions and lifted rims. Along and on top of these rims, we discovered rather long crevasses and small scarps in the sediment, indicating recent deformation of the seafloor. On one of these small ridges we found single spots densely covered by Pogonophora, completing our collection of characteristic seep communities. At the end of the dive, the ROV pilots transferred all deployed tools back to the Ocean Elevator Lander. As, due to weather conditions, it was not clear when we would be able to retrieve the lander, the Benthic Chamber was placed on the porch of the ROV and thus brought up to the surface.

After successful recovery of the ROV, we conducted another night-time OFOS survey on the accretionary wedge. Gravity core sampling here had resulted in interesting geochemical anomalies of the pore water. The pore water profiles of the sediments of the accretionary wedge had shown enhanced concentrations of elements such as chlorine and bromide. These possibly result from alteration of volcanic ashes in the deep sediment whereby large amounts of pore water are integrated into freshly generated minerals which normally behave conservatively i.e. they are not part of any geochemical or biological processes in the sediment. Further geochemical and isotopical investigations on land will add to our understanding of the importance of such ash-alteration-processes for the geochemical budget in the subduction zone.

On the following day, the Profiler Lander could be recovered while the weather got worse. The subsequent TV-multicorer deployment reminded of the view of a bungee jumper above the seafloor. After successful sampling, we abandoned the further sampling stations as well as the recovery of the two remaining landers and continued the mapping of the landslides south of Concepcion.

Decreasing wind enabled us to do this on the following day. Both landers were recovered and the tenth ROV dive could be conducted. Again, sampling of carbonates was the main focus and this time we were able to sample carbonates at an active venting hole. In the following nights, two more gravity cores were taken at a splay fault and a thrust fault in the forearc.

On the 23<sup>rd</sup> of October, the 11<sup>th</sup> dive of the ROV was conducted along a ridge structure which had been investigated during an OFOS survey at the beginning of the cruise. We succeeded in sampling numerous carbonates as well as single seep communities on the site. Similar to an oasis in the desert we discovered locally restricted but active vent holes at the base of a slope, around which bacterial mats, gigantic clams of the genus *Archivesica* sp. and tube worms had settled. This habitat was intensely sampled to assess the heterogeneity of methane impact and



chemosynthetic activity in close vicinity. During the night until midday of the following day, we tried to sample the Valdez and Reloca slides using the gravity corer.

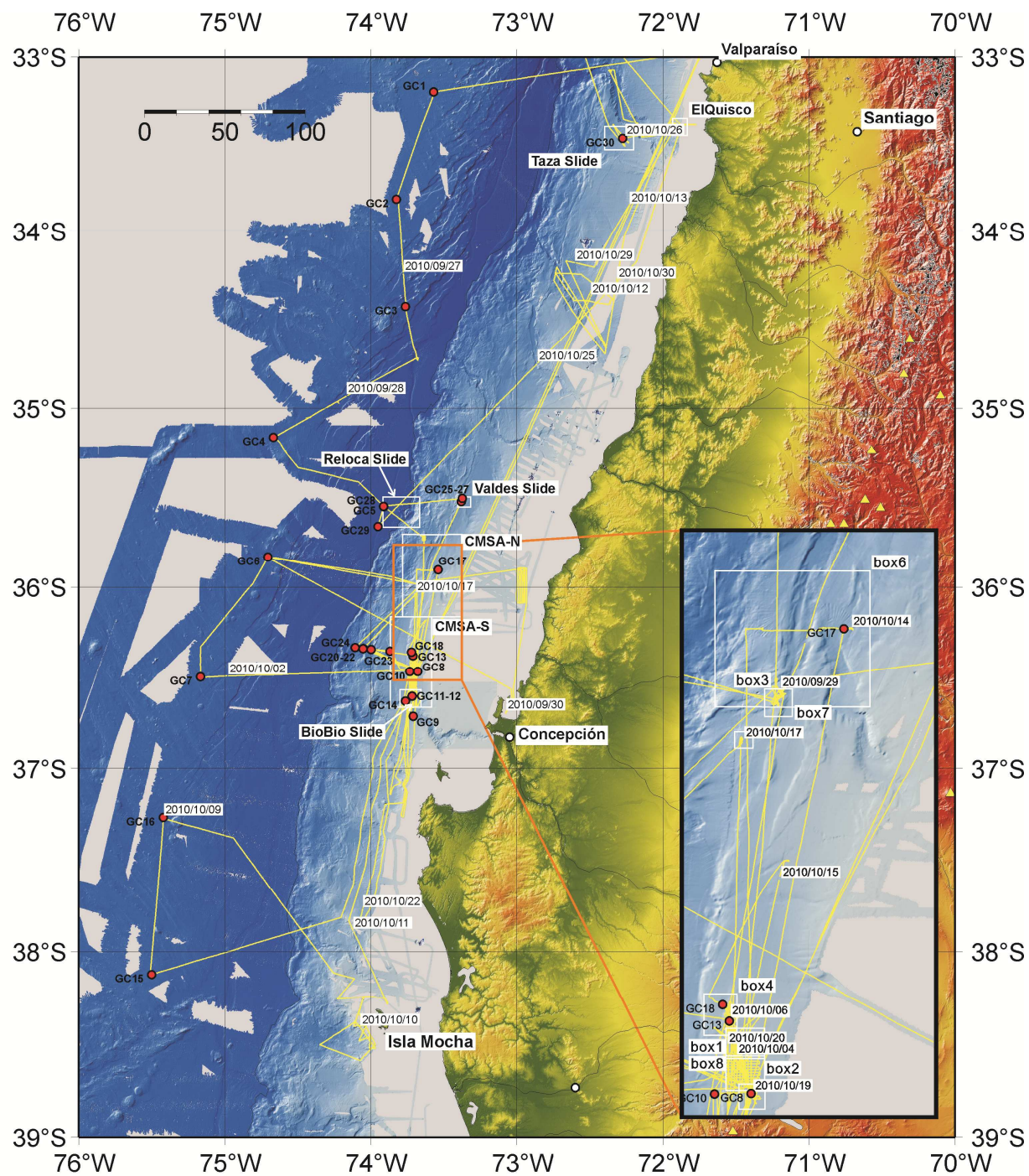
Subsequently, we once more started a transit to the El Quisco working area, located closely to the harbour of Valparaiso. Here, the Profiler Lander was deployed for the remaining days of the cruise. Results of the first two deployments of the lander had given clear indications of a coupling between oxygen flux and the bottom current regime, which is to be verified by the present measurement of the Profiler Lander.

Furthermore, we started to obtain a profile by CTD- and Multicorer-casts through the oxygen minimum zone and a gravity core was taken in the vicinity of the Tasca slide. Mapping of this area had shown a cover of the slide by recent sediments and we thus hope to obtain information on the age of the slide.

On the 26<sup>th</sup> of October 2010 the ROV Team finally wanted to know whether their gear with all its technical components deserves its name – KIEL 6000. In perfect weather conditions and after three long hours of descent, the bottom came into sight on the monitors in the control van. The onboard-CTD showed a depth of 5988 m, while the DigiQuartz depth sensor went up to 6057 m. We are all happy to have reached the maximum dive depth without any damages, especially after the accident earlier during the cruise and the successful repair of the ROV.

In the morning of the 27<sup>th</sup> of October the ROV was launched for the last dive of the cruise at El Quisco. After this the multicorer deployments at the profile were continued and the vessel transitted to the coring stations in the San Antonio Canyon. Gravity coring within the slopes of the San Antonio Canyon was performed without success and we completed the multicorer profile through the oxygen minimum zone at El Quisco. At 15:00 on October 28 station work for sampling ended and we started with mapping profiles for de-installation and packing of the equipment.

In the morning of October 30 we arrived at Valparaiso and started demobilisation of equipment and loading of containers on shore which was continued on the next day. On the 1<sup>st</sup> of November, a catholic holiday in Chile, the cruise SO210 ended by disembarkment of the scientific crew.



GM 2011 Apr 27 12:38:23

Fig. 4.1: Cruise tracks, working areas, and gravity corer (GC) stations of leg 1 and 2 of cruise SO210.

## **5 Scientific Equipment**

### **5.1 Shipboard Equipment**

(D. Völker, J. Geersen)

#### **5.1.1 Parasound**

The hull-mounted parametric subbottom profiler Parasound P70 (Atlas Hydrographic GmbH, Bremen) was operated whenever the ship was moving. It provides real-time information on sedimentary structures of the uppermost 50-200 m of sediment with a resolution of tens of cm and can image features such as gas flares in the water column. Parasound P70 works as a narrow beam sediment echo-sounder, simultaneously emitting two primary frequencies of 18 kHz (PHF, fixed) and 18.5 – 28 kHz (adjustable), thus generating parametric secondary frequencies in the range of 0.5 – 10 kHz (SLF) and 36.5 – 48 kHz (SHF). The secondary frequencies develop by nonlinear acoustic interaction of the primary waves at high signal amplitudes. This effect is restricted to the emission cone of the primary signals, which is limited to an aperture angle of only 4°. Therefore the footprint size is only 7% of the water depth and vertical and lateral resolution is significantly improved compared to conventional 3.5 kHz echosounder systems.

The fully digital system offers a number of features like simultaneous recording of the 18 kHz primary signal and both secondary frequencies, continuous recording of the water column, beam steering, different types of source signals (continuous wave, chirp, barker coded) and signal shaping. Digitization is done at 96 kHz to provide sufficient sampling rates for the secondary frequency. A down-mixing algorithm in the frequency domain is used to reduce the amount of data and allow data distribution over ethernet. For the standard operation, a parametric frequency of 4 kHz and a sinusoidal source wavelet of 2 periods was chosen to provide a good relation between signal penetration into the seafloor and vertical resolution of sedimentary structures. The system was operated either in Quasi-Equidistant-Transmission mode (water depth > 1000m) or in Single Pulse Mode (water depth < 1000m). Both modes worked reliably throughout the entire cruise. The water depth was taken from the PHF signal.

A 400 m long reception window centered at the seafloor was recorded in PS3 and SEG-Y format with Phase and Carrier to allow processing with standard seismic processing software (e.g. VISTA Seismic Processing). About 25% of the Parasound data were directly processed on board. Processing included adding of delay, applying a wide band pass filter to improve the signal-to-noise ratio and writing a navigation file. All lines were then loaded to a Kingdom Suite Project. The processed data provide detailed information of variations in sea floor morphology, sediment thickness, sedimentation patterns and gas flares in the water column along the ship's track.

The real-time Parasound data images were used to fine-tune the location of sediment-penetrating instruments such as gravity cores as well as for the detection of gas emission sites. On the cruise, three particular sites were chosen for a survey combining Parasound and EM120 multibeam on a dense rectangular grid.

#### **5.1.2 Kongsberg EM120 Multibeam Bathymetry System**

Parallel to the Parasound system, a multibeam bathymetry system was operated whenever the ship was not on station. The Kongsberg EM120 system is a deep-water multibeam echosounder. It provides accurate bathymetric mapping up to full ocean depth. Basic

components of the system are two linear transducer arrays in a Mills cross configuration with separate units for transmission and reception. The nominal sonar frequency is 12 kHz with an angular coverage sector of up to 150° and 191 beams per ping. The emission beam is 150° wide across track, and 2° along track direction. The reception is obtained from 191 beams, with widths of 2° across track and 20° along track. Thus the actual footprint of a single beam has a dimension of 2° by 2°. Achievable swath width on a flat ocean floor can be up to six times the water depth, dependent on the character of the seafloor and the chosen angle of the emission beam. The angular coverage sector and beam pointing angles can be set to vary automatically with depth. This maximizes the number of usable beams. The beam spacing is normally equidistant with equiangle available. For depth measurements, 191 isolated depth values are obtained perpendicular to the track for each ping. Using the two-way-travel-time and the beam angle known for each beam, and taking into account the ray bending due to refraction in the water column by sound speed variations, depth is calculated for each beam. A combination of amplitude (for the central beams) and phase (slant beams) is used to provide a measurement accuracy practically independent of the beam pointing angle.

Standard processing of multibeam data requires two sequences of processing steps: a profile-oriented sequence followed by area-based processing. The profile-oriented processing of the EM120 data comprises the check of navigation data, interpolating missing navigation values, the calculation of water depth and positions of the footprints of the beams by raytracing through the water-column taking into account the sound velocity profile, and removing artefacts and erroneous data points. Area-based processing comprises the calculation of a digital terrain model (DTM) and the visualisation of the data. For these purposes the NEPTUNE software package from Kongsberg is available onboard RV SONNE. However, mainly for easier integration of other data from different systems in various data formats, the “open source software” packages MB-System (Caress and Chayes, 1996) and GMT (Wessel and Smith, 1995) were used for the processing of the multibeam data.

Data of the multibeam system Kongsberg EM-120 is stored continuously during operation on the disks of the operator workstation in a vendor specific raw-data format. Data is organized in Surveys. A survey is initiated by the operator on the operator console. Generally a new survey was initiated on a daily basis. In the MB-System software the Kongsberg vendor specific raw data format is defined as format 56. Further processing of the data requires the conversion of the data to the MB-System format 57. In addition, some auxiliary files have to be created, containing meta-information for each file. In MB-System the management of the data is maintained by so-called datalist-files, that contain names, paths, format-ID and a weighting factor for each file. Datalist files are set up recursively, i.e. entries in a datalist refer to other datalists, that point to the actual data files. This structure helps to keep track of the data files which grow to several thousands for a normal-sized project. The format conversion, the creation of ancillary files and the set up or updating the respective datalist files is accomplished by shell scripts.

The cleaning of the raw data by flagging outliers and artefacts is done with the programme mbedit for each of the raw data files. This time-consuming step requires inspection of all pings and beams in each raw data file. Following this the navigation has is checked interactively with the programme mbnavedit for each raw data file. The interactive editor programmes do not modify the data files, but store the edit instructions to separate files. Following the interactive editing, the data files are updated by a call to the programme mbprocess. After successful completion of mbprocess the profile-oriented data processing is finished.

The new seafloor depth information was then integrated into a bathymetric grid based on former cruises on a daily basis for the production of regional maps and DEMs. Georeferenced maps, essential for other on board operations like ROV diving, TV grabs and OFOS observations were provided on demand. Apart from the depth information, the signal backscatter information was used to create maps of the backscatter properties of the seafloor, which were helpful to locate former seep sites in those regions where a dense survey was performed.

## 5.2 Water Column Measurements

(L. Rovelli, S. Sommer, L. Bryant, P. Wefers)

At the different seep sites water samples were taken during several CTD casts in order to detect methane anomalies that might be related to seabed methane release. Beside for chemical analyses, these CTD casts were important to gain necessary background information about the physical properties of the water column. Furthermore, they provide valuable data for the calibration of other instruments such as sound velocity for hydro-acoustic devices or absolute concentrations of solutes for in-situ sensors (oxygen, methane, pH).

### *CTD technical notes, methane and oxygen analysis*

Water column measurements were mainly carried out with the onboard CTD (Conductivity-Temperature-Depth) system. Additionally to these conventional CTD casts a Microstructure-CTD was deployed during the first leg.

The CTD system consisted of a carousel with a SBE9plus CTD (Sea-Bird Electronics, Inc., Washington, USA) equipped with standard sensors (Conductivity, Temperature, Pressure and Dissolved Oxygen) a pH sensor and a 24 Niskin bottle rosette for discrete water sampling. During the second leg an optical backscatter sensor was added. A HydroC CH<sub>4</sub> methane sensor (Contros GmbH, Kiel, Germany) was mounted into the CTD water sampling rosette to act as a sniffer for high methane concentrations.

As is common practice, undisturbed physical profiles were taken during the downcasts, while the water sampling occurred during the upcasts. Water sampling was conducted primarily in the lower water column as well as along sharp gradients of oxygen and temperature (oxycline, thermocline) indicating high biological activity and changes of water masses.

Methane and oxygen measurements were carried out on the water samples by means of gas chromatography fitted with a FID detector using He as carrier gas for the detection of CH<sub>4</sub> and Winkler titration for dissolved oxygen. Methane was extracted from the water samples using the vacuum degassing method according to Keir et al. (2008). Subsequent to gas extraction, the gas phase was sub-sampled into headspace vials at atmospheric pressure for onboard methane measurements. Methane-carbon stable isotope measurements will be conducted at IFM-GEOMAR. During the first leg oxygen concentrations were determined only occasionally, mainly to calibrate the CTD readings, while during the second leg each Niskin bottle was sub-sampled for oxygen measurements.

### *ROV and lander based water sampling*

In addition to water sampling during CTD casts, further water samples were taken during ROV dives and during the lander deployments. An advantage of lander and ROV based water sampling is that the samples were taken very close to the sea floor whereas CTD casts

generally only provide CH<sub>4</sub> and O<sub>2</sub> data to within ~ 5 m above the sea floor. In this distance from the sea bed a substantial fraction of the original methane concentration might be lost during mixing.

#### *Microstructure-CTD*

In order to allow the calculation of methane and oxygen fluxes in the water column, vertical turbulent transport was determined using a Microstructure-CTD. We deployed a MSS90-D profiler (Sea & Sun, Trappenkamp, Germany). The MSS90 is a specialized oceanographic tool that is capable of profiling the water column with a high resolution (mm scale, depending on the sensors). The profiler was equipped with 2 shear sensors (for turbulence measurements), a fast temperature sensor and standard CTD sensors. As the study sites were characterized by strong dissolved oxygen gradients we tested an experimental fast oxygen sensor that should be able to resolve the oxygen fine structures at a cm scale which is not possible for standard oxygen sensors.

Using the high resolution data collected with the Microstructure-CTD, it is possible to quantify the vertical transport of solutes by mean of the vertical eddy diffusion coefficient which is derived from the turbulence level according to Osborn (1980). Flux estimations can be carried out using the gradient method in which concentration gradients are multiplied by the vertical eddy diffusion coefficient.

### **5.3 Seafloor Observations by OFOS**

(P. Linke)

OFOS (Ocean Floor Observation System) is a frame equipped with the following instruments: two video cameras, a digital still camera system with two remote flash heads (Ocean Imaging Systems), two Xenon lights (Oktopus), CTD (RBR) and 3 red lasers (Oktopus).

The frame is towed behind the vessel at a speed of about 0.5-0.8 knots (kn). The distance of about 1.5 m to the seafloor is adjusted manually by the winch operator. For this purpose, a ground weight (20 cm wide) is suspended below the sled on a rope of 1.5 m length. Two laser pointers were used to scale the video and the still camera images. The laser pointers are parallel and 50 cm apart, while a third one points at an oblique angle, getting in line with the other 2 lasers when the sled is 1.5 m away from the sea floor. The images were taken by remote control.

## 5.4 ROV Operations

(F. Abegg, P. Cuno, G. Engeman (leg 2), A. Foster (leg 1), T. Grossmann (leg 2), H. Huusmann, A. Meier (leg 1), A. Petersen, M. Pieper, W. Queisser, I. Suck)

The ROV (remotely operated vehicle) KIEL 6000 is a 6000 m rated deep diving platform manufactured by Schilling Robotics LLC. As an electric work class ROV of the type QUEST, this is build no. seven, and is based at the Leibniz Institute for Marine Sciences, IFM-GEOMAR in Kiel, Germany. The UHD vehicle is equipped with 7 brushless thrusters, with 210 kgf peak thrust each. Power is supplied through an umbilical with up to 4160VAC/460 Hz. The data transfer between the vehicle and the topside control van is managed by a digital telemetry system (DTS<sup>TM</sup>) which consists of two surface and four subsea nodes, each representing a 16-port module. Each port may be individually configured for serial, video or ethernet purposes. The vehicle is linked to the topside control unit via a 19 mm diameter steel armed umbilical. No tether management system (TMS) is used. To unlink the vehicle from ship's movements, floats are attached to the umbilical. For further details please visit the GEOMAR homepage. Tools standardly installed on the vehicle include a HDTV camera, two high-resolution colour zoom cameras and one digital still camera as well as three black and white observation cameras. Besides the video capabilities, the two manipulator arms are the major tools used on this platform. One is a seven-function position controlled manipulator of the type ORION and the other one is a five-function rate controlled manipulator, type RIGMASTER. Further tools include a DIGIQUARTZ depth sensor, a SIMRAD sonar system, a PNI TCM2-50 compass, a motion reference unit (MRU) containing a gyro compass, and an RDI doppler velocity log (DVL). For navigation the USBL-based IXSEA POSIDONIA<sup>TM</sup> system was employed. The tool sled (Fig. 5.4.1) in the lower-most part of the vehicle is especially dedicated to take up the scientific payload. An SBE49 FastCAT CTD is permanently mounted. Located on portside front of the tool sled is a sample tray which can be opened hydraulically. On starboard front there is a drawer, likewise hydraulically driven, which can take up sample containers, probes or other scientific tools continuously mounted or handled by the manipulator. Port aft and starboard aft are reserved for additional scientific payload which differ from mission to mission.





Fig. 5.4.1: View of the ROV KIEL 6000 front with the scientific tooling most frequently used during the SO 210 cruise.

During cruise SO210, the port side sample tray was rigged for sampling push cores and hard rocks. Additionally, it contained two nets and two chisels. On the front plate of the drawer, two 5 l Niskin bottles for water samples were mounted. The starboard drawer was equipped with a sample box with six compartments of different sizes. On the starboard aft of the tool sled, a Falmouth Scientific Instruments CTD was mounted. A pH-sensor which was connected to the FSI probe was mounted on the starboard front leg of the ROV frame. A premiere was the application of an underwater hydraulically driven chain saw (Figs. 5.4.2 a & b). The necessity of obtaining samples of carbonates let to the integration of the saw into the hydraulic cycle of the ROV. The chain saw was mounted that way that it could be reached and operated by the ORION manipulator. During several deployments, a successful sampling strategy was developed which let to a large set of samples (s. chapter 6.4).



Figs. 5.4.2 a & b: Chain saw used to sample carbonates.



## 5.5 Lander Operations

(S. Sommer, P. Linke, L. Bryant, S. Cherednichenko, M. Türk, S. Kriwanek)

Sea bed methane seepage represents a global phenomenon that occurs predominantly at continental margins and is related to subduction, but also to salt tectonics or mud volcanism. Beside the green-house potential of methane when reaching the atmosphere, seabed methane release significantly affects benthic cycling of major elements, particularly carbon and sulfur. One aim of this research cruise was to measure in situ seabed methane emission rates and associated fluxes of sulfide and major electron acceptors such as oxygen at seep sites along the Chilean margin and to understand its controls.

To approach this aim we used the benthic lander BIGO (Biogeochemical Observatory), a benthic chamber module as well as a transecting micro profiler for the high resolution measurements of oxygen-, sulfide-, and pH gradients in the surface sediments. Additionally, the POZ-Lander was deployed for measurements of the physical control parameters in the benthic boundary layer and the elevator for the deployment and recovery of modules handled by the ROV. A TV-guided launching system allowed smooth placement of the landers at selected sites on the sea floor.

### *BIGO type lander and benthic chamber module deployed by a ROV*

BIGO contains two circular flux chambers (internal diameter 28.8 cm, area 651.4 cm<sup>2</sup>). Two to three hours after the observatories were placed on the sea floor the chambers were slowly driven into the sediment ( $\sim 30 \text{ cm h}^{-1}$ ). During this initial time period where the bottom of the chambers was not closed by the sediment, the water inside the flux chamber was periodically replaced with ambient bottom water. The water body inside the chamber was once further replaced with ambient bottom water after the chamber has been driven into the sediment to flush out solutes that might have been released from the sediment during chamber insertion. To trace fluxes of methane, O<sub>2</sub>, NO<sub>3</sub><sup>-</sup>, NO<sub>2</sub><sup>-</sup>, NH<sub>4</sub><sup>+</sup>, sulphide, and total alkalinity 8 sequential water samples were taken from inside each benthic chamber by means of glass syringe water samplers. The syringes were connected to the chamber using 1 m long Vygon tubes with a dead volume of 5.2 ml. To monitor the ambient bottom water an additional syringe water sampler (hosting 8 glass syringes) was employed. The positions of the sampling ports were about 30 – 40 cm above the sediment water interface. During the BIGO deployment the sediments were retrieved for latter pore water analyses, pore water methane determination and microbiological studies.

In addition to the BIGO a single chamber was deployed during ROV dive #9. This ROV deployed chamber was carefully inserted into the sediment using the ROV arm. After chamber insertion the overlying water body was replaced with ambient sea water in order to establish start conditions which are not affected by solutes that are released from the sea bed during insertion. Similarly to the BIGO the sediment inside the chamber was retrieved for latter onboard analyses.

### *Profiler Lander*

The profiling unit consists of a lower and upper glass fibre frame, which are connected by four glass fibre poles. The upper frame extends about 50 cm towards the front defining the area across which sensors can be moved in mm increments along the x and the y axis. Along the vertical z axis, the sensors can be moved freely selectable increments. The rear part contains

pressure housings for data logging, for the control unit controlling the movements of the sensors, and batteries. For the deployment the profiling unit was mounted into a lander frame (Fig. 5.5.1). Commercially available oxygen, sulfide and pH sensors (tip diameters:  $\sim 50 \mu\text{m}$ . Unisense, DK) were used to measure in-situ micro-profiles in the sediment. Two optodes, one mounted at the same height as the micro-sensors, the second one mounted in  $\sim 1 \text{ m}$  above the seafloor recorded time series of  $\text{O}_2$  and temperature in the bottom water.

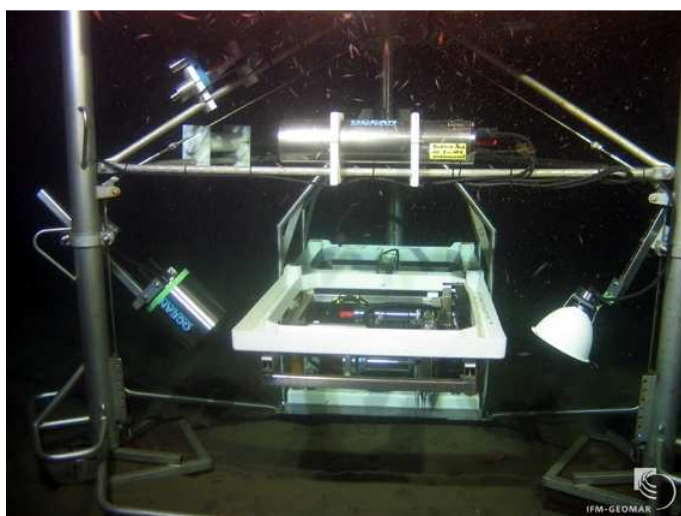
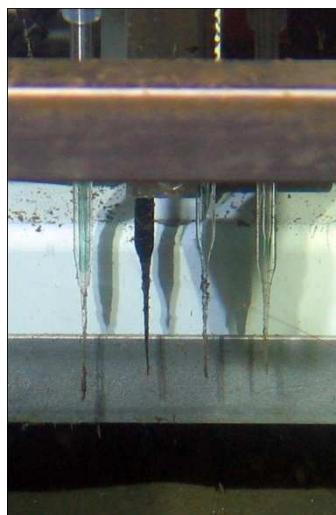
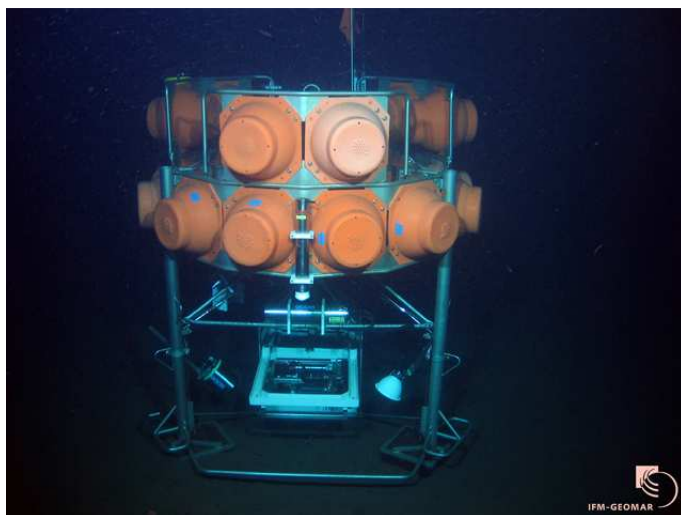


Fig. 5.5.1: Profiler Lander to conduct microscale spatial measurements of oxygen, sulfide and ph in sediments. Profiler is mounted within a benthic lander frame (top left). The picture is taken by ROV during deployment at El Quisco.

In addition to the profiling unit during deployment #1 and #2 the lander hosted an upward looking ADCP (300 KHz, sentinel, RDI), a camera system (Ocean imaging system) taking image series of the sediment surface, as well as an RBR CTD. During deployment #3 furthermore a downward looking Aquadopp Profiler (2 MHz, Nortek) was installed to measure currents close to the bottom (Fig. 5.5.1).

#### *POZ-Lander*

The POZ-Lander is a low-profile lander equipped with a 300 kHz ADCP and a RBR CTD with pressure sensor. Aim of this design was to decrease the size of the instrument in settings with high bottom water current velocities. Additional, the design put all sensors close to the sediment at  $\sim 50 \text{ cm}$  above the seafloor. The floatation is provided by modular syntactic foam cylinders. The POZ RBR CTD was equipped with temperature, conductivity, and a Digiquartz pressure sensor to monitor and log tidal-driven hydrographic changes. During this cruise the

lander was deployed with the launcher in the vicinity of the area where lander and ROV operations were conducted. The anchor weight underneath the lander keeps the system in a horizontal plane during free-fall descent and deployment at the sea floor (Fig. 5.5.2).

Upon recovery the lander rises to the sea surface with the floatation, flag, radio beacon and strobe light first while the heavy ADCP and CTD are oriented vertical below and are protected during recovery.

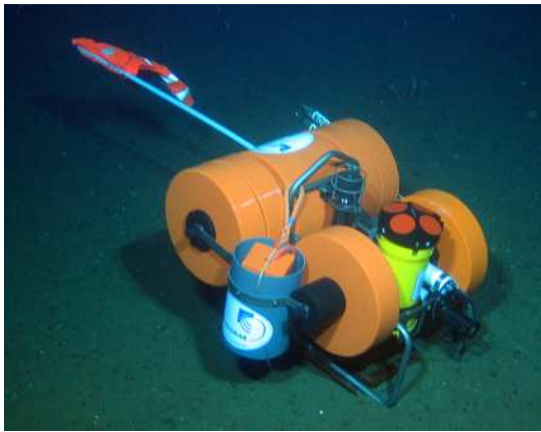


Fig. 5.5.2: POZ-Lander deployed on soft sediment in Box 4.

### *Ocean Elevator*

The elevator is a newly designed lander which serves as a carrier system for scientific payloads which are handled by the ROV on the seafloor. The stainless steel frame of the lander is of squared design and has two platforms on which scientific ROV modules can be transported. Two large blocks of syntactic foam are used for buoyancy, additional blocks or cylinders can be added to achieve a total payload of approx. 200 kg. Beneath these blocks 2 drawers can be used for transport of push corers or other scientific samples. The lander is equipped with 2 acoustic releasers and a release line which can be handled by the ROV to drop the anchor weight.

During the cruise the elevator was used for the first time and served as a platform to deploy 2 benthic chambers, 2 eddy correlation modules and the pore water sampler in the vicinity of the seep sites. The lander and the ROV modules were equipped with Homer beacons for relocation. After its video-guided deployment with the launcher (Fig. 5.5.3), the ROV unloads these modules from the elevator and deploys them at distinct sites at the seeps. After the end of the measurement or sampling the ROV carries them back to the Elevator, secures the modules on the platform by hooks and rubber bands. After recovery of the ROV the anchor weight of the elevator is released by acoustic command and the lander is picked up by the vessel (Fig. 5.5.4).

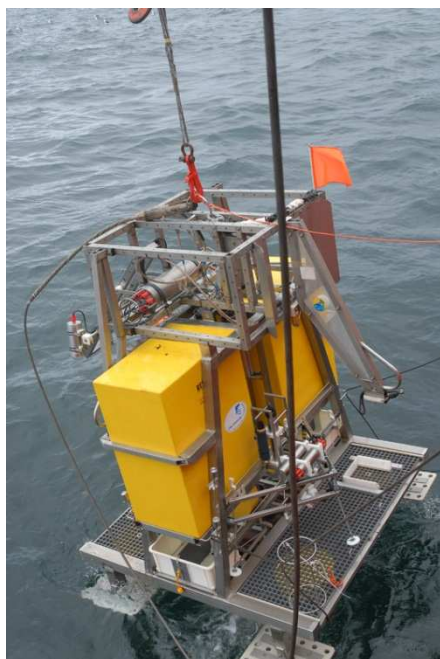


Fig. 5.5.3: Video-guided deployment of the elevator with launcher on top.

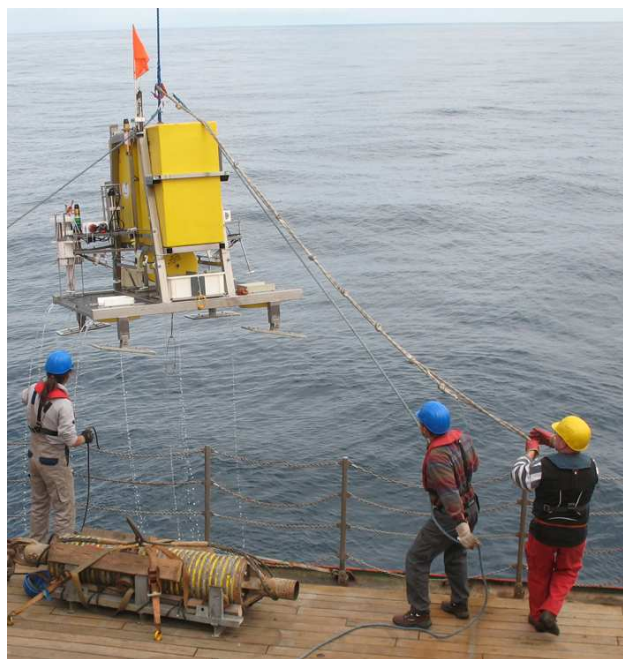


Fig. 5.5.4: Recovery of the elevator with 2 Eddy Correlation modules and pore water sampler.

### *Eddy correlation modules*

The Eddy Correlation (EC) technique is a well established technique to measure constituent fluxes in the atmosphere (Lee et al. 2004). Its use to measure fluxes at the sediment-water interface in the BBL of lakes and oceans, however, is still a relatively new approach. So far Berg et al. (2003, 2007, 2008, 2009) and Kuwae et al. (2006) used the EC technique to determine DO fluxes in coastal marine systems, over various marine sediments. McGinnis et al. (2008) and Brand et al. (2008) studied DO flux dynamics in a riverine reservoir and a freshwater seiche-driven lake, respectively.

The general idea of the eddy correlation is that by correlating the vertical velocity fluctuations  $w'$ , with the fluctuations of the constituents (DO, T)  $C'$ , the instantaneous exchange flux  $w'C'(t)$  can be calculated in a straight-forward manner. Its average  $\overline{w'C'}$  yields the net flux directed towards (consumption) or away from (production) of the sediment.

Since Berg et al. (2003) first tested the EC technique, by combining oxygen micro-sensor and acoustic velocimeter (ADV) measurements, the experience and confidence have increased with respect to instrumentation, deployment and data analysis. An extensive method paper is now being published by Lorrai et al. (2010).

The outstanding advantage of the EC technique over i.e. benthic chambers and in-situ microprofilers, is the potential to record undisturbed fluxes with high temporal resolution. The EC techniques will not disrupt the hydrodynamics of the system and is less affected by localized bioturbation.

Using the IFM-GEOMAR facilities and technical skills, we have developed the next generation of EC for oxygen measurements. Two complete systems were developed based on knowledge and experience gained from Eawag system (McGinnis et al., 2008), together with experience from internationally recognized experts (P. Berg, R. Glud, V. Meyer). Our system consists of a Nortek ADV coupled with a Clark-type oxygen microsensor. The sensor microamplifiers as well as the ROV deployable light inox steel EC frame were completely designed at IFM-GEOMAR (Fig. 5.5.5).



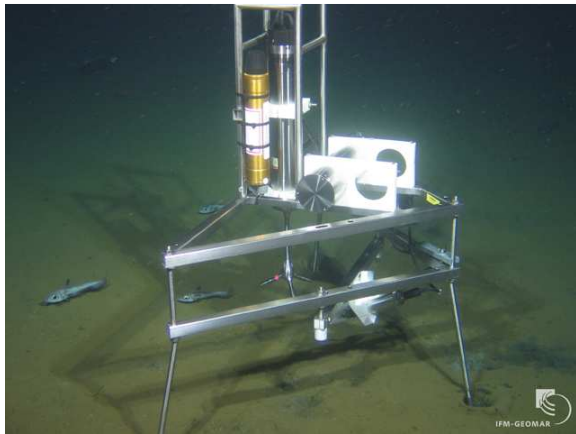


Fig. 5.5.5: Eddy Correlation module deployed by ROV next to bacterial mats in Box 2.

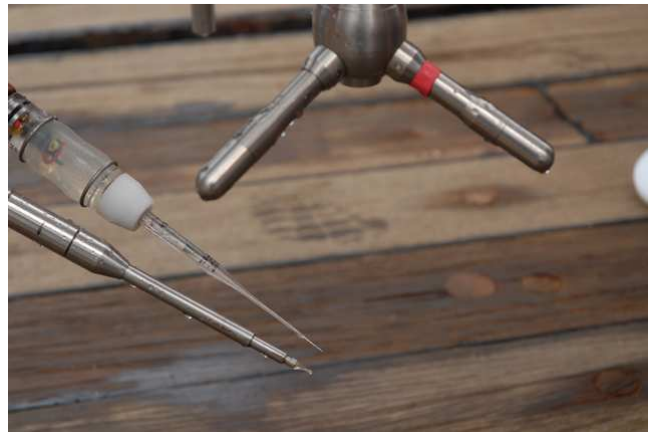


Fig. 5.5.6: View on the sensors: Temperature sensor (left) addition to the oxygen sensor (middle) and the ADV in the upper part.

During this cruise one of our goals was to extend the existing O<sub>2</sub> Eddy Correlation (EC) systems (McGinnis et al., 2011) to include heat flux measurements with fast (7-12 ms response time) FP07 temperature microsensor system (sensor, amplifier and housing). The new EC system now non-invasively and simultaneously measures temperature, O<sub>2</sub> and velocity and their associated turbulent fluctuations (Fig. 5.5.6). The coupling of benthic heat and O<sub>2</sub> fluxes is expected to help determine if, and to which extent, O<sub>2</sub> fluctuations are due to active turbulence or to non-active (fossil) signals. The combined EC system will also help determine temperature dependencies on O<sub>2</sub> fluctuation as well as the extraction O<sub>2</sub> fluxes. By integrating concurrently measured water column turbulence data, it is then possible to more accurately characterize the transport of dissolved gasses and heat within both the water column and at the sediment-water interface.

#### *Pore water sampler (PWS)*

The PWS has been used for the first time in the North Sea for high-resolution extraction of pore water within a depth range of up to 40 cm below the sediment surface. The advantage of this method is to separate pore water and sediment before sample retrieval, which prevents artifacts by decompression and temperature changes. The device basically consists of a lance with small filtering elements (Rhizones) and a syringe carrier. After penetration of the lance into the seafloor the Rhizones can be moved laterally out into the sediment. Pore water will be ingested by applying a vacuum through pressure-resistant syringes.

## **5.6 TV-Grab Operations**

(V. Liebetrau)

During various OFOS tracks (see 5.3. and 6.3.) different types of authigenic cold seep carbonates were observed and potential sites (see 6.6.) could be defined for the recovery of large samples with a video guided grab (TVG). This grab (Fig. 5.6.1), made out of approx. 2.5 t of steel, was originally designed to dig into soft sediments and very successful used for the recovery of Fe-Mn-concretions or gas hydrates from the seafloor. This tool is characterized by a penetration depth of 0.5 to 1 m, a sample volume of around 1 m<sup>3</sup> and a deployment depth of up to 6000 m. The integrated online video system allows a detailed search for suitable targets

and sampling documentation by a straight vertical seafloor observation through the open jaws of the grab. Due to the fact of a closing pressure of around 2 t, provided by the integrated battery-driven hydraulics, the claws can hold and recover samples even larger than the volume of the closed grab. The successful deployment on large rock samples depends strongly on the coordination of ship positioning, winch control and the timing of jaw closure. A final challenge is getting the recovered sample on deck when its weight is more than doubled by leaving the water column. Often several attempts are necessary for successful sampling of a seep site. Nevertheless, this technique provides unique large samples for detailed profile studies through the uppermost calcified sediments and chemoherm structures. Vertical cross cuts enable the detailed sub-sampling and reconstruction of long sequences of fluid activity and reflect new insights into growth structures, calcification processes and fluid-pathway systematic in one sample. Furthermore, the recovery of big boulders and blocks includes quite often the sampling of whole habitats, with typical seafloor fauna on the hard-substrates (e.g. coldwater corals, in this context important geochemical archive of the bottom water column) and adjacent or during calcification incorporated typical cold seep fauna (tube worms, clams, bacterial mats; as indicators of seep activity). The TVG technique for sampling of large single blocks and detailed continuous depth profiles therein is an important completion of the surface oriented ROV sampling. The latter provides unique lateral profile samples covering the extension of whole seep structures.



Fig. 5.6.1: Video guided grab (TVG) of RV SONNE during cruise SO210.

## 5.7 Sediment Sampling and Sedimentology

(S. Kutterolf, D. Völker)

Gravity coring was performed using a gravity corer with a headweight of 2t and a steel pipe, fitted to contain PVC-liners of 120 mm diameter. The pipe was composed of segments of 3 or 6 m. Depending on the sediment type, either 3 m, 6 m or 12 m were used. Liners were cut into ~ 1 m segments, sealed and stored at 5 degree C. Altogether, 32 cores were retrieved (Annex III). With the exception of six cores that are destined for geotechnical experiments at the

University of Kiel, the gravity core segments were cut into halves, one being the work half to be sampled and one the archive half to be kept for non-destructive analysis and description.

The archive half of the split core segments were routinely photographed digitally. We used a home-designed photographic rack, where the camera is moved at a fixed height and with constant illumination in defined steps over the split segment, in order to obtain a series of photos that can later be assembled to photo mosaics. These mosaics reveal much of the surface structure and internal composition of the cores and serve as addition to the visual core description protocol.

A visual core description (vcd) of the archive halves of the split cores was performed, according to ODP standards and classifications, taking into account the grain size composition, colour (according to MUNSELL soil colour charts), sedimentary structures and major as well as minor components of the sample. The written protocols were transformed into digital core descriptions after the cruise (Annex IV).

At particular sedimentary layers (ash layers, turbidites), smear slides were prepared and later fixed for inspection of the mineral and microfossil content under a microscope. This was done by rubbing a small quantity of material with water onto a microscope carrier.

## 5.8 Zoology

(F. Valdés)

The faunal assemblage of the Concepción methane seep area (CMSA; 36°27' 87'S ; 73° 43, 25' W) is diverse, and comprises a large proportion of species that are new to science. Among the reported chemosymbiotic species are *Calymene gallardoi* (Sellanes & Krylova, 2005), *Archivesica* sp. and the siboglinid tubeworms *Lamellibrachia* sp. Although taxonomic analysis is still under way, most of the chemosymbiotic species seem to be endemic. The CMSA is also a hotspot for non-seep benthic megafauna too; 101 taxa were present, but most of them are colonists or vagrants (i.e. not endemics of methane seeps). The objective of the zoological study was the collection of samples of megafauna and meiofauna in the CMSA and other seep zones.

### *Material and methods*

**Study area.** The Concepción methane seep area (CMSA) is located 72 km northwest of Concepcion Bay (36°22' S ; 73°73' W), on the mid-slope (740 –870 m water depth). Previous piston-core deployments have found large gas hydrate deposits with carbon isotopic values of  $-62.8 \pm 1.0\text{‰}$  for both the hydrates themselves and sedimentary porewater (Coffin *et al.*, 2006); this value is indicative of a biogenic origin of the methane (Ussler *et al.*, 2003). There are abundant blocks formed by carbonate-cemented mud, i.e. mud breccia. Previous faunal studies have indicated the presence of eight species of chemosymbiotic bivalves belonging to the families Vesicomidae, Lucinidae, Thyasiridae and Solemyidae, as well as three species of polychaetes (families Siboglinidae, Antonbruunidae and Nautiliniellidae). An abundant accompanying heterotrophic fauna has been also reported, composed of more than a hundred species of benthic organisms (Sellanes *et al.*, 2004; Sellanes and Krylova, 2005; Sellanes *et al.*, 2008).

### *Biological sampling*

Different methods were used for biological sampling, including the Kiel 6000 ROV, TV-Grab and TV-MUC, at different stations within and nearby the CMSA. Megafaunal sampling with the ROV was performed by a collecting net and meiofaunal samples through push-corers, both devices manipulated with the ORION arm during the 11 dives performed. Samples were put in the ROV sample basket and transported to the surface. The TV-Grab allowed selecting through online video the sampling sites at the 8 deployments performed. The fauna contained in the large sediment blocks recovered was sorted onboard. Meiofaunal samples were also obtained from TV-MUC deployments. All the samples were fixed using 10% formalin or absolute ethanol for morphological or genetic analysis, respectively.

### *Video survey and analysis*

Still images and video footage were collected both by the Ocean Floor Observation System (OFOS) as well as by the ROV Kiel 6000. Ocean floor observation allowed to obtain important insights on the identification, distribution, zonation, spatial heterogeneity of the fauna and allowed a visual identification of the hydrocarbon seep sites. Videos and high resolution still images taken by both devices at the different transects will be studied in greater detail at home.

## **5.9 Microbiological Studies**

(T. Treude)

### *Multicorer Cores*

Four sediment cores taken from each multicorer were used for (1) microbial turnover rate measurements (methane oxidation and sulfate reduction), (2) molecular studies (Fluorescence In-situ Hybridization = FISH, RNA/DNA, biomarker), (3) flow through experiments, and (4) sampling of active sediments. Microbial turnover rates of methane and sulfate were measured in three parallel sub-cores (i.d. 26 mm), respectively, by radiotracer techniques. Fifteen  $\mu\text{l}$  of  $^{14}\text{C}$ -methane tracer (activity 2 kBq) and 6  $\mu\text{l}$  of the  $^{35}\text{S}$ -sulfate tracer (activity 200 kBq) were injected into the sediment, respectively, in 1-cm intervals. After an incubation time of 18-24 hours at in-situ temperature, the reactions were stopped by slicing the cores into 1-cm intervals and transferring the sediment into 2.5% (w/w) sodium hydroxide and 20% (w/w) zinc acetate, respectively (Table 5.9.1). For molecular studies, the first five centimeters of one sediment core was sliced into 1-cm intervals. Below five centimeters, the core was sliced in 2-cm intervals. Each depth section was sub-sampled for different purposes (Table 5.9.1). A sub-core (i.d. 60 mm) was taken from one multicorer core for sediment flow-through experiments in the home laboratory. The core liner was specifically designed to be installed into a flow-through system enabling biogeochemical studies under controlled fluid flow settings. To gain active sediments for in-vitro studies, one core was sliced into larger depth sections depending on sediment stratigraphy. Sediments were transferred into glass bottles, sealed with a rubber stopper, and cooled.



Table 5.9.1: Sampling scheme for the microbiological studies during SO210.

Parameter	Vial	Chemical	Sample Volume (ml)	Storage
<b>Microbial turnover rate measurements (1 core)</b>				
3 x methane oxidation	40 ml Snapvials	20 ml 2.5% NaOH	ca. 5 ml sediment	room temperature
3 x sulfate reduction	50 ml Corningvials	20 ml 20% ZnAc	ca. 5 ml sediment	room temperature
<b>Molecular studies (1 core)</b>				
FISH	10 ml PE Testtubes	1.5 ml 4% Formalin	0.5 ml sediment	→ further processing on board
RNA/DNA	4 ml Cryovials	-	fill vial 2/3 <sup>rd</sup> w/ s.	-80°C
Biomarker	Aluminum + Ziplock	-	Ca. 30g sediment or carbonates	-20°C
<b>Sediment flow through studies (1-2 cores)</b>				
For flow-through studies	-	-	Sediment core 60 mm i.d., length ca. 20 cm.	+ 4°C
<b>Active sediments (1 core)</b>				
For in-vitro studies.	100 or 250 ml glass vials, rubber stopper, screw cap	-	100 or 250 ml sediment	+ 4°C

### ROV-Pushcores

Pushcores (i.d. ~80 mm) taken by the ROV KIEL 6000 were sampled basically after the same scheme as multicorer cores. For flow through experiments two special pushcores (i.d. 60 mm) were used per sampling site that can later directly be installed into the flow-through system.

### Authigenic carbonates

Authigenic carbonates gained during TV-Grab or ROV deployments were frozen for biomarker analyses. In some cases (see Table 6.9.1) the carbonates were also sampled for further molecular and in-vitro studies.

### Whale bones

Two whale vertebrae were sampled from an old natural whale fall. One bone was sub-sampled similar to sediments (sulfate reduction, FISH, RNA/DNA, biomarker, active bone pieces kept cooled in seawater). The bone was cut in the middle with a saw and then cut into smaller pieces from surface to center. The second bone was frozen completely at -80°C.

### Clams

Four clams (*Archivesica* Sp.) were frozen at -80°C for molecular studies.

## 5.10 Pore Water Geochemistry

(F. Scholz)

### Sediment sampling and pore water recovery

Sediments were retrieved by means of gravity (GC) and multiple corers (MUC) as well as ROV-guided push cores (PC). Sediment samples were taken from the GCs at depth intervals of 20 to 60 cm. The MUCs and PCs were stepwise extruded from the core liners and cut into 1 – 5 cm thick discs. Depending on sample type and the respective parameters to be analyzed, pore waters were recovered by pressure filtration (Argon gas at 4 – 7 bar), centrifuging after sediment processing in an Argon-flushed glove bag (20 minutes at 4000 rpm) or by the aid of rhizons (obtained from Rhizosphere, the Netherlands). Pore water samples were filtered

through 0.2  $\mu\text{m}$  cellulose acetate membrane filters. Between 5 and 20 ml of pore water could be recovered per depth interval by the techniques described above. About 5 ml of wet sediment sample were stored for the determination of water content and porosity.

For methane and hydrocarbon isotope headspace analyses a defined sediment volume of 6  $\text{cm}^3$  was sampled into glass vials that contain 3ml 10% KCl or 3ml 0.1 M NaOH solution, tightly crimped, and suspended. The above procedures were performed at approximately in situ temperature of 6°C in a cold room.

Sediments remaining after pressure filtration (squeeze cakes) and centrifuging were stored for potential solid phase analyses in shore-based laboratories.

#### *On-board chemical analyses*

Analyses for ammonium ( $\text{NH}_4^+$ ), phosphate ( $\text{PO}_4^{3-}$ ), silicate ( $\text{SiO}_4^{4-}$ ) and dissolved sulfide ( $\text{HS}^-$ ) and iron ( $\text{Fe}^{2+}$ ) were completed onboard using a Hitachi U2800A spectrophotometer. The respective chemical analytics follow standard procedures and are described in detail in Grasshoff et al. (1999) and on the IFM-GEOMAR webpage ([www.ifm-geomar.de](http://www.ifm-geomar.de)), respectively. Aliquots for  $\text{NH}_4^+$  analyses were partly diluted prior to measurements in order to avoid interferences with  $\text{HS}^-$ . For the same purpose, aliquots for  $\text{PO}_4^{3-}$  and  $\text{SiO}_4^{4-}$  analyses were acidified and bubbled with argon for at least one hour.

The total alkalinity of the pore water was determined by titration with 0.02 N HCl using the Tashiro indicator, a mixture of methyl red and methylene blue. The titration vessel was bubbled with argon to strip any  $\text{CO}_2$  and  $\text{H}_2\text{S}$  produced during the titration. The pore water contents of chloride ( $\text{Cl}^-$ ), bromide ( $\text{Br}^-$ ), sulfate ( $\text{SO}_4^{2-}$ ) and nitrate ( $\text{NO}_3^-$ ) were determined by ion-chromatography (Metrohm 761 Compact). The IAPSO seawater standard was used to check the reproducibility and accuracy of all chemical analyses.

In addition to the shipboard analyses, sub-samples were taken for shore-based analyses of major and minor cations (acidified with  $\text{HNO}_3$ ), iodine and methane concentrations as well as oxygen and carbon isotopes (poisoned using mercury chloride). Table 6.10.1 gives an overview about the analyses carried out and sub-samples taken at each station.

## **5.11 Volcanology**

(S. Kutterolf, A. Freundt)

Tephra layers are typically much better preserved on the ocean floor than under the commonly erosive conditions on land. Offshore sediment gravity coring thus potentially improves the determination of areal distribution particularly of thin, fine-grained distal tephra. All volcanic fallout layers of the Chilean southern volcanic zone mapped on land show dispersion axes directed to the east (into Argentina), reflecting the (presently) strictly eastward directed wind at all but the very lowest atmosphere altitudes. However, little fallout tephra is preserved in the central valley and coastal cordillera west of the volcanic front. In contrast, the central valley is filled by numerous ignimbrites, deposits of pyroclastic flows of which many probably reached the coast. The search for tephra beds on the Pacific ocean floor thus aimed to identify distal deposits related to ignimbrites emplaced on land, and to detect any unusual fallout dispersal to the west.

## **6 Work Completed and First Results**

### **6.1 Hydroacoustic Work**

(D. Völker, J. Geersen)

#### **6.1.1 Parasound**

Parasound data was collected whenever the ship was moving. In addition, detailed surveys were carried out (a) on the shelf between Concepción and Constitución, (b) along flanks of submarine canyons and across previously known submarine slides.

On the continental shelf between Concepción and Constitución off Punta Lugurne, Chilean colleagues had reported on a change in the water depth of up to 50 m after the Maule earthquake in relation to existing nautical charts. Here, the idea was to see whether this apparent change is result of an earthquake triggered submarine slide. However, the Parasound profiles display undisturbed shelf sediments of about 50 ms two-way-traveltime (TWT) thickness, absent of indications for recent mass wasting (Fig. 6.1.1.2). The apparent discrepancy in seafloor depth is therefore likely a result of imprecise nautical charts.

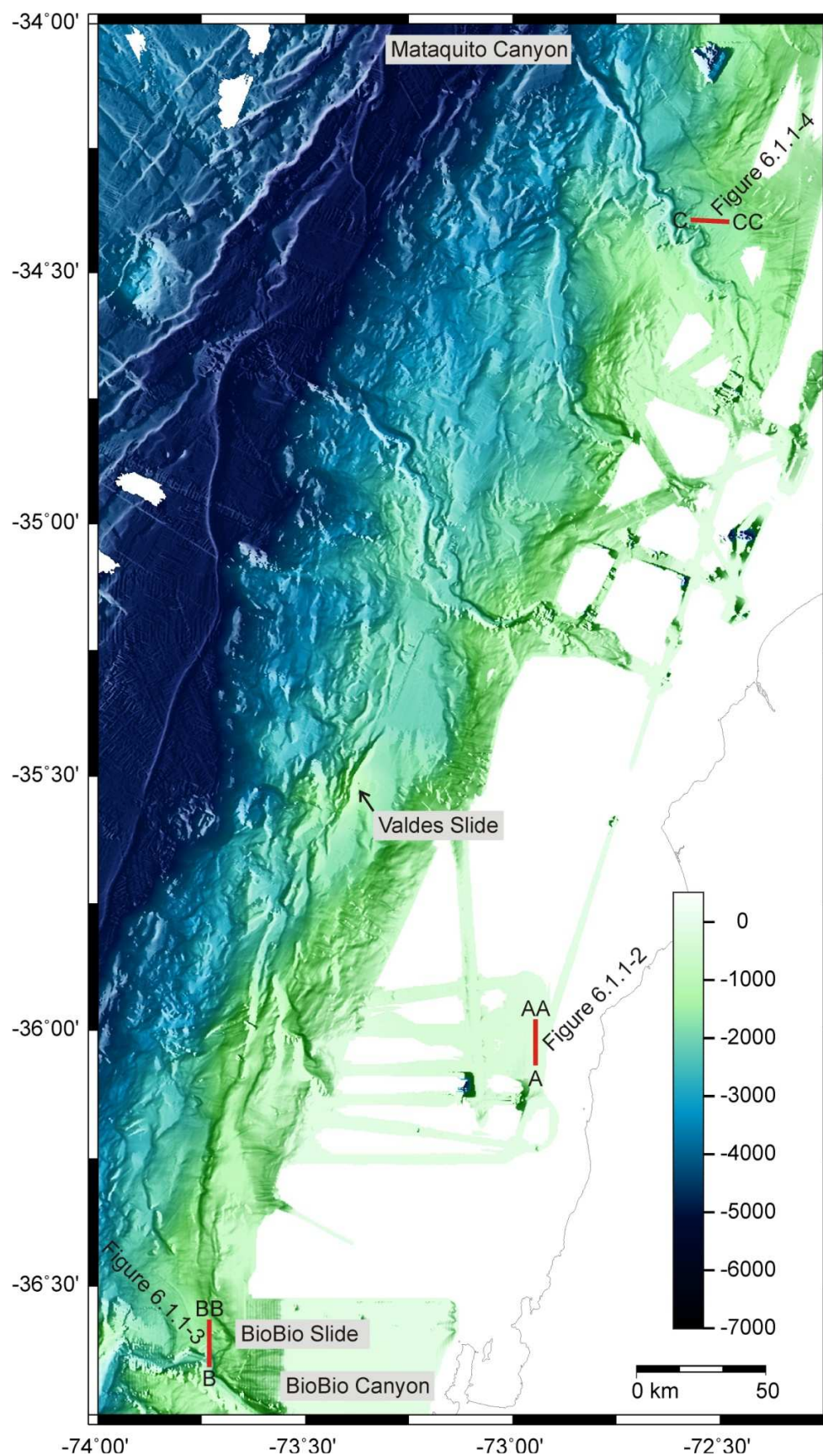


Fig. 6.1.1.1: Position of Parasound profile lines shown in the consecutive figures, on the continental shelf offshore Punta Lugurne (line A-AA, Fig. 6.1.1.2), at BioBio Slide (line B-BB, Fig. 6.1.1.3), as well as to the north of Mataquito Canyon (line C-CC, Fig. 6.1.1.4).

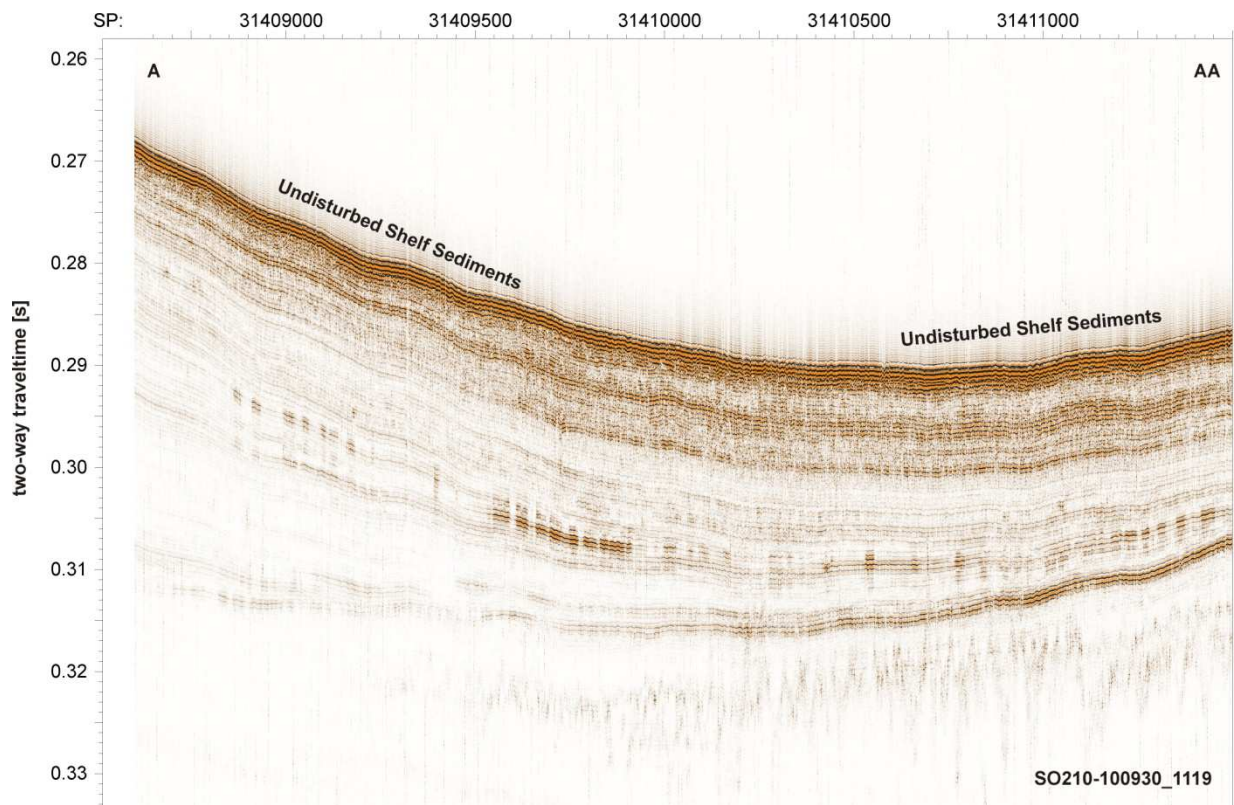


Fig. 6.1.1.2: Parasound profile of the continental shelf between Constitución and Concepción (off Pta Lujurne) where a change in water depth had been reported after the Maule Earthquake of 27 February 2010 in relation to nautical maps. The profile line shows a unit of undisturbed shelf sediments lacking indications for mass movement. Profile length is 20 km.

Detailed surveys around previously mapped slides and canyon walls were done in order to search for mass wasting features triggered by the recent (27 February 2010) Mw 8.8 Maule Earthquake. One of the targets was the BioBio Slide (Fig. 6.1.1.1) which is a 5 by 6 km wide depression of 29 km<sup>2</sup> extent that is 55-160 m deep in relation to the surrounding sea floor. The depression lies at the northern edge of and opens to the deeply incised BioBio Canyon. The steep head- and sidewalls of the slide are indented by a number of smaller and less deep, flat-floored depressions which are interpreted as retrogressive failures of the canyon walls. Parasound profiles give a comprehensive insight into the deformation associated with the BioBio Slide (Fig. 6.1.1.3). Outside and upslope of the depression, parallel reflections are interpreted as undisturbed (e.g. not affected by mass wasting) part of the continental slope. Here the seafloor appears smooth. At the headwall, parallel reflectors of the undisturbed strata are bluntly truncated and the style of the seafloor changes to a rough and blocky morphology. This morphology is interpreted as caused by slump debris that originates from the headwall area. Further towards the BioBio Canyon, a strong seafloor reflector that appears less blocky represents the glide plane of the slide. Within the BioBio Canyon, a terrace that is also found in the bathymetric data is visible above the thalweg and may represent a fraction of the sediment volume displaced by the major causing slide or retrogressive events.





Fig. 6.1.1.3: Parasound profile across the BioBio Slide. The profile shows main morphological features of the slide. A 20° steep headwall truncates a 60m thick sediment unit upslope of the slide. At the floor of the evacuation site, the slide scar is partly exposed and partly covered by debris. The slide opens to the deeply incised BioBio Canyon. Profile length is 8.5 km.

Similar work was done in the vicinity of the Taza Slide, the Valdes Slide, the Mataquito Canyon, and the San Antonio Canyon (Figs. 2.2.2 and 6.1.1.1). These profiles need to be processed in the future to further analyze, if recent (possibly seismically triggered) mass wasting took place. Taza Slide appears to be much older than BioBio Slide or Valdes Slide, as the bottom of this depression and presumable glide plane of the slide is covered by tens of meters of well-stratified hemipelagic sediments. The flanks of the canyons are ornamented by mass-wasting features that extend from the canyon walls onto the open slopes to the sides of the canyons (see chapter 6.1.2). Parasound data show that retrogressive sediment deformation upslope of failed segments of the canyon wall takes place as sediment creep, where 75 ms TWT thick, well-stratified sediments form sinusoidal folds (Fig. 6.1.1.4).



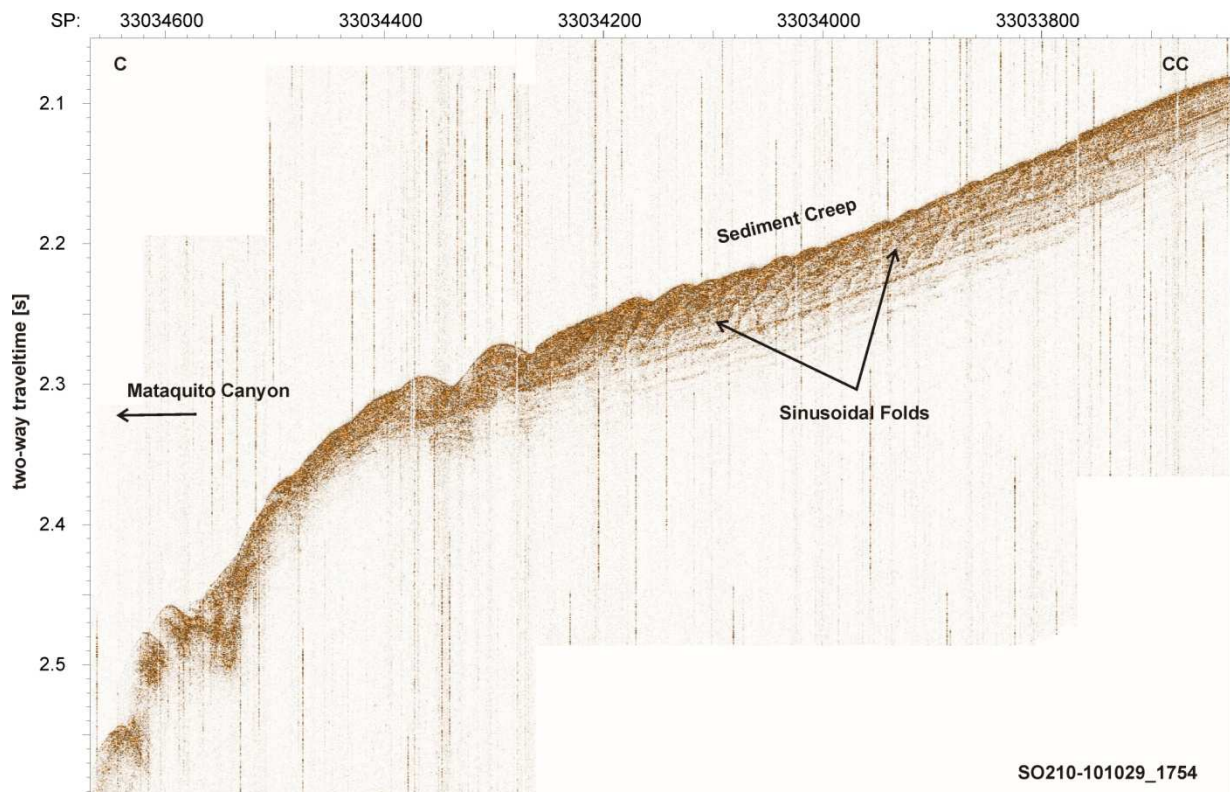


Fig. 6.1.1.4: Parasound profile to the north of Mataquito Canyon. Here, the collapse of canyon walls has led to retrogressive, translational failure of the slope to the canyon side as well as sediment creep structures. The profile shows regular, small-scale folds that are observed exclusively in the direct vicinity upslope of the sites of failure. Profile length is 12 km.

## 6.1.2 EM120

Main goals of the multibeam bathymetric mapping during SO210 were (a) to fill data gaps in the existing bathymetric data (Fig. 6.1.2.1) and (b) to remap critical areas for mass wasting, such as flanks of submarine canyons or head- and sidewalls of previously detected submarine slides. Data gaps were particularly annoying at the upper and middle continental slope off Arauco Peninsula (Figs 6.1.2.1), where there is indication of continental slope indentations that may evidence giant slope collapses in the past (Geersen et al., 2011-B). The newly gathered data in fact show that these depressions are delimited by escarpments (sidewalls) of some 100 m height and that some of them extend from the Chile Trench floor to the shelf where they modify the course of the shelf edge, thus spanning the full depth range of the continental margin. In total, ~1600 km<sup>2</sup> of the continental slope and ~4150 km<sup>2</sup> of the abyss were newly mapped, whereas most of the mapped areas were already covered by previous cruises. The detailed remapping of previously known areas offers the possibility to directly monitor seafloor deformations related to a Mw 8.8 earthquake by comparison of DEMs of the bathymetry and derived seafloor attributes such as slope gradient, aspect and curvature of before and after the event. Differential gradient maps which provide an easy visual way of monitoring seafloor deformation were calculated for the areas mapped on cruises of RRS JAMES COOK, RV SONNE and RV METEOR prior to the Maule Earthquake.

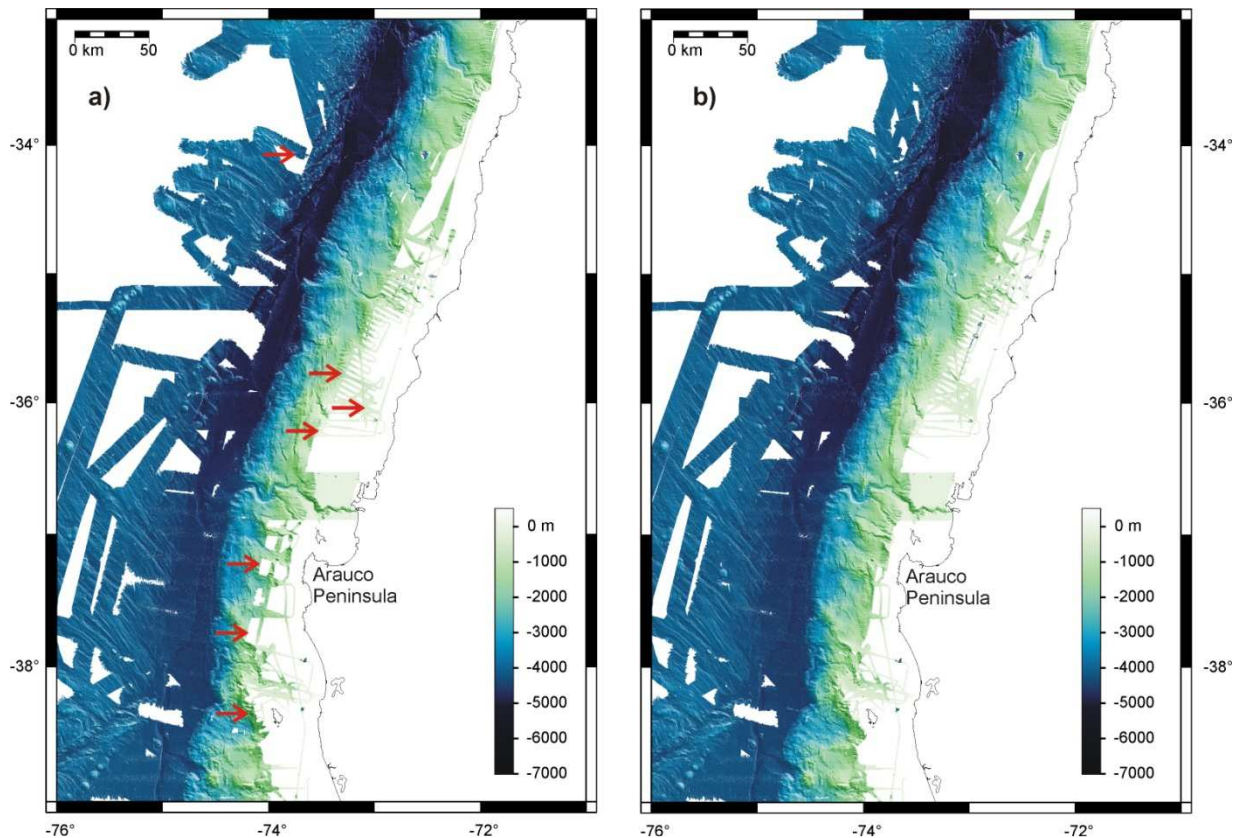


Fig. 6.1.2.1: Bathymetric dataset of the working area prior to cruise SO210 (a) and after it (b). A number of gaps in the combined dataset of previous cruises of RV SONNE, METEOR and RRS JAMES COOK were filled (red arrows). At the continental slope, the mapping of three large slope failure embayments offshore Arauco Peninsula was nearly completed.

As a first result, we can say that in spite of the Maule Earthquake (the fifth largest ever instrumentally recorded earthquake), no newly formed retrogressions were found at the headwall of BioBio Slide although a number of older retrogressive failures of the headwall are obvious (Fig. 6.1.2.2). At first sight, the same is true for a number of other previously known slides (Taza Slide, Valdes Slide). The sidewalls of BioBio, Mataquito and San Antonio Canyon are ornamented by a number of canyon wall collapses as well as translational slides that appear to origin from the first and extend onto the open slopes to the sides of the canyons. Here, no immediately apparent changes were noted, nor were newly formed slide-related depressions found on the open continental slope. On horizontal scales of  $< 1$  km however, new slides may exist and could show up in further and more thorough data revision.

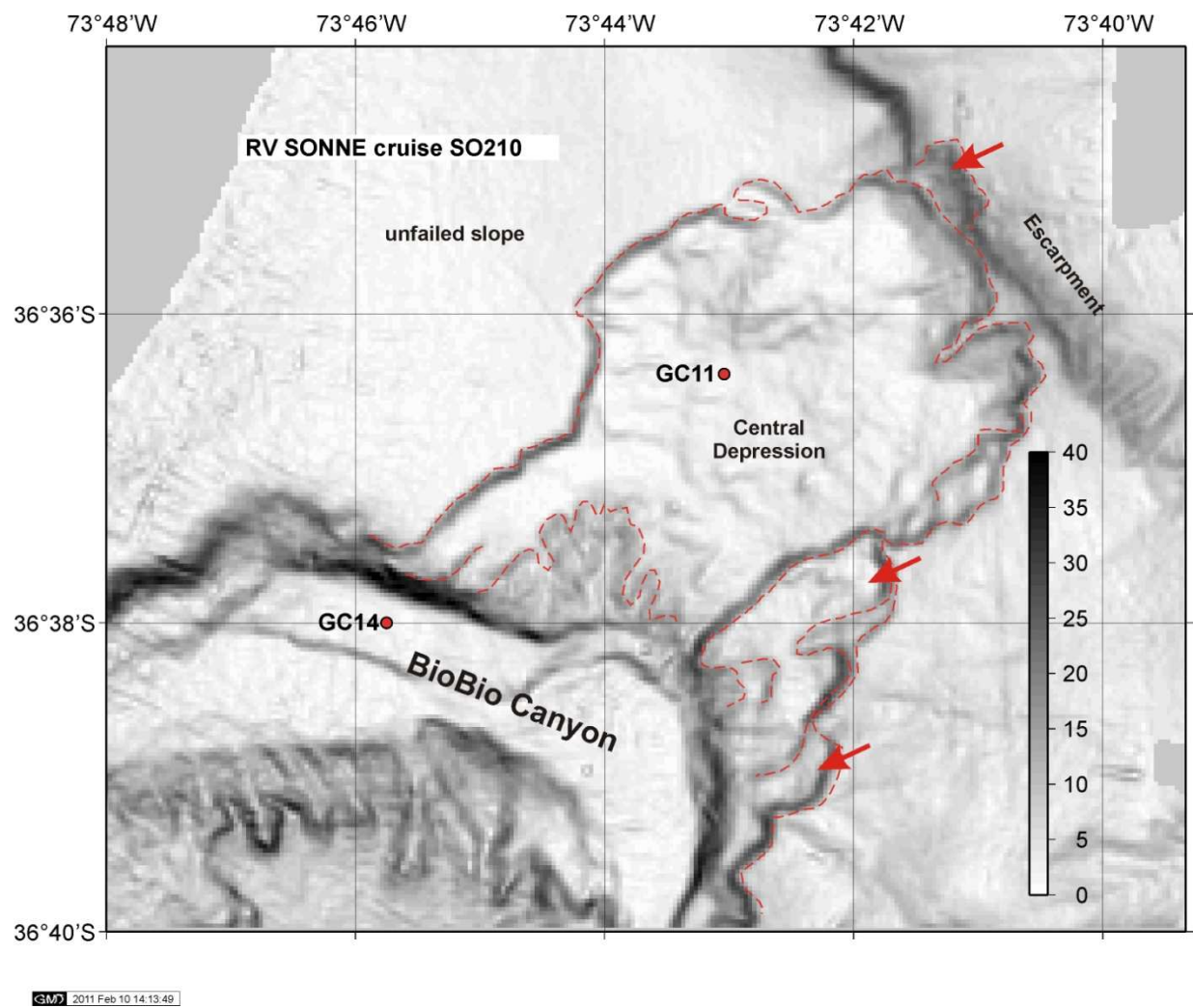


Fig. 6.1.2.2: Slope gradient map of BioBio Slide area with headscarp, central depression and retrogressive secondary slides (arrows).

## 6.2 Water Column Studies

(L. Rovelli, S. Sommer, L. Bryant, P. Wefers)

The research areas CMSA Box 1, Box 2 and Box 4 were investigated with several CTD casts. With the exception of the well mixed surface boundary layer (SBL) the water column was stratified (Fig. 6.2.1). With the CTD casts profiling down to 5 m above the sea floor it was not possible to detect a well mixed bottom boundary layer (BBL) thus suggesting that its extent might be confined to the first couple of meters above the sea floor.

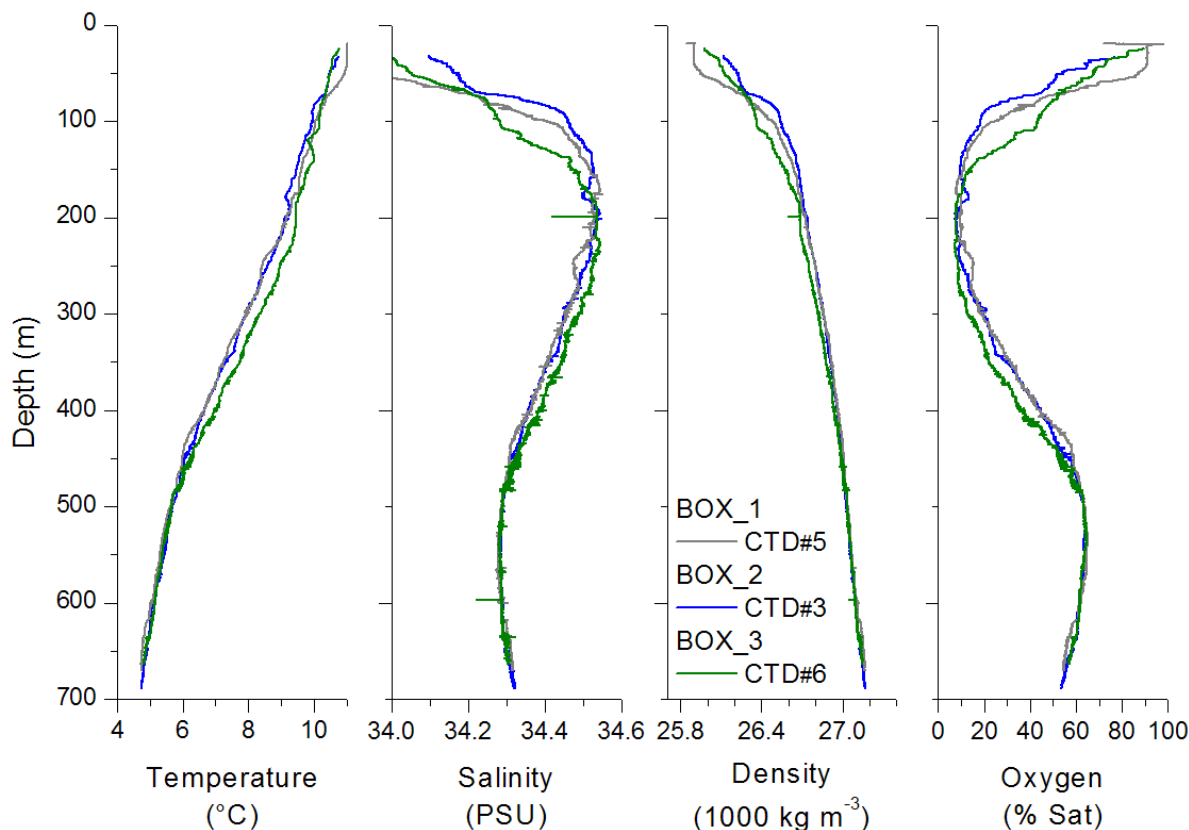


Fig. 6.2.1: Physical information on the water column in the different study sites as collected from selected CTD casts. It shows, from left to right, potential temperature, salinity, potential density and dissolved oxygen.

Oxygen measurements showed an oxygen minimum (8% saturation) at ~200 m and a deep water maximum (64%) at ~540 m depth respectively. Due to the presence of a great variability in the oxygen concentrations (multiple oxyclines), the CTD readings were corrected according to absolute values from Winkler titrations to provided more accurate results.

Furthermore, the oxygen dynamics was also investigated using the Microstructure-CTD, which was equipped with a standard sensor (Oxyguard), with time constants similar to the ship CTD one, and a fast oxygen sensor (0.2 s time constant). The preliminary results on a selected casts (Fig. 6.2.2) revealed that the oxygen variability is larger than it is measured by the standard sensors and that the depth location and magnitude of the oxyclines might be larger than thought. This is of major importance not only for the oxygen transport but also for the fate of methane in the water column (i.e. methane oxidation).



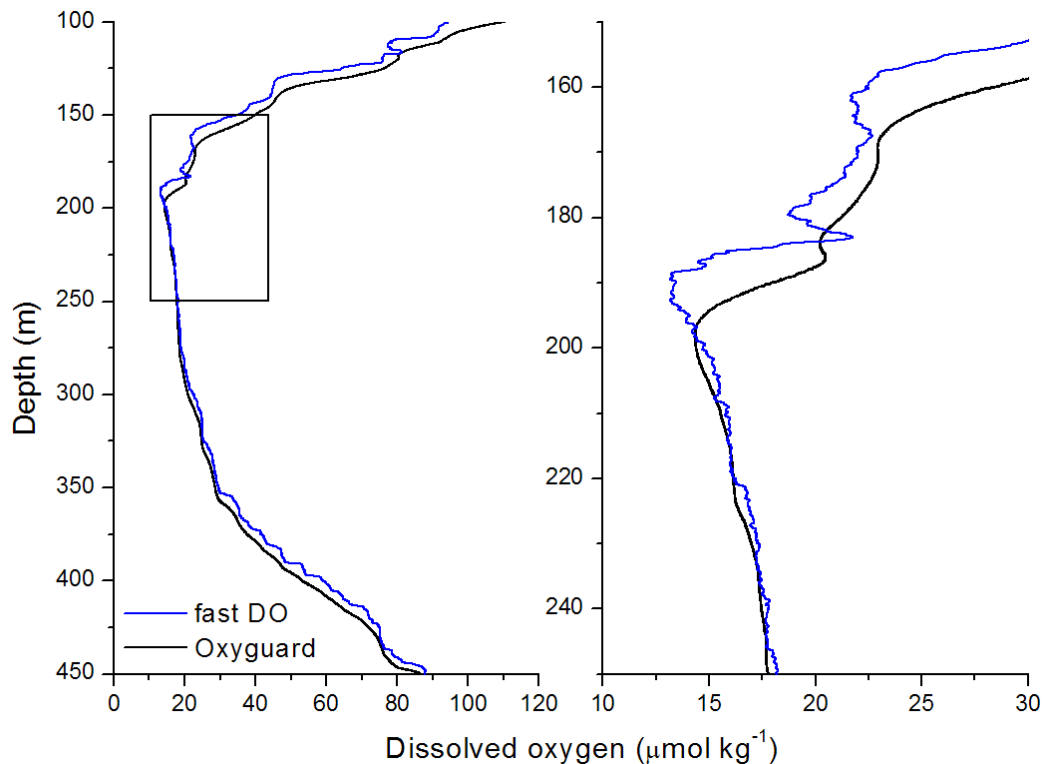


Fig. 6.2.2: High resolution oxygen profile from a selected Microstructure CTD cast. Left: Oxycline and oxygen minimum as measured by the standard oxygen sensor (Oxyguard) and the fast sensors. Right: Zoom-in of the upper part of the oxygen minimum. Note the considerable displacement of the oxycline caused by the standard oxygen sensors resolution at the profiling speed (0.6 m s<sup>-1</sup>).

Water sampling for methane measurements was conducted at the different seep sites by using the CTD and the ROV (Fig. 6.2.3 left and right panel, respectively).

During CTD casts at all sites elevated methane concentrations of up to ~ 170 nM were determined close to the bottom. Highest CH<sub>4</sub> concentration was found at CMSA Box 4 over a dead clam bed. However at this site variability appeared high as a second CTD cast that was sampled 18 days later did not reveal high CH<sub>4</sub> levels. Overall bottom water CH<sub>4</sub> concentration was about 50 – 100 nM.

In contrast to the CTD casts, the CH<sub>4</sub> concentrations determined in water samples obtained by the ROV were generally strongly elevated. Above the clam bed (CMSA Box 4) up to ~ 3800 nM CH<sub>4</sub> was measured indicating that methane release at this site was still active although the clams were dead. The high variability of methane at this site presently cannot be explained conclusively.

In addition, near bottom water sampling was performed during ROV dives and during the lander deployment BIGO #1 at CMSA Box 2. During ROV dives water samples were taken at locations where methane seepage was suspected based on the presence of bacterial mats, distinct fractures within carbonate crusts or specific fauna such as tubeworms.

Future activities will include methane carbon isotope measurements and the analyses of the microstructure CTD data in conjunction with the conventional CTD data. Based on this data processing it will be tried to calculate fluxes of oxygen and methane in the water column. This analysis will be conducted in close consideration of the water column data that were obtained during the BIGO and Profiler deployments.

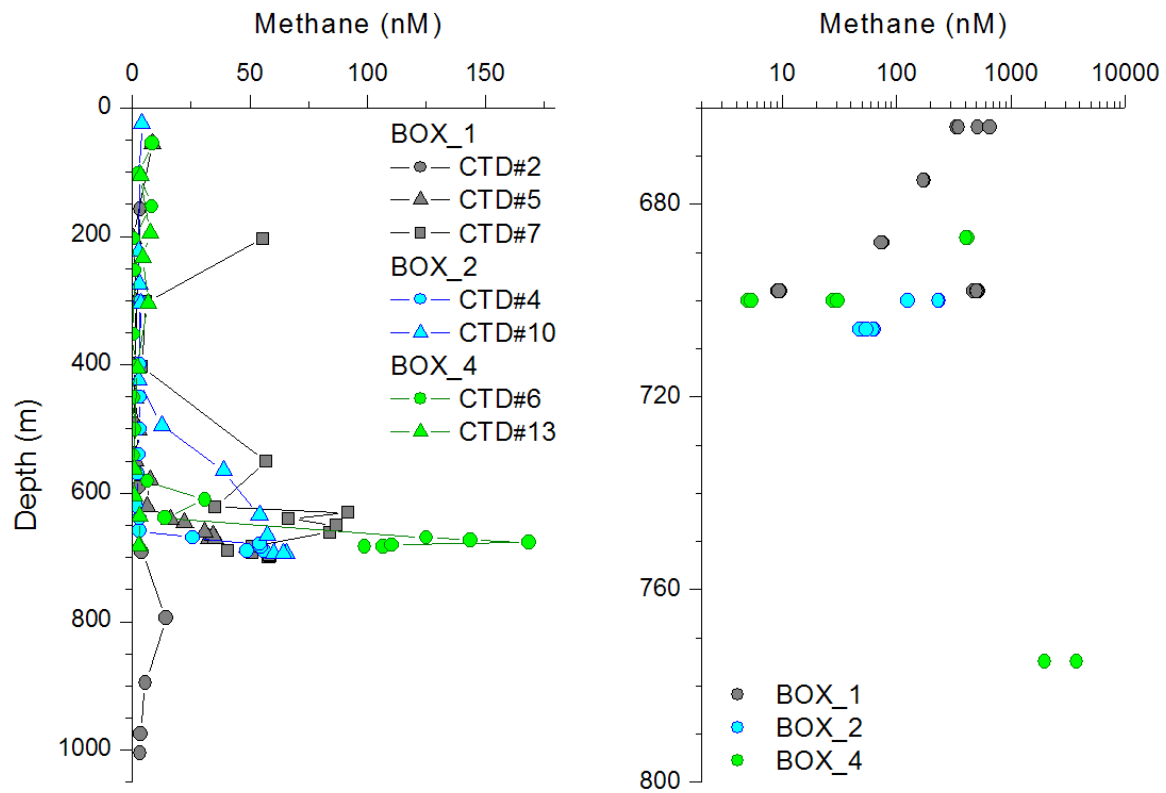


Fig. 6.2.3: Left panel: methane concentrations above the different seep sites (CMSA Box 1, CMSA Box 2, CMSA Box 4), water sampling was by CTD casts; right panel: methane concentrations (log scale) determined at these seep sites in water samples obtained by the ROV.



### 6.3 Seafloor Observations (OFOS, ROV)

(P. Linke)

During the cruise the OFOS and ROV were used for ground-truthing of information which indicated possible seep activity and has been obtained during previous cruises to the Chilean fore-arc. Of special help in our search for cold seep activity were the sidescan sonar images obtained in the Concepcion Methane Seep Area (CMSA) during cruise JC23 with RRS JAMES COOK (Flüh & Bialas, 2008). In this geophysical study, several indications for fluid venting were observed on ridges on the upper and middle slope between 35.5 and 36°S (CMSA North) and on the upper-slope between 36.5 and 36.8°S (CMSA South) along the seaward margin of an intra-slope basin (Klaucke et al., in press). Here, backscatter anomalies indicated widespread authigenic carbonate precipitation, which was suspected to result from the expulsion of methane-rich fluids.

During cruise SO210 a total of 11 OFOS deployments in 6 working areas were conducted (Table 6.3.1). If manifestations of fluid discharge were seen, the survey was followed by ROV dives and subsequent sampling of bottom water, sediments, carbonates and fauna. A complete list of the 13 ROV dives is given in Table 6.4.1 in the following chapter.

Table 6.3.1: Summary of OFOS tracks during the SO210 cruise (\*followed by ROV dive)

Station No. SO210	OFOS No.	Date	Time Start (UTC)	At Bottom (UTC)	Off Bottom (UTC)	Time End (surface) (UTC)	Picture No. taken at seafloor	Location
8	1	28.09.10	22:59	23:22	03:42	04:09	7 – 130	CMSA Box 3*
11	2	30.09.10	21:45	22:18	02:45	03:17	5 - 138	CMSA Box 3*
14-1	3	02.10.10	05:58	06:20	08:08	08:33	5 - 68	CMSA Box 2*
14-2	4	02.10.10	09:06	09:30	11:24	11:50	69 - 110	CMSA Box 2*
18	5	02.10.10	20:11	20:41	02:22	02:42	5 - 500	CMSA Box 1*
19	6	03.10.10	04:06	04:33	08:46	09:20	5 - 81	CMSA Box 4*
56	7	13.10.10	22:49	23:38	04:49	05:18	3 - 185	CMSA Box 6
57	8	14.10.10	06:04	07:16	10:20	11:00	186 - 221	CMSA Box 6
71-1	9	16.10.10	23:16	23:57	00:51	01:25	5 - 102	CMSA Box 7
71-2	10	17.10.10	01:50	02:24	03:19	03:54	103 - 197	CMSA Box 7
89	11	21.10.10	00:55	02:18	07:00	08:20	6 - 354	Accret. prism

The first two OFOS surveys were conducted in Box 3 in the vicinity of Itata Canyon (CMSA North). The sidescan sonar images showed areas of high backscatter intensity that are several hundreds of meters in diameter with highly irregular outlines and forming elongate ridges or domes (Klaucke et al., in press). The OFOS surveys showed that the steep flanks of the ridges were covered with large carbonate boulders and crusts. In between the carbonates bacterial mats (Fig. 6.3.1), shells of vesicomid clams and large Siboglinid tubeworms of the genus *Lamellibrachia* were visible (Fig. 6.3.2).

Box 3 was revisited during the 10h-long ROV dive 115 (98ROV-11) starting from the southerly ridge towards the summit of the northern ridge. Similar to an oasis in the desert we discovered locally restricted but active vent holes at the base of a slope, around which bacterial mats, gigantic vesicomid clams of the genus *Archivesica* sp. and tube worms had settled (Fig. 6.3.3). This habitat was intensely sampled to assess the heterogeneity of methane impact and chemosynthetic activity in close vicinity. The slope of the northern ridge was covered with carbonates and large fields of vesicomid clams and Siboglinid tubeworms of the genus *Lamellibrachia*. On the top of the northernmost elevation we found an uplifted carbonate block which was sticking like a pinnacle in the sediment (Fig. 6.3.4).

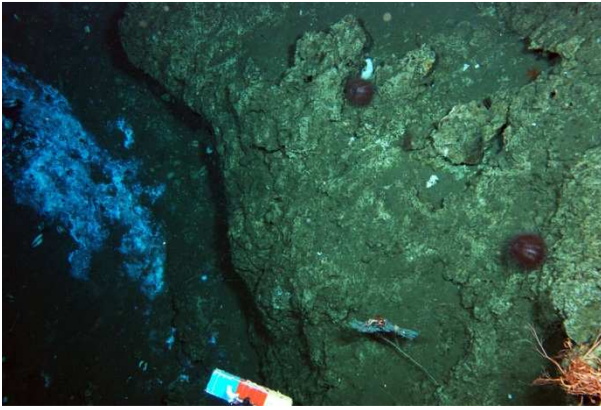


Fig. 6.3.1: Bacteria mats near a large carbonate block in Box 3.



Fig. 6.3.2: Shells of vesicomyid clams and large Siboglinid tubeworms of the genus *Lamellibrachia*.



Fig. 6.3.3: A seep community with bacterial mats, clam field (*Archivesica* sp.) and tube worms.

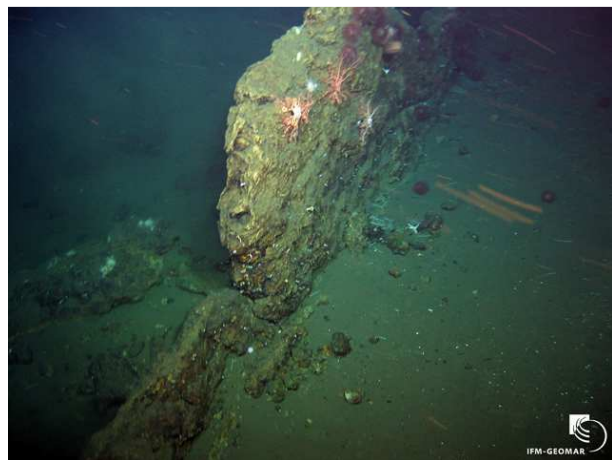


Fig. 6.3.4: Uplifted carbonate block on top of the northernmost elevation in Box 3.

The OFOS surveys 9 and 10 were conducted in Box 7, where the sidescan sonar survey had shown a fault trace (Klaucke et al., in press). Faults appear to be the pathway for fluids, as patchy high backscatter intensity around the fault suggested. This fault has been imaged during cruise JC23 for at least 1 km surrounding the surface expression of the fault. It widens from east to west reaching a width of about 500 meters at the western end of the sidescan sonar profile. However, the OFOS surveys did not reveal any signs of present seepage, only some single carbonates were found (Fig. 6.3.5). At the end of the track indications for a slide event or canyon fill were seen (Fig. 6.3.6).

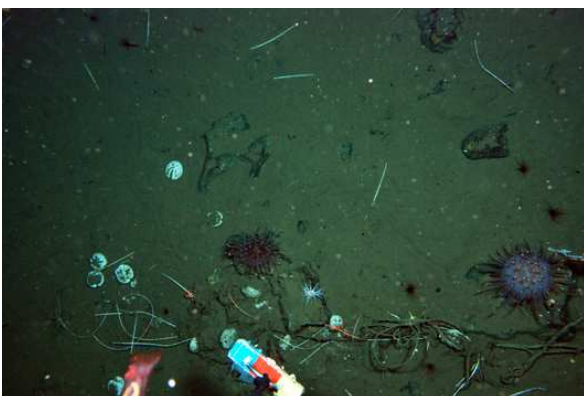


Fig. 6.3.5: Single carbonates and a rope (no tube worms) at the seafloor, Box 7.

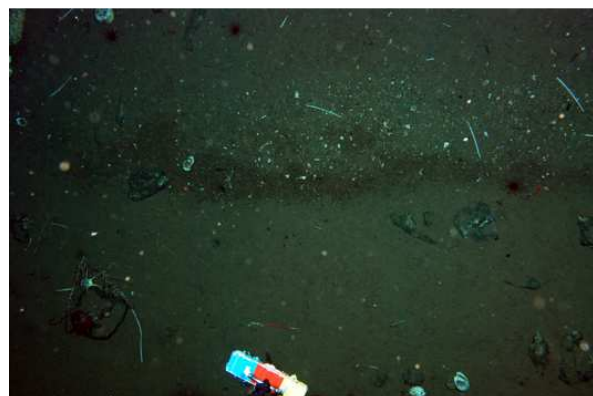


Fig. 6.3.6: Indications for a slide event or canyon fill.

Box 6 was chosen due to a heat flow anomaly measured in the sediments on transect HF0307 at 35.8°S by Grevemeyer et al. (2006). This transect was followed by OFOS tracks 7 and 8. During this survey only buried carbonates (Fig. 6.3.7) and no indication of recent fluid discharge were visible (Fig. 6.3.8).

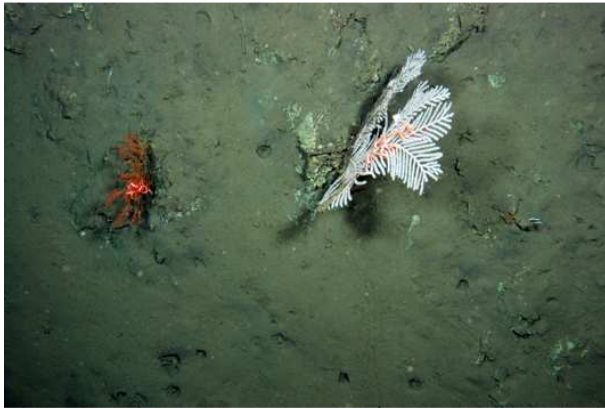


Fig. 6.3.7: Sediment-covered carbonates, Box 6.



Fig. 6.3.8: Indications for a slide event.

OFOS surveys 3 and 4 covered Box 2 in the southern part of the CMSA. In the sidescan sonar record, ellipsoidal to elongated patches of high backscatter intensity indicated the presence of either authigenic carbonate precipitates and/or gas-charged sediments (Klaucke et al., in prep.). The OFOS surveys showed only some authigenic carbonates (Fig. 6.3.9). Most of the area was covered with sediments and some patches with bacterial mats were found (Fig. 6.3.10). Push coring with the ROV revealed sub-surface carbonates and rising gas bubbles from the methane-charged sediments. During the subsequent ROV dives 108 and 109 the bacterial mat patches were found and sampled with push cores and landers (see chapters 6.4 and 6.5).

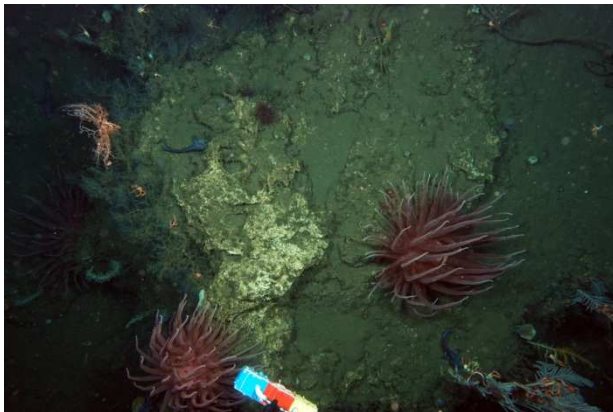


Fig. 6.3.9: A small ridge with carbonates, Box 2.



Fig. 6.3.10: Patches with bacterial mats.

Box 1 was selected as the sidescan sonar mosaic showed areas of high backscatter intensity that are several hundreds of meters in diameter with highly irregular outlines and forming elongate ridges or domes (Klaucke et al., in press). OFOS survey 5 showed massive blocks and pavement of authigenic carbonate in the areas of increased backscatter activity. In the cracks of carbonate small patches of clams, bacterial mats and large clusters of Siboglinid tubeworms of the genus *Lamellibrachia* were found (Fig. 6.3.11). On the southernmost summit in this box large numbers of ray egg cases were discovered (Fig. 6.3.12). This box was investigated in great detail by 4 subsequent ROV dives.



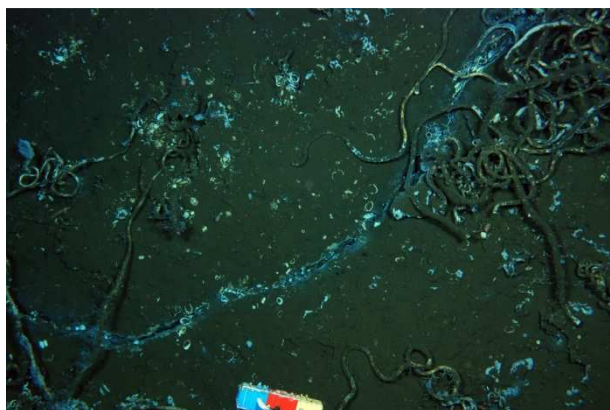


Fig. 6.3.11: Cracks in the carbonate with manifestations of fluid seepage, Box 1.



Fig. 6.3.12: Large number of ray egg cases.

During the first ROV dive (21ROV-1) the observations with OFOS were confirmed and investigated in greater detail (Fig. 6.3.13). Towards the end of the dive the remains of a whale fall were discovered (Fig. 6.3.14). Parts of the skeleton were sampled for microbial and biomarker studies (see chapter 6.9). During the other 3 ROV dives carbonates were sampled by a chain saw and fauna for biological investigations.



Fig. 6.3.13: Typical cold seep community in Box 1



Fig. 6.3.14: Remains of a whale fall.

Box 4 was selected as Agassiz trawls and the analysis of water samples from CTD casts during the INSPIRE cruise with RV MELVILLE in March 2010 revealed indications for active methane discharge (A. Thurber, pers. com.). OFOS track 6 confirmed this by the observation of large fields of clam shells and patches with bacterial mats on top of the small ridge. Closer inspection of one extended clam field revealed dead vesicomyid clams on top of sediments with high sulfide concentrations (see chapter 6.10). During 3 subsequent ROV dives these fields and patches were sampled in great detail. During dive 113 (88ROV-9) inspection of the surface morphology and fauna of the hill-top showed a characteristic sequence of plate-like depressions and lifted rims. Along and on top of these rims, we discovered rather long crevasses and small scarps in the sediment, indicating recent deformation of the seafloor (Fig. 6.3.15). On one of these small ridges we found single spots densely covered by Pogonophora (Fig. 6.3.16), completing our collection of characteristic seep communities.



Fig. 6.3.15: Crevasses in the sediment, Box 4.



Fig. 6.3.16: Sampling of Pogonophora.

The last OFOS survey (11) was conducted along a profile on the accretionary wedge. Gravity core sampling here had resulted in interesting geochemical anomalies of the pore water. The pore water profiles of the sediments of the accretionary wedge had shown enhanced concentrations of elements such as chlorine and bromide. These possibly result from alteration of volcanic ashes in the deep sediment whereby large amounts of pore water are integrated into freshly generated minerals which normally behave conservatively i.e. they are not part of any geochemical or biological processes in the sediment. However, during the OFOS survey no visible manifestation for this anomaly was found.

ROV dive 110 (74ROV-6) was conducted in Box 8 which was selected as PARASOUND images obtained during this cruise hint to the presence of a mud diapir. The dive showed several areas with small carbonate pebbles and bacterial mats which might indicate an early stage of carbonate precipitation (Fig. 6.3.17). These sites were sampled by push corers and nets (Fig. 6.3.18).



Fig. 6.3.17: Seep site with small carbonate pebbles and bacterial mats, Box 8.



Fig. 6.3.18: Sampling of a seep by push corer.

The last ROV dive (118ROV-13) was conducted in the El Quisco seep area. This area has soft sediment and some small patches of bacteria mats indicative for the presence of methane in the sediment. During the dive the deployment site of the Profiler Lander was visited, which had been deployed in the immediate vicinity of the bacterial mats (see chapter 5.5). Large swarms of shrimps and squids followed the lights of the ROV during the dive. Pockmark-like



depressions were seen in the scanning sonar and inspected on the gently dipping slope (Fig. 6.3.19) but no visible and clear sign of fluid or gas seepage was found (Fig. 6.3.20).



Fig. 6.3.19: Pockmark like depression in the El Quisco seep area.



Fig. 6.3.20: Possible bacterial mat and large number of shrimps.

## 6.4 ROV Deployment and Sampling

(P. Linke)

In total, the ROV conducted 13 scientific dives (Table 6.4.1), 12 of which were generally shallower than 1000 m. The ROV reached a bottom time of almost 80 hours, which in relation to the total dive time of approx. 100 hours is a rate of more than 78% bottom time. The maximum diving depth was 5988m in the trench off the Chilean slope.

Table 6.4.1: Summary of ROV dives during cruise SO210.

Station No. SO210	Dive No.	Date	Time Start (UTC)	At Bottom (UTC)	Off Bottom (UTC)	Time End (surface) (UTC)	ROV Bottom Time	% Bottom Time	Location
		25.9.2010							Harbour Test Valparaiso
21ROV-1	105	3.10.2010	17:00	17:30	22:56	23:14	05:26	87.17	CSMA Box 1
25ROV-2	106	4.10.2010	14:21	15:03	21:04	21:39	06:01	82.42	CSMA Box 4
30ROV-3	107	5.10.2010	12:45	13:23	19:23	19:54	06:00	83.92	CSMA Box 1
37ROV-4	108	6.10.2010	14:52	15:21	22:44	23:10	07:23	88.96	CMSA Box 2
42ROV-5	109	7.10.2010	13:00	13:26	20:08	20:48	06:42	85.90	CMSA Box 2
74ROV-6	110	17.10.2010	15:54	16:28	21:29	22:05	05:01	81.13	CMSA Box 8
78ROV-7	111	18.10.2010	12:14	12:45	20:51	21:49	08:06	84.52	CSMA Box 1
84ROV-8	112	19.10.2010	15:39	16:04	20:47	21:26	04:43	81.56	CSMA Box 4
88ROV-9	113	20.10.2010	13:57	15:05	22:01	22:48	06:56	78.34	CSMA Box 4
95ROV-10	114	22.10.2010	12:56	13:27	22:01	22:31	08:34	89.39	CSMA Box 1
98ROV-11	115	23.10.2010	11:40	12:17	22:24	23:15	10:07	87.34	CSMA Box 3
112ROV-12	116	26.10.2010	11:27	14:44	14:52	17:15	00:08	2.30	Trench
118ROV-13	117	27.10.2010	12:13	12:34	17:15	17:44	04:41	84.89	El Quisco
Total: 13 scientific dives							<b>79:48</b>	<b>78.29</b>	



Beside observation and ground-truthing (see chapter 6.3), the ROV was used to obtain distinct samples and deploy instrumentation on the seafloor during these dives. This instrumentation was either on board the vehicle (chapter 5.4) or deployed by the elevator lander (chapter 5.5) in the vicinity of the seep site.

The 2<sup>nd</sup> ROV dive aimed towards an area (Box 4) with extended clam fields and bacterial mats, which were sampled with push cores for microbiological and geochemical analyses (Fig. 6.4.1). Living specimens of vesicomyid clams were recovered with a net (Fig. 6.4.2).



Fig. 6.4.1: Push core recovery.

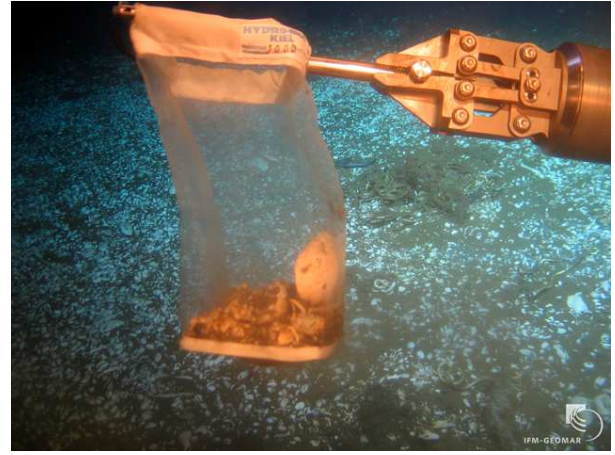


Fig. 6.4.2: Recovery of clams.

The 3<sup>rd</sup> dive was conducted in the working area of the first dive (Box 1) and was dedicated to the sampling of authigenic carbonates. For this purpose the ROV was equipped with a hydraulic chain saw which was used with the ORION manipulator (see chapter 5.4). The ROV was positioned in front of a carbonate block, its side above a crevasse was covered by white bacteria. The first sawing attempts under water were set in full length (Fig. 6.4.3) showing the methodological potential and the ability of the several components. Even horizontal cuts were performed by the well-coordinated ROV pilots. The following cut was made to obtain a smaller sample segment at the front of the carbonate block. Finally, the sample had to be retrieved from the block by using a chisel. During this manoeuvre, the hydraulics of the 2<sup>nd</sup> manipulator, the Riggmaster, here used to keep the ROV away from the rock, failed and we had to abandon the dive.



Fig. 6.4.3: Sampling of carbonates with the hydraulic chain saw by the ORION manipulator.



Fig. 6.4.4: View on the carbonate block with the missing sample section, Box 1.

However, on ROV dive 111 and 114 we returned to this working area. After carefully choosing the cutting level, this new in-situ tool was able to show its capabilities and several pieces of carbonates were retrieved (Figs. 6.4.5 a-d). Even the sample we were not able to retrieve during the first use of the chain saw, due to a failure of the hydraulics, could be retrieved now (Fig. 6.4.4).

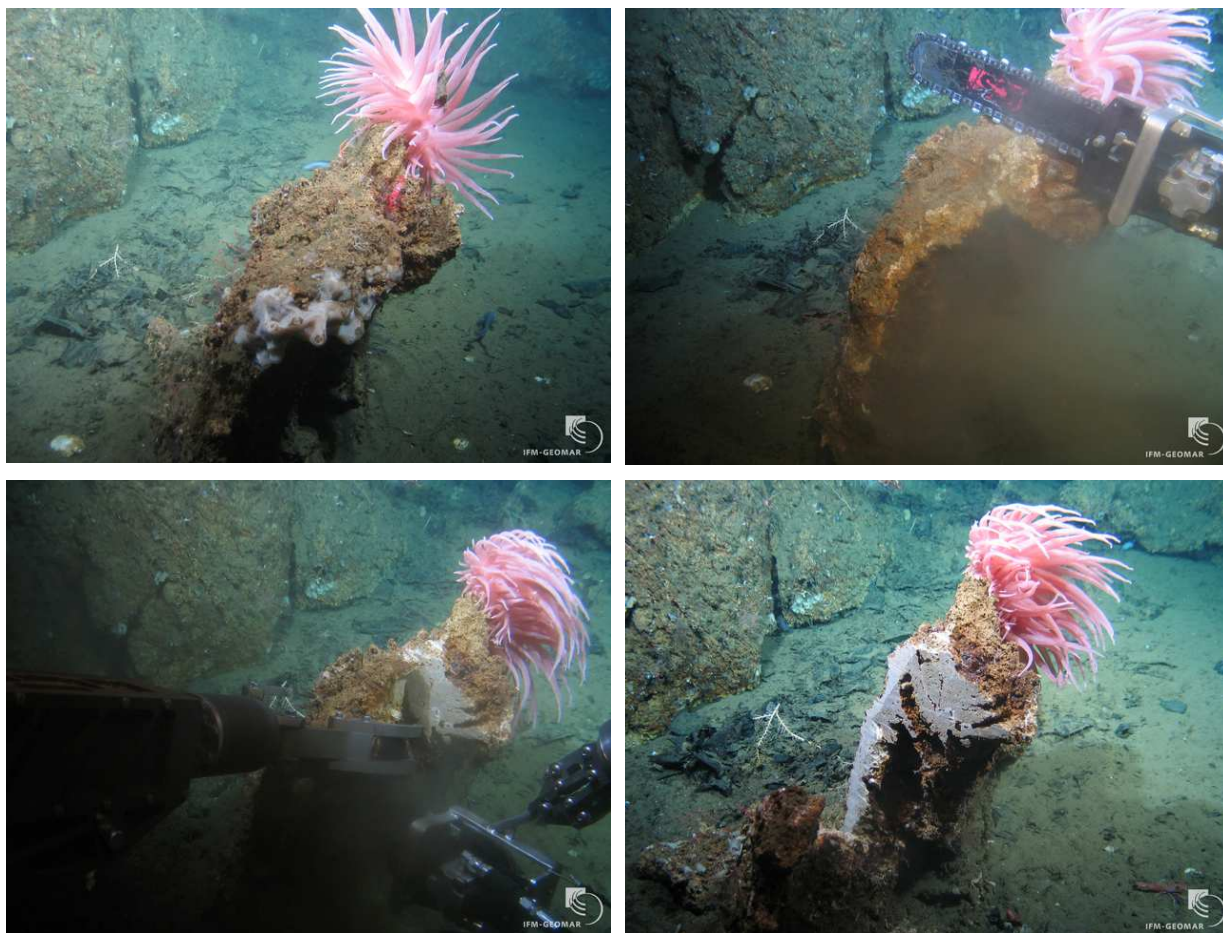


Fig. 6.4.5 a: Vertically oriented carbonate block with an epifaunal anemone; b: first cut of the chain saw; c: „co-operation“ of the two manipulators for recovery of samples; d: the vertical cutting face with visible fine-structure of carbonate precipitation (Box 1).

In summary, the work-class ROV proved to be the ideal tool for the sampling of carbonates by diamond chain saw from massive build-ups, breaking single heavy fragments, picking-up fragile biological substrates (e.g. cold water coral, clam shells, tube worms). This accompanied by well positioned bottom water sampling, combined with CTD monitoring enables unique and well targeted investigation of lateral and surface penetrating profiles across large scale cold seep structures.

On cruise SO210 four different work areas were addressed by this technique (see appendix IV) and supported by TVG based sampling (chapter 6.6) of oversized single blocks for detailed local depth profiles.

In areas with sediments, e.g. Box 2 and 4, the ROV was deployed in combination with the elevator lander. In Box 2 the elevator carried the pore water sampler (PWS) and 2 Eddy Correlation (EC) modules which were deployed by the ROV (dive 108) on bacterial mats or in their vicinity and recovered during the subsequent dive (Fig. 6.4.6 a-d).



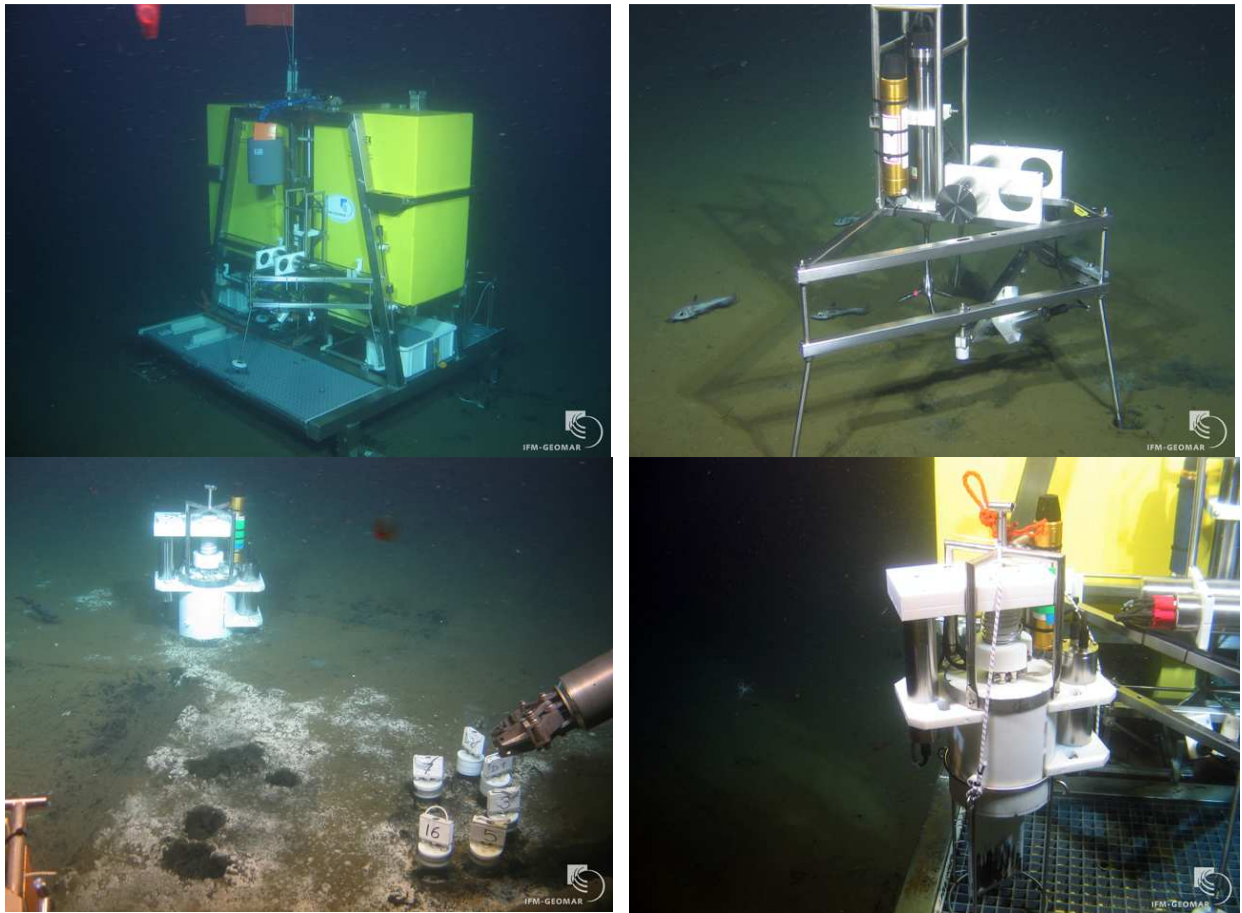


Fig. 6.4.6 a: Deployment of ROV modules by the elevator in Box 2; b: EC module deployed on soft sediment next to bacterial mats; c: PWS and push cores deployed in bacterial mats; d: recovery of the PWS on the elevator.

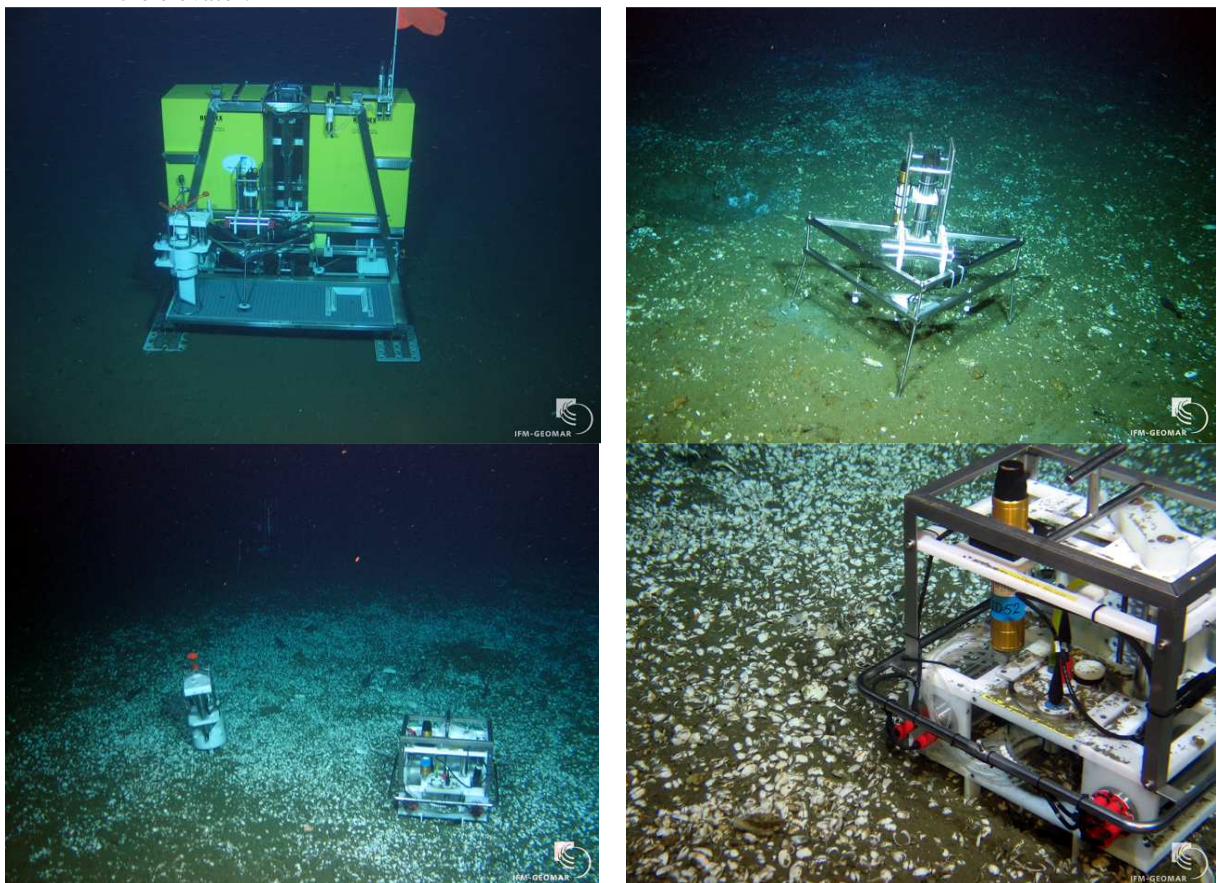


Fig. 6.4.7 a: Deployment of the elevator in Box 4; b: EC module at the fringe of the large clam field; c: PWS and benthic chamber in the clam field, EC visible in the upper part; d: close-up of the BC.

In Box 4 the elevator carried additionally a benthic chamber (BC) which was deployed together with the PWS and the two EC modules in and around a large clam field (Fig. 6.4.7 a-d) which had been discovered during the 2<sup>nd</sup> ROV dive. All modules were successfully retrieved on the subsequent dive and after recovery of the elevator.

## 6.5 Lander Deployments

(S. Sommer, P. Linke, L. Rovelli, L. Bryant, S. Cherednichenko, M. Türk, S. Kriwanek).

The area around CMSA was extendedly covered with carbonate crusts that did not allow an intense lander sampling programme (Table 6.5.1). Therefore, our work focused on Box 2 characterized with sediments that were covered with small-sized bacterial mats and CMSA Box 4 where a dead clam bed has been discovered during leg 1. At El Quisco a third profiler deployment was conducted at a site which was reported as a seep site (Thurber pers. comm.). In this region we found small patches of bacterial mats and placed the profiler next to them.

Table 6.5.1: List of lander deployments

Gear	Date	Location/Habitat	Parameter
Profiler #1, Stat. 58	14.10.2010	CMSA Box 2, Seep bacterial mat	O <sub>2</sub> , S, current, CTD, image
BIGO #1, Stat. 75	17.10.2010	CMSA Box 2, close to bact. mat	Geochem, CH <sub>4</sub> , O <sub>2</sub>
Profiler #2, Stat. 79	18.10.2010	CMSA Box 2, reference	O <sub>2</sub> , S, current, CTD, image
ROV #9, Stat. 88	20.10.2010	CMSA Box 4, clam bed (dead)	Geochem, CH <sub>4</sub> , O <sub>2</sub>
MUC #5, Stat. 91	21.10.2010	CMSA Box 2, close to bact.mat	Geochem, CH <sub>4</sub> , pH
Profiler #3, Stat. 109	25.10.2010	El Quisco, close to seep	O <sub>2</sub> , S, current, CTD, image

During the transecting micro-profiler deployment #1 bottom water time series of O<sub>2</sub> and temperature indicated periodic O<sub>2</sub> fluctuations that apparently were related to tidal forcing (Fig. 6.5.1).

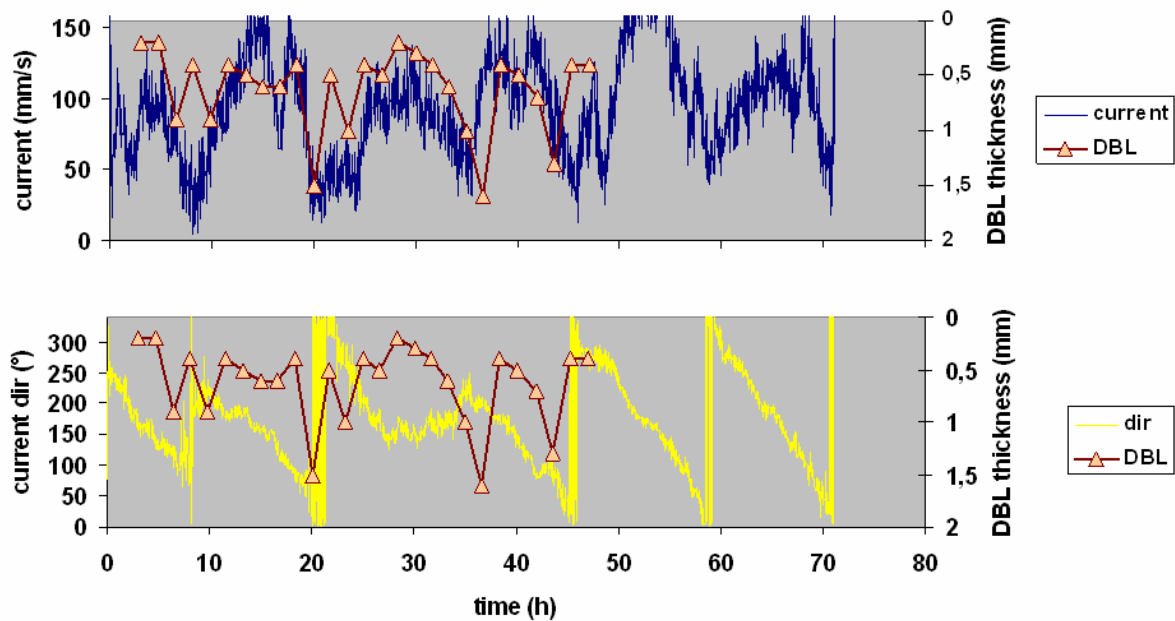


Fig. 6.5.1: Upper panel: Temporal variability of the current magnitude that was measured in ~ 9 cm above the sea floor (bin 6) plotted in relation to the thickness of the diffusive boundary layer. Lower panel: Direction of the current plotted in relation to the thickness of the diffusive boundary layer.

During each profiler deployment #1 and #2 a total of 54 O<sub>2</sub>- and 27 sulfide profiles were obtained. The distance between each successive profile along the x-axis was 16 mm. Vertical resolution was 100  $\mu$ m and maximum profile depth 24 mm. Unfortunately the pH sensor failed during these deployments. A typical example of a sulfide and oxygen gradient within the bacterial mat is depicted in Figure 6.5.2. Oxygen penetration depth was about 2.3 mm. The depth distribution of oxygen and sulfide was separated by a ~ 10 mm thick suboxic zone.

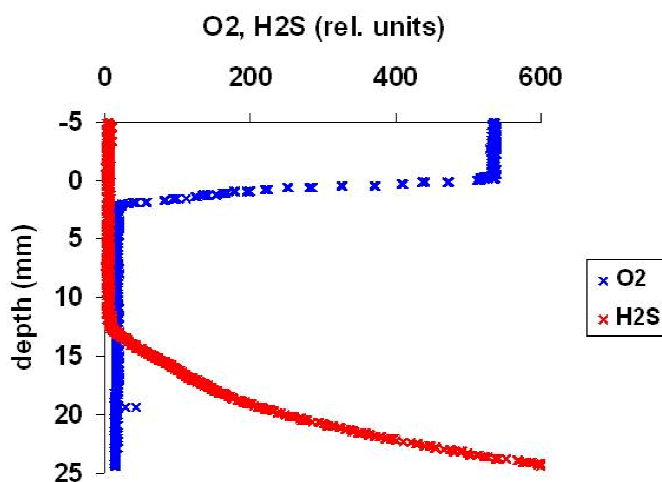


Fig. 6.5.2: Micro-gradients (profile #14) of oxygen and sulfide measured during Profiler deployment #1 at a methane seep site in CMSA BOX 2 covered with bacterial mats. Depth within the sediment is indicated in positive numbers, negative figures indicate vertical distance in the bottom water. The position of the sediment water interface was deduced from the change in the slope of the O<sub>2</sub>-gradient that occurs when moving through the water column into the sediment.

Solutes that were taken up or are released from the sediment must pass the diffusive boundary layer, DBL, which covers the sediment as a thin carpet. Within this layer transport is mediated via molecular diffusion rather than via turbulent advection which proceed much faster. Hence, a thick DBL can impede benthic material turnover even if organic carbon is not limiting. The thickness of the DBL is related to the current strength as is indicated in Figure 6.5.1. Hence, shifts in the current regime will have strong effects on the benthic turnover as well as on release and uptake of solutes.

Future activities will include analyses of the methane fluxes as well as post processing of the profiler data. This post processing comprises calculation of diffusive oxygen uptake rates and sulfide fluxes at methane seep sites in contrast to nearby reference sediments.

During the cruise four Eddy Correlation (EC) module deployments were carried out. Due to not suitable sea conditions on the first leg, the EC module deployment in Box 2 (Fig. 5.5.5) was interrupted prematurely, although 22 hrs of consecutive measurements were collected before the ROV safely placed the devices on the elevator. On the second leg the deployment lasted for slightly more than two days in Box 4. From the four EC module deployments only one was subject to severe electrical noise and a sensor malfunction leading to an overall deployment failure, i.e. no usable data. All other deployments were successful and the preliminary results are very promising. Figure 6.5.3 provides an overview of the dissolved oxygen fluxes from the Oxygen/Temperature EC system, as deployed during the first leg in Box 2. The average dissolved oxygen fluxes were  $-1.8 \pm 1.4 \text{ mmol m}^{-2} \text{ d}^{-1}$  on average although fluxes up to  $7 \text{ mmol m}^{-2} \text{ d}^{-1}$  were measured.

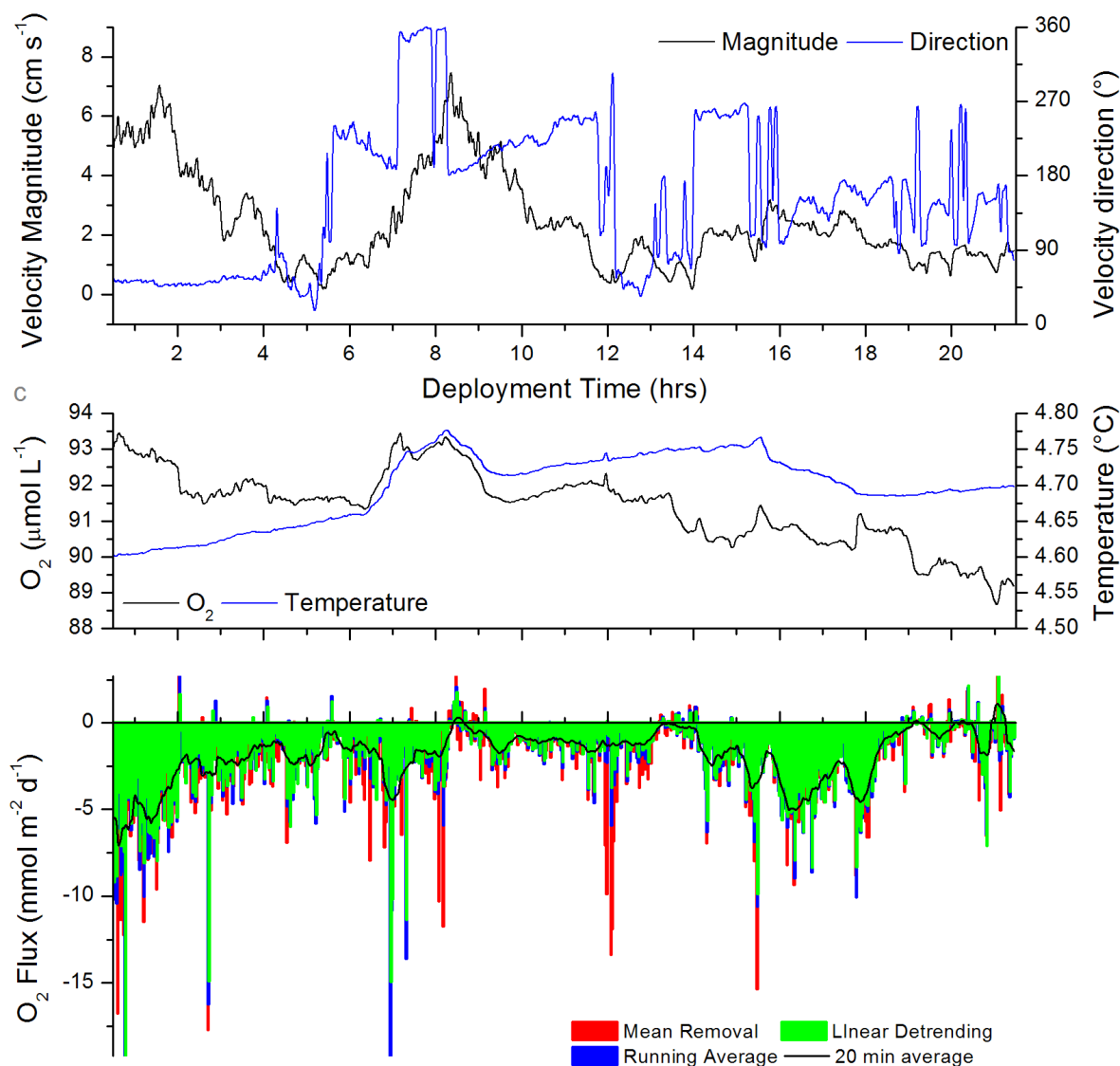


Fig.6.5.3: Overview of the Oxygen/Temperature EC system data. Top panel: water current velocity magnitude and direction as measured from the ADV. Center panel: dissolved oxygen and temperature time series. Bottom panel: Dissolved oxygen fluxes calculated by using different methods over a 2 min window size. The black line the fluxes over a 20 min average.



Future processing of the collected data involves the correction of the oxygen reading according to other in-situ oxygen measurements such as from optodes to obtain more robust fluxes, and the processing of the high resolution temperature to resolve heat fluxes. Furthermore, the EC data will be coupled with the water column measurements (CTD and MSS) to better understand the oxygen dynamics in the studied area.

## 6.6 TV-Grab Deployments

(V. Liebetrau)

During the cruise six TVG deployments were conducted and resulted in 4 samples (Tab. 6.6.1) of different size from 3 locations, CMSA Box 3 (2 sites) and CMSA Box 1 (1 site).

Table 6.6.1: TVG sampling.

Station	TVG_no	area	Lat. "S"	Long. "W"	Depth	figure no. & remarks
24	1	CMSA Box 1				not successful
31	2	CMSA Box 1	36°25.108	73°42.188	638	no sample retrieved
63	3	CMSA Box 3	35°58.549	73°38.410	1026	massive carbonate block, 2 buckets mud (no spec. fig.)
64	4	CMSA Box 3	35°58.558	73°38.388	1022	1a & b, largest block recovered on cruise including solitary cold water coral ( <i>Bathycyathus chilensis</i> )
69	5	CMSA Box 1	36°25.117	73°42.180	670	2a & b, 1 large block from NW-base of NW-top, cold water corals ( <i>Caryophyllia huinayensis</i> ) on top and in downside niches, disrupted contact to 2nd medium size carbonate block visible, additional fragments with thin white layers
70	6	CMSA Box 1	36°25.457	73°41.975	678	no chance for TVG, massive carbonate

The most promising and impressive sample (Fig. 6.6.1a) represents a large block retrieved in CMSA Box 3 from a water depth of 1022 m. It reflects the dominating type of calcification with a network of thin white layers within a calcified sediment matrix and porous surface structures. The latter is often combined with high tube worm abundances.



Fig. 6.6.1a & b: Large authigenic cold seep carbonate block from 1022 m depth in CMSA Box 3 (approx. 140 x 70 x 80 cm, TVG-4). The red-brownish colored part was visible on top of the sediments and the greyish part was within the sediment partly connected to deeper carbonate structures (visible at freshly broken surfaces of the bottom side). The big white scratch is just a trace of a grab claw. Living cold-water corals are visible in the upper left and in the center as red and a white dot, respectively (b: picture width approx. 12 cm).



Fig. 6.6.2a & b: Authigenic cold seep carbonate block from 670 m depth in CMSA Box 1 incl. living cold-water coral *Caryophyllia huinayensis* recovered with TVG-5 (b: picture width approx. 1 cm).

Due to the spread of the two major sampling sites on different depth levels, a comparison and reconstruction of cold vent activity for potentially different geological settings seems achievable and is one aim of the on-going isotope geochemical investigation.

Additionally, cold-water corals were recovered as an important archive of chemical changes in the bottom water (Fig. 6.6.1b and 6.6.2b).

## 6.7 Sediment Sampling and Sedimentology

(S. Kutterolf, D. Völker)

Sediment sampling and sediment description was aimed at two goals, (a) the description of volcanic ash layers from eruptive volcanic centres of the Southern Volcanic Zone (SVZ) of the Andes that were either deposited as fallout onto the oceanic Nazca Plate or, alternatively, were transported down the slope and across the Chile Trench in large mass transport processes and (b) the description and dating of previously mapped submarine landslides as well as retrieval of slide-related material for geo-technical experiments.

Eight gravity cores (Annex III, List of core stations) of 12 m length (GC1-GC4, GC6, GC7, GC15, GC16) were retrieved seaward of the Chile Channel on the outer rise of the Nazca Plate. The distance from the trench and the relative elevation were chosen to minimize the influence of turbiditic trench sedimentation at the sites. In total we found 34 horizons in 7 cores that exhibit ash layers, ash pods or pod layers. Only in GC2 we did not recover any tephra. 22 of those 34 horizons mark distinct ash layers that have whitish to black colors. This is also reflected by the transparent through brownish and dark brown glass shards that presumably represent the whole range of magmatic compositions from basalt to rhyolite. Most of the layers have sharp basal contacts to the underlying sediment but erosional contacts or diffuse transitions into the overlying sediment.

In the northern working area (33-36°S), we found a very prominent, normal graded ash layer (GC1-664-670 cm) that has mineral and lithic fragments enriched at the base. Transparent glass shards are highly vesicular. The occurrence of lithic fragments at the base of the ash layer, next to mineral enrichment, at a distance of probably more than 200 km away from the source and against the prevailing wind directions, is unusual and will be investigated in detail. First results on major element compositions of glass shards suggest this ash layer correlates to

the Diamante Tuff erupted from the Diamante Caldera, which today hosts the Maipo volcano (Fig. 6.7.1). Since the Diamante ignimbrite is widely distributed in the Central Valley of Chile between Santiago and Rancagua, we assume transport by a density current down the continental slope, across the trench and onto the incoming plate seems a plausible scenario for emplacement of the ash layer.

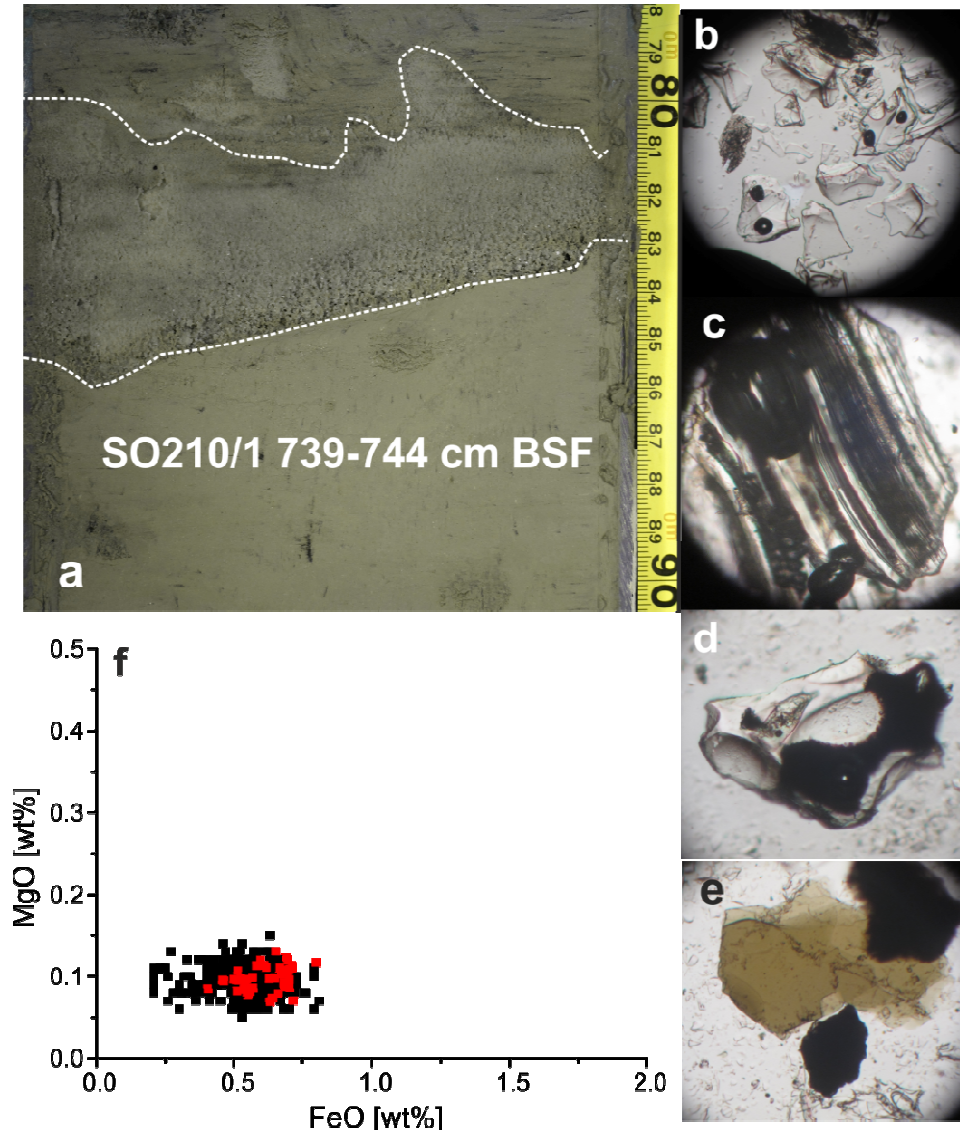


Fig. 6.7-1: 4cm thick, normal graded, ash layer with biotite and lithic components enriched at the base (a); typical transparent glass shards (b); tubular glass shard with elongated vesicles (c); glass shard showing structures of round vesicle remnants (d); biotite (e); (f) MgO versus FeO plot of glass shards from Diamante Ignimbrite on land (black) and SO210/1 739-744 cm (red).

A black tephra layer found in cores GC15 and GC16 is cross-bedded and was thus emplaced by flow processes rather than simple fallout. In both cores (GC15/746-765 cm; GC16/786-799cm) the tephra layer is overall normally graded but consists of three units: a massive basal unit overlain by a parallel and cross stratified middle unit that is followed by a massive or planar stratified unit of very fine ash mixed with hemipelagic sediment (Fig. 6.7.2). Further investigations will clarify the apparently variable emplacement processes of these marine tephra layers and their source.

Ten gravity cores (Annex III, List of core stations) of 3 to 6 m barrel length were collected on the continental slope at mass-wasting sites (GC5, GC9, GC11, GC12, GC14, GC25-28,



GC30). The sites were chosen to sample reference cores upslope of slides, the glide plane and redeposited material downslope of the slide evacuation area. This strategy aimed at (1) determining the general nature and rheology of the background sediments as well as sedimentation rates, (2) determining the nature of the glide plane (potential “weak layer”) and (3) dating the transition of slide deposits to post-slide sedimentation. In general, the sampling of such locations is critical, as it involves a combination of old and redeposited or exposed and lithified material, steep slopes ( $>10^\circ$ ) and/or blocky surfaces which explains the high number of four attempts that either failed or gained very short cores.

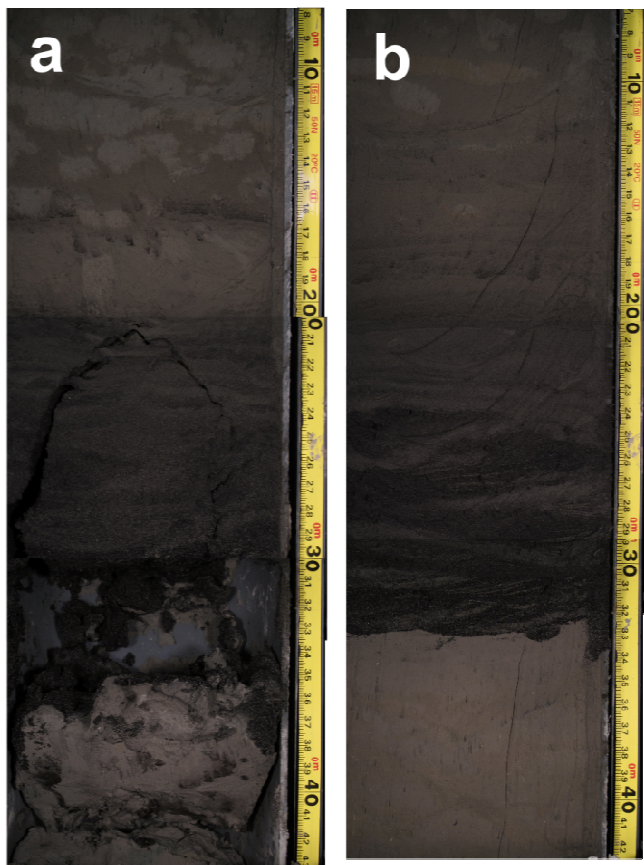


Fig. 6.7-2: Mafic marine ash layers showing distinct internal structures. (a) GC15/746-765 cm; (b) GC16/786-799cm.

We were successful at the BioBio Slide, where a very young small-scale slide deposit is observed in the central depression of an older, larger slide plane (core GC11). Multiple sliding is evident in a core from an elevated bank within the BioBio Canyon (GC14). At Reloca Slide and Valdes Slide, material for geo-technical tests was retrieved which will complement cores retrieved during RRS James Cook cruise JC23b. We refrained from taking samples at Taza Slide, as Parasound Data clearly showed that this feature is buried beneath a post-slide hemipelagic sediment unit too thick to be penetrated by our 6m barrel. We also tried to sample a bank within San Antonio Canyon for remains of canyon wall collapse material (GC30), similar to GC14 in the BioBio Canyon. Here, however, the little retrieved material consisted of chiseled, angular metamorphic hard rock gravel, thus showing that presently no sediments are deposited here.

## 6.8 Zoological Studies

(F. Valdés)

### Sampling

A diverse set of biological samples has been obtained. We recovered 79 different taxa; the taxonomic composition and details of the sampling station are compiled in Annex III.

Two taxa appear to be species new to science: the gastropod Provannidae defined as *Provanna* sp., and the bivalve Mytilidae of the genus *Adipicola*. *Provanna* sp. was collected from a block of carbonate, recovered by the ROV in Box 4 from 775 m water depth (Fig. 6.8.1). *Adipicola* was collected at Box 4, but unfortunately only articulated valves. This is the first record of a chemosymbiotic mytilid in the SE Pacific off Chile (Fig. 6.8.2).

Six live specimens of the giant clam *Archivesica* sp. were collected in Box 3, this material is crucial for future taxonomic classification (Fig. 6.8.3).



Fig. 6.8.1: Gastropod *Provanna* sp., some individuals were collected at station 25, Box 4, during ROV-2, Bar = 0.5 cm.



Fig. 6.8.2: Probably mytilid of the genus *Adipicola*. The animal was collected in Box 4, in the soft sediments near *Calymene gallardoi*.



Fig. 6.8.3: Vesicomylid clam *Archivesica* sp. collected in Box 3. Bar = 2 cm.

In addition, six live specimens of the siboglinid tubeworm *Lamellibrachia* sp. were collected. The collection made by the ROV allowed to obtain complete individuals, including the caudal region or opisthosome. This segment is crucial for the taxonomic characterisation (Fig. 6.8.4).





Fig. 6.8.4: Siboglinid tubeworm of the genus *Lamellibrachia* sp. (A) vestimentum, (B) opisthosome, (C) calcareous tube of body. Bar = 3 cm.

It has not been possible to establish the taxonomic status of several species collected. The samples were stored at the Laboratory of Subtidal Benthic Ecosystems (ECOBENS) of the Universidad Católica del Norte. Some examples of the collected fauna are shown in figures 6.8.5 to 6.8.10.



Fig. 6.8.5: Colony of *Clavularia magelhanica*, the colony is attached to the tube of the polychaete *Eunices* sp. Bar = 2 cm.

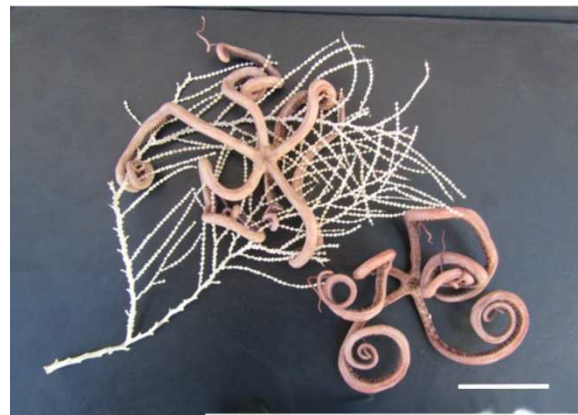


Fig. 6.8.6: The ophiuroid *Astrodia tenuispina* in the cold water coral *Callogorgia* sp. Bar = 5 cm.



Fig. 6.8.7: The ophiuroid *Ophiocantha antarctica*. The samples were collected from the TV-Grab at station 64, Box 4. Bar = 2 cm.



Fig. 6.8.8: The sea star *Pteraster gibber*. The samples were collected during ROV-9, station 88, Box 4. Bar = 2 cm.



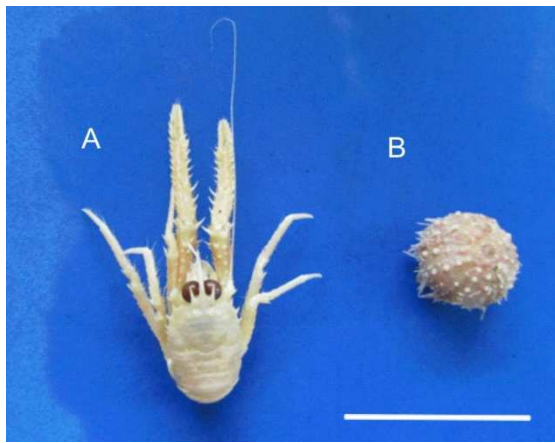


Fig. 6.8.9: (A) *Munida propinqua* and (B) *Sterechinus* cf. *meumayeri*. The samples were collected during TV-Grab-5, station 69, Box 1. Bar = 3 cm.

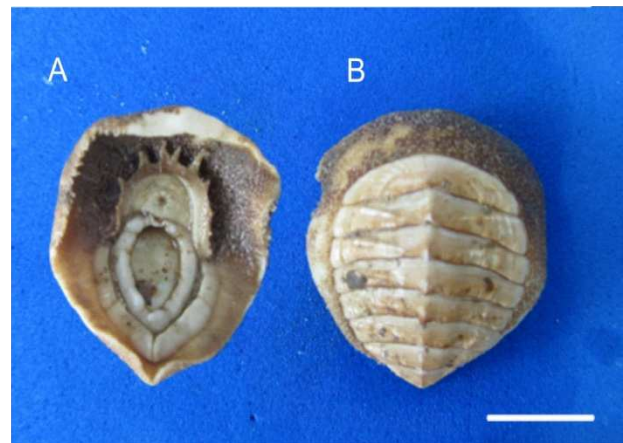


Fig. 6.8.10: *Leptochiton americanus*. (A) ventral view, (B) dorsal view. The samples were collected during ROV-10, station 95, Box 1. Bar = 1 cm.

The meiofaunal biological samples were stored in the ECOBENS laboratory, from a total of seven stations. The details of the sampling of the meiofauna and the stations are compiled in Annex III.

#### Observation

The detailed visual observation of the CMSA was performed for the first time during the cruise SO210 by using the OFOS (Ocean Floor Observation System) and the ROV (remotely operated vehicle) Kiel 6000. Both instruments belong to the Leibniz Institute of Marine Sciences (IFM-GEOMAR) in Kiel, Germany.

Different transects were made, the beginning of each transect, as well as the location and type of instrument used is described in Annex III.

According to the video surveys, an enhanced diversity is observed at the sites where methane is seeping, probably associated to the spatial heterogeneity generated by carbonate crusts.

#### Chemosymbiotic fauna

Siboglinid tubeworms of the genus *Lamellibrachia* were distributed in small and large aggregations (Fig. 6.8.11). They were often attached to carbonate crusts at sites where seepage is active. These bushes are used as a substrate for sessile species and as refuge by some mobile species, which in turn serve as food for larger organisms. Among the most abundant sessile taxa observed were cnidarians, sponges and bryozoans among others. Bushes of living tubeworms were abundant at the CMSA sites (Box 2 and Box 4) and a new seep located 26 miles south of the CMSA (Box 3).

Patches of clams and bacterial mats (Fig. 6.8.12) also suggest an enhanced chemosynthetic activity in the area. Most abundant clam species identified in the videos were *Calymene gallardoi* and *Archivesica* sp. Another abundant bivalve is *Thyasira methanophila*, whose distribution seems not to be obligate to seep sites, since Thyasirids as well as Lucinids seem to be facultative. Another bivalve, apparently a mytilid of the genus *Adipicola* was collected at Box 4, but unfortunately only articulated valves. This is the first record of a chemosymbiotic mytilid for the SE Pacific off Chile. Different areas covered by patches of white bacteria belonging to the genus *Beggiatoa*, Pogonophoran tubeworms, Vesicomylid clams belonging to species *Calymene gallardoi* and *Archivesica* sp.; also siboglonid polychaetes of the genus

*Lamellibrachia* sp. are indicators of chemosynthetic activity. The coverage of these taxa will identify areas where seepage is more active.



Fig. 6.8.11: Living Siboglinid tubeworms of the genus *Lamellibrachia* sp. from CMSA, the ensemble is formed by several individuals. Picture was obtained at station 84, ROV-8, Box 4.



Fig. 6.8.12: Cluster of living clams of the species *Archivesica* sp., the animals live in soft sediments. Picture was taken during station 98, ROV- 11, Box 3.

#### *Non chemosymbiotic fauna*

The faunal assemblage of the CMSA is diverse, and comprises a large proportion of species that are new to science (Sellanes *et al.*, 2008). Spatial heterogeneity at seep sites promotes a great biological diversity (Levin, 2005).

At the CMSA at least 10 species of cold water coral species have been reported, with *Callogorgia* sp., *Paragorgia* sp., *Swiffia* sp., *Touarella* sp and *Antipathes speciosa* being the most abundant. Corals in turn provide habitat for other species of ophiuroids, actinians, bryozoans and crustaceans. The ophiuroids *Astrothoma agassizi*, *Gorgonocephalus chilensis*, *Astrodia* sp., *Ophiomusium biporicum*, *Ophiacantha antarctica*, and five other species are the most abundant. The galatheid *Munidopsis trifida* dominates among the decapod crustaceans, which prefer the black coral *Antipathes speciosa* (Fig. 6.8.13).

Most abundant among the gastropods were *Bathybembix macdonaldi*, *B. humboltii*, *Margarites huloti*, *Zetela alphonsi*, *Calliostoma chilena*, *C. crustulum*, *Fusitriton magellanicus*, *Trophon ceciliae*, *T. condei*, *Miomelon alarconi* among others. The giant Humboldt squid *Dosidiscus gigas* is also abundant and has been often seen in several videos preying on fish and crustaceans. Among bivalves, *Ennucula grayi*, *Limopsis ruizana*, and *Acesta patagonica* are the most often seen species at the CMSA.

Among the several species of polychaetes collected, *Eunice* sp. was dominant at the CMSA. Several individuals were collected attached to the carbonates obtained by the ROV and the TV-Grab. Different species of decapods of the family Galatheidae (genus *Munidopsis* and *Munida*) were observed with the ROV and OFOS. Identification at the species level is still pending.

Within the crevices of the carbonates lithodid crabs of the genus *Paralomis* were also observed. Main species of echinoids observed at the CMSA were *Dermechinus horridus*, *Sterechinus* sp. and *Cidaridites* sp. while *D. horridus* and *Cidaridites* sp. have an aggregated patchy distribution (Fig. 6.8.14), *Sterechinus* sp. is more sparsely distributed over the carbonates and also over black corals. Swarms of pelagic holothuroids of the genus *Enypniastes* were also

often seen (Fig. 6.8.15). The most prevalent fish in the CMSA correspond to *Coelorinchus fasciatus*, *C. chilensis* and *Coryphaenoides ariommus* species, also different Squalidae and more other fish species that occupy the tubes of *Lamellibrachia* sp. as a hideout.

Over soft substrates where no seep activity is observed biological diversity and abundance of the fauna is diminished. Dominant species is the polychaete *Hyalinoecia* sp. which is sparsely distributed over the substrate. Other abundant taxa are the ophiuroid *Stegophiura* sp. and three other species, the asteroids *Hippasteria hyadesi*, *Solaster regularis* and *Luidia magellanica*. The solenocerid shrimp *Haliporoides diomedeeae* is quite abundant.

Further detailed analysis of the video footage as well as the still images obtained during the SO210 cruise will certainly help to improve our understanding of the ecology, diversity and biogeography of the seep habitats at the SE Pacific.



Fig. 6.8.13: The cold water coral *Antipathes speciosa*, and the little crustacean *Munidopsis trifida*. Picture was obtained during station 21, Box 1.

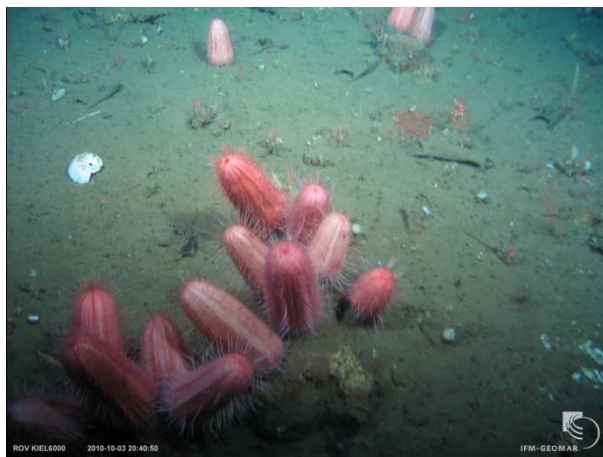


Fig. 6.8.14: Clusters of the echinoid *Dermechinus horridus* in a patchy distribution. Picture was taken during station 21, ROV- 1, Box 1.

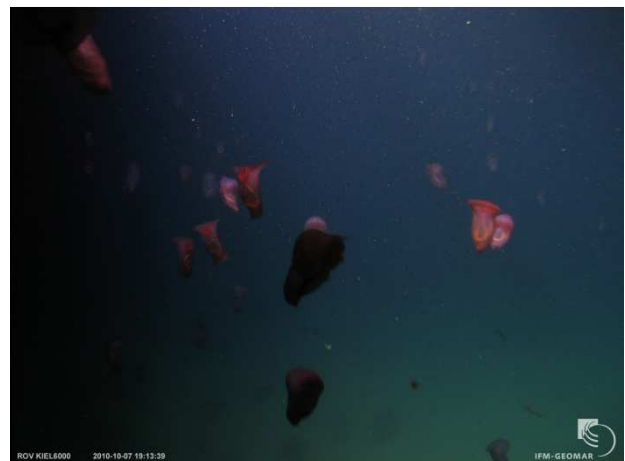


Fig. 6.8.15: The benthopelagic holothurian *Eunipniastes* sp. uses the water column for displacement. The picture was taken during station 42, ROV- 5, Box 2.



## 6.9 Microbiological Studies

(T. Treude)

We detected and sampled active chemosynthetic communities in CMSA Box 2-4 and at Mound Felix. Whereas in Box 2 chemosynthetic communities were found on extended sediment areas, they occurred within rather localized sediment islands embedded in carbonate outcrops in Box 3, 4, and at Mound Felix. Box 2 was dominated by patchy black sediment spots or bacterial mats (Fig. 6.9.1). Even "normal" appearing sediment with an oxidized brown sediment coverage featured a reduced sulfidic layer underneath, suggesting that the seepage area must be much larger than visible from the top. Besides bacterial mats (most likely *Beggiatoa* Sp.) we found living specimens of the clam *Thyasira* Sp. (Fig. 6.9.2) inside the sediment (at depths between 5 and 9 cm) as well as indications for the presence of the giant sulfur bacteria *Thioploca* Sp. (sheaths retrieved). In the Box 3 area, seepage appeared much localized. We discovered a small but diverse chemosynthetic community at the bottom of a hill. Two seepage openings (through carbonate rock) inside the sediment were found surrounded by tubeworms, bacterial mats as well as large dead and living clams (*Archivesica* Sp.). The sediment in each area (Fig. 6.9.1) and some specimens of the clam *Archivesica* Sp. (Fig. 6.9.2) were sampled for analyses. In Box 4, a large dead (but very sulfidic) clam field as well as patches of Pogonophorans (Fig. 6.9.2) were sampled. On Mound Felix, the sediments were covered by small (4-6 cm diameter) carbonate nodules. Here, two sites dominated by either clams or bacterial mat were sampled (Fig. 6.9.1).

Table 6.9.1 Overview of stations, sample type (sediment or carbonates), and use (analyses) of samples.

Station	CMSA-BOX	Sample type	Rates	CARD-FISH, RNA/DNA	Biomarker	Cooled (alive) samples	Flow-through cores
16, MUC-1	2	beside black spot - sediment	x	x	x	x	x
21, ROV-1	1	whale fall - bones and sediment	x	x	x	x	-
25, ROV-2	4	dead clam field - sediment	x	x	x	x	x
42, ROV-5	2	bacterial mat - sediment	x	x	x	x	x
52, MUC-2	2	reference - sediment	x	x	x	x	x
64, TV-Grap-4	4	carbonates	-	x	x	x	-
66, MUC-3	4	dead clam field - sediment	x	x	x	x	x
68, MUC-4	Reference	"outside seep" reference - sediment	x	x	x	x	x
69, TV-Grap-5	1	carbonates	-	-	x	-	-
74, ROV-6	Mound Felix	carbonate-rich bacterial mat and clam field	x	x	x	x	x
78, ROV-7	1	carbonates	-	-	x	-	-
82, BIGO-1	2	beside bacterial mat - sediment	x	-	-	-	-
84, ROV-8	4	carbonates	-	-	x	-	-
88, ROV-9	4	pogonophoran field- sediment	x	x	x	x	x
95, ROV-10	1	carbonates	-	-	x	-	-
98, ROV-11	3	bacterial mat, tubeworm, clams - sediment	x	x	x	x	x



Fig. 6.9.1: Examples of sediment cores that were retrieved and analyzed for microbiological studies. Station numbers are given.

Beside sediments we sub-sampled carbonates (mainly for biomarker analyses) that were retrieved from Box 1 and 4.

In Box 1 an old whale fall was discovered on top of a carbonate hill (probably an extinct cold seep site, Fig. 6.9.3). The skeleton was very porous and showed no signs of chemosynthetic activity. It was surrounded by a few clam shells; however, it was impossible to identify whether the clams used to be associated to the whale fall or to former seepage activity. We sampled two whale vertebrae (Fig. 6.9.3) as well as some sediment from around the whale fall for analyses. The sediment coverage was very thin. After just a few centimeters, pushcores could not penetrate deeper, probably due to a solid carbonate plate situated underneath.



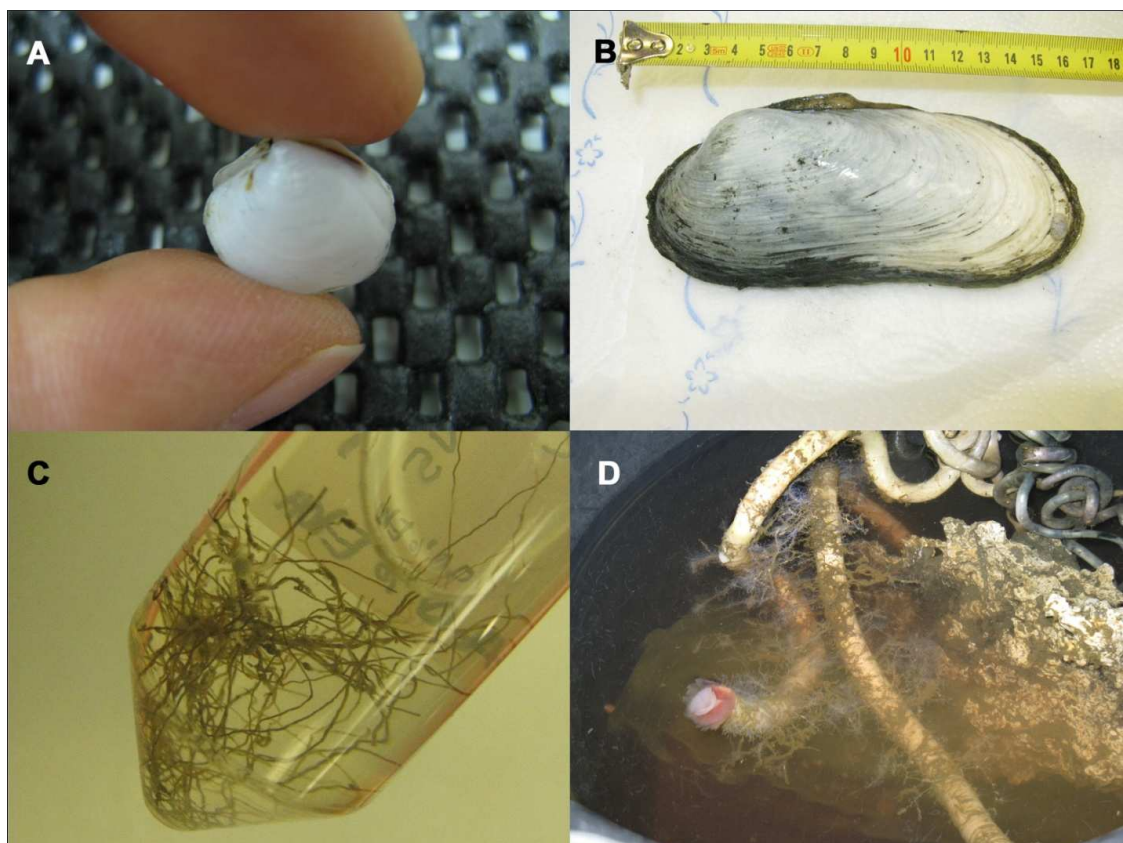


Fig. 6.9.2: Examples of chemosynthetic organisms collected during the cruise: (A) the clam *Thyasira* Sp., (B) the clam *Archivesica* Sp., (C) pogonophorans, (D) tubeworms on carbonate nodules.

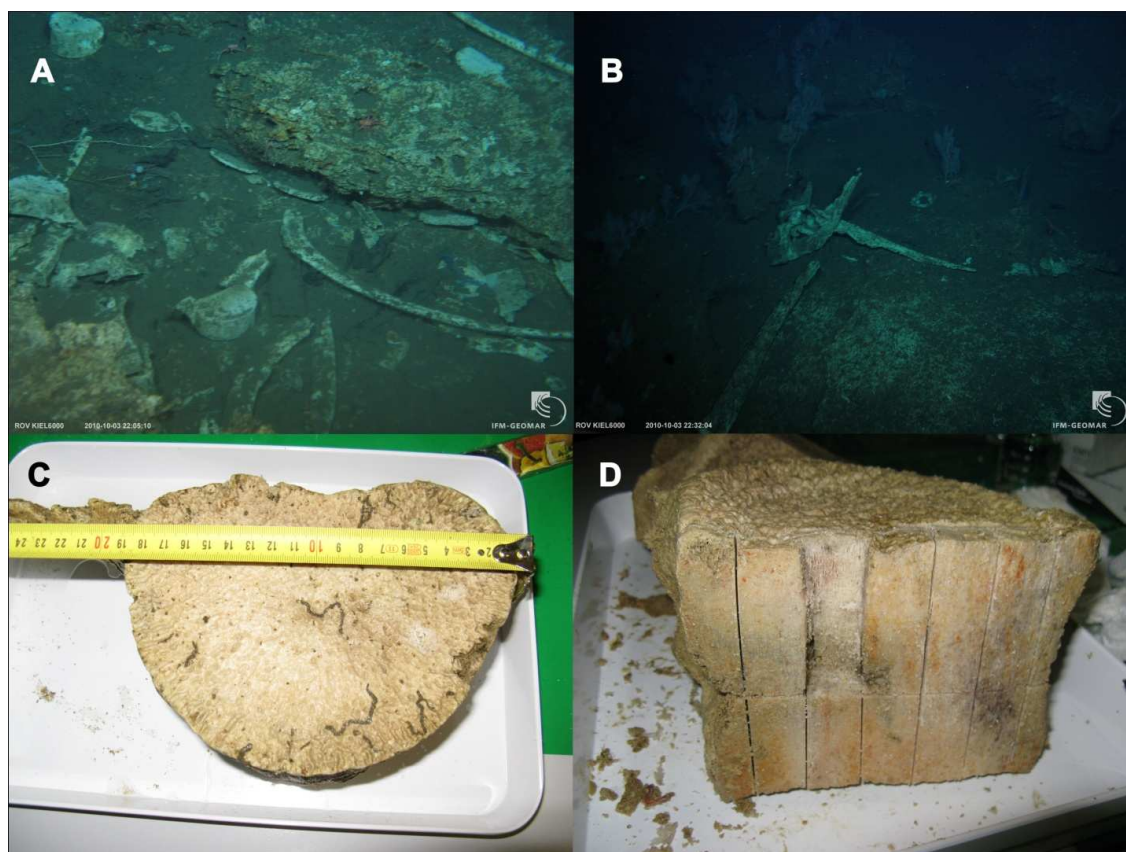


Fig. 6.9.3: Whale fall discovered in Box 1: (A) and (B) skeleton on the seafloor, (C) and (D) one of the two vertebrae that were retrieved and sub-sampled for microbiological studies.



## **6.10 Pore Water Geochemistry**

(F. Scholz, B. Domeyer, R. Surberg, U. Lomnitz)

The pore water geochemistry group participated in essentially all research activities during the cruise SO210 resulting in a total number of 19 GCs, 12 PCs and 12 MUCs (Table 6.10.1). Coring locations were selected according to the results of previous surveys using Side Scan Sonar, Parasound, Multibeam bathymetry or a deep-towed camera sled (OFOS). Furthermore, 1 benthic chamber, the samples of 2 in situ pore water sampler deployments and 1 Biogeochemical Observatory (BIGO) were analyzed for their pore water chemistry. The results for the different working areas will be discussed on the basis of appropriate examples in the following sections.

Table 6.10.1: Stations which were processed by the pore water geochemistry group during SO210.

#	Station	Device		Longitude	Latitude	Water depth	Region/	Sample	
				(dec deg)	(dec deg)	(m)	purpose	#	
1	01	GC	01	-73.571	-33.200	3785	Oceanic plate	18	
2	05	GC	04	-74.667	-35.167	4306	Oceanic plate	19	
3	12	GC	06	-74.705	-35.833	4387	Oceanic plate	21	
4	13	GC	07	-75.167	-36.500	4043	Oceanic plate	20	
5	16	MUC	01	-73.679	-36.471	700	Cold seep, CMSA	15	
6	25	ROV	02	PC02	-73.711	-36.383	680	Cold seep, CMSA	10
7	25	ROV	02	PC05	-73.712	-36.381	682	Cold seep, CMSA	8
8	25	ROV	02	PC16	-73.713	-36.381	681	Cold seep, CMSA	8
9	29	GC	08	-73.678	-36.471	707	Cold seep, CMSA	14	
10	35	GC	10	-73.734	-36.471	1008	Reference site	14	
11	37	ROV	04	PC03	-73.669	-36.473	688	Cold seep, CMSA	9
12	39-1	GC	11	-73.717	-36.607	1448	BioBio Slide	10	
13	41	GC	13	-73.711	-36.383	697	Cold seep, CMSA	7	
14	42	ROV	05	PC05	-73.679	-36.471	707	Cold seep, CMSA	9
15	42	ROV	05	PWS01	-73.679	-36.471	707	Cold seep, CMSA	10
16	43	GC	14	-73.763	-36.634	1824	BioBio Canyon	18	
17	44	GC	15	-75.512	-38.128	3950	Oceanic plate	18	
18	45	GC	16	-75.417	-37.271	4213	Oceanic plate	18	
19	54	MUC	02	-73.679	-36.470	707	Cold seep, CMSA	12	
20	55	GC	17	-73.540	-35.904	1417	Cold seep, CMSA	15	
21	60	GC	18	-73.721	-36.364	859	Cold seep, CMSA	14	
22	61	GC	19	-73.623	-36.188	716	Cold seep, CMSA	14	
23	66	MUC	03	-73.713	-36.381	679	Cold seep, CMSA	12	
24	68	MUC	04	-73.735	-36.471	1006	Reference site	15	
25	72	GC	20	-74.053	-36.343	3544	Accretionary wedge	14	
26	74	ROV	06	PC05	-73.691	-36.443	699	Mound Felix	9
27	74	ROV	06	PC12	-73.690	-36.443	697	Mound Felix	8
28	75	BIGO	01	-73.678	-36.470	700	Cold seep, CMSA	36	
29	80	GC	21	-73.999	-36.347	3192	Accretionary wedge	13	
30	81	GC	22	-74.053	-36.343	3491	Accretionary wedge	14	
31	88	ROV	09	PC01	-73.710	-36.381	685	Cold seep, CMSA	8
32	88	ROV	09	BC01	-73.712	-36.381	688	Cold seep, CMSA	11
33	88	ROV	09	PWS02	-73.712	-36.381	688	Cold seep, CMSA	10
34	91	MUC	05	-73.679	-36.470	705	Cold seep, CMSA	13	
35	96	GC	23	-73.869	-36.366	2199	Accretionary wedge	14	
36	97	GC	24	-74.107	-36.337	3842	Accretionary wedge	14	
37	98	ROV	11	PC05	-73.632	-35.986	1008	Cold seep, CMSA	7
38	98	ROV	11	PC13	-73.632	-35.986	1009	Cold seep, CMSA	6
39	98	ROV	11	PC16	-73.632	-35.986	1008	Cold seep, CMSA	6
40	104	MUC	06	-71.880	-33.390	334	El Quisco/OMZ	12	
41	107	MUC	07	-71.780	-33.391	120	El Quisco/OMZ	17	
42	113-2	MUC	09	-71.867	-33.390	235	El Quisco/OMZ	11	
43	119	MUC	10	-71.897	-33.390	438	El Quisco/OMZ	16	
44	121	MUC	11	-71.921	-33.390	599	El Quisco/OMZ	16	
45	124	MUC	12	-71.850	-33.390	165	El Quisco/OMZ	14	
46	125	MUC	13	-71.903	-33.390	485	El Quisco/OMZ	14	

CMSA Concepcion methane seepage area  
 OMZ Oxygen minimum zone at 33°23.385'S  
 GC Gravity core  
 MUC Multiple corer (video guided)  
 ROV Remotely operated vehicle

### *Ash alteration and early diagenesis on the incoming plate*

GCs (12 m) from the incoming Nazca Plate were retrieved in order to evaluate the geochemical composition of sediments and pore fluids prior to subduction. An example for a core from the incoming plate is shown in Figure 6.10.1. Deep-sea sediments on the incoming plate contain little organic matter, thus hosting a rather sluggish microbial activity. This is reflected in the small decrease of dissolved  $\text{SO}_4^{2-}$  from seawater-like concentrations at the top to 23.1 mM over the entire core length of almost 10 m. Three distinct ash layers were observed in the core, each with a thickness of several centimeters. The presence of ash layers is accompanied by significant deflections in the pore water profiles of alkalinity,  $\text{NH}_4^+$ ,  $\text{PO}_4^{3-}$  and, to a lesser extent, silica. For alkalinity and silica the deflections might be directly related to the production of  $\text{HCO}_3^-$  and the release of silica during the alteration of volcanic ashes to clay minerals (e.g. smectite). Ion exchange processes and desorption could account for the peaks in  $\text{NH}_4^+$  and  $\text{PO}_4^{3-}$ . Some of the cores on the incoming plate did not display any pore water anomalies, although they contained ash layers of comparable thickness. This could be related to the age, and thus reactivity, of the ash layers. Determination of the age and provenance of the ash will help to solve this question.

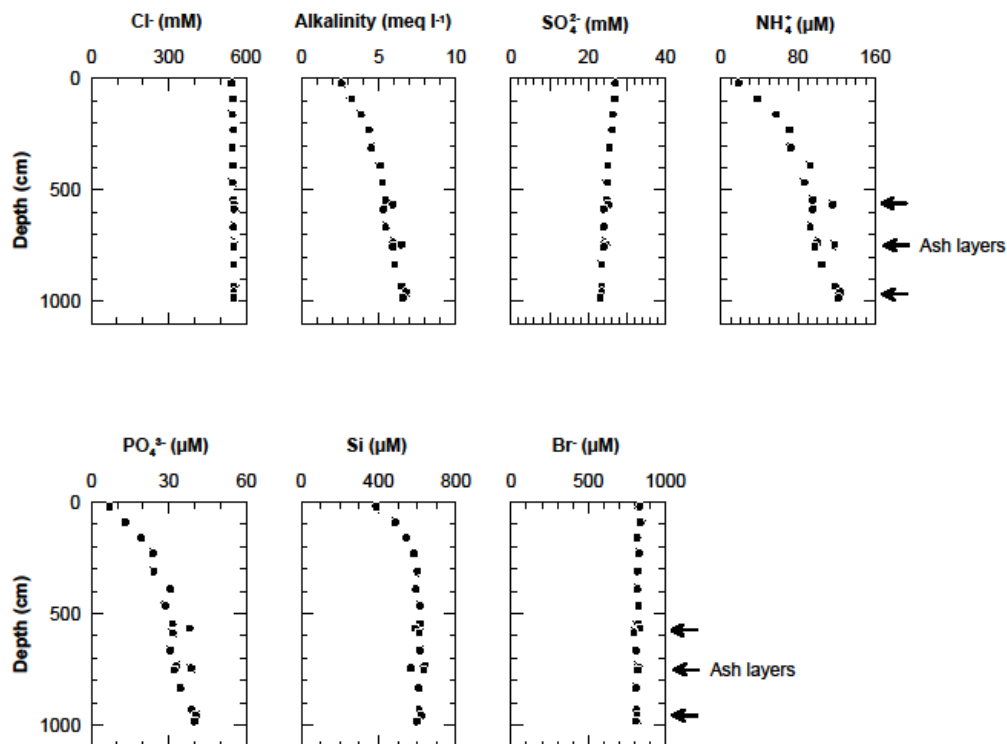


Fig. 6.10 1: Pore water profiles of chloride, alkalinity,  $\text{SO}_4^{2-}$ ,  $\text{NH}_4^+$ ,  $\text{PO}_4^{3-}$ , silica and bromide for 01-GC01 from the incoming place (3785 m WD).

### *Pore water geochemistry of sediments in Concepcion Methane Seepage Area*

Previous findings from Side Scan Sonar surveys indicated the presence of authigenic carbonates related to methane seepage at water depths around 700 m in the in the Concepcion Methane Seepage Area (CMSA). This could be confirmed by the aid of video-guided seafloor surveys (ROV, OFOS). The apparently most active sites (i.e. presence of bacterial mats, clams and tube worms) were sampled using ROV-guided PCs and 3 to 6 m long GCs. Examples for short and long sediment cores from the CMSA are given in Figure 6.10.2 and 6.10.3. The red lines represent the pore water profiles of reference cores that were retrieved away from the

seep site. The cold seep cores display a comparably shallow zone of sulfate depletion (<1 m and <10 cm as opposed to 4.5 m in the reference core) which is likely the result of anaerobic methane oxidation. During this microbially mediated process, the reduction of seawater sulfate is coupled to the oxidation of methane derived from deeper sediment strata.

The concentration of chloride in pore water is a meaningful parameter for the detection of subduction-related diagenetic processes such as the large-scale alteration of volcanic ashes ( $\text{Cl} > \text{seawater}$ ) or clay mineral dehydration ( $\text{Cl} < \text{seawater}$ ) in the subsurface. However, 60-GC18, 42-ROV05-PC05 (Fig. 6.10.2 and 6.10.3) and all other sediment cores from the CMSA display seawater-like chlorinity profiles throughout the sampled depth intervals. It is therefore preliminarily concluded, that the CMSA does not possess a hydrological connection to the deep subsurface. Accordingly, the methane which is transported upwards in this area should have a comparably shallow and biogenic origin. This will be further investigated by means of carbon isotope analyses.

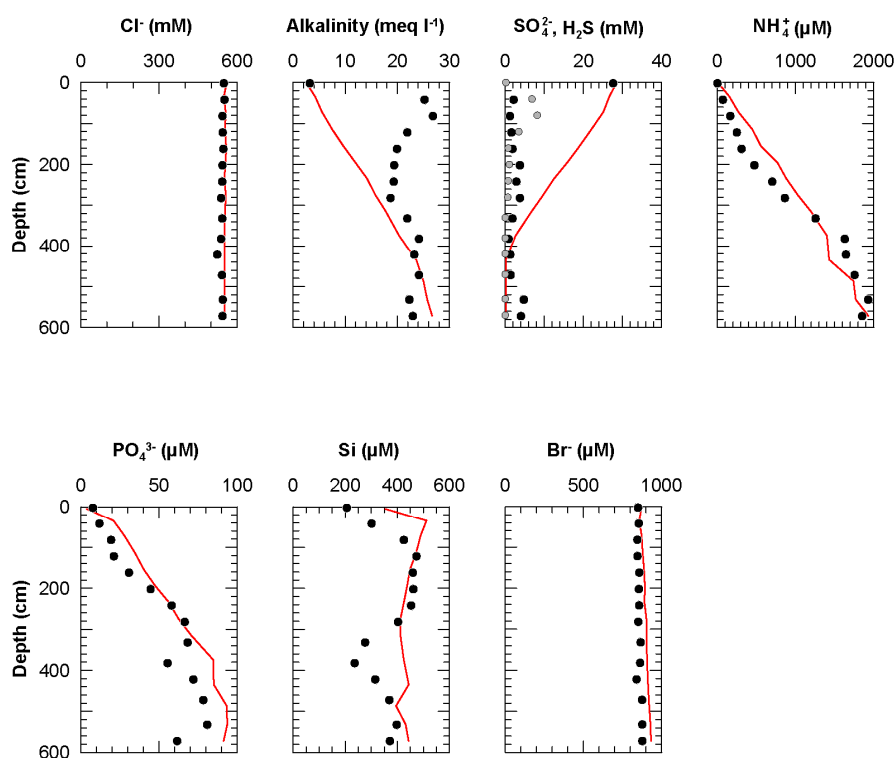


Fig. 6.10.2: Pore water profiles of chloride, alkalinity,  $\text{SO}_4^{2-}$  (black circle),  $\text{H}_2\text{S}$  (gray circle),  $\text{NH}_4^+$ ,  $\text{PO}_4^{3-}$ , silica and bromide for 60-GC18 from the Concepcion Methane Seepage Area (859 m WD). The red lines represent a reference core (35-GC10) which was retrieved close by and which is not influenced by methane seepage.

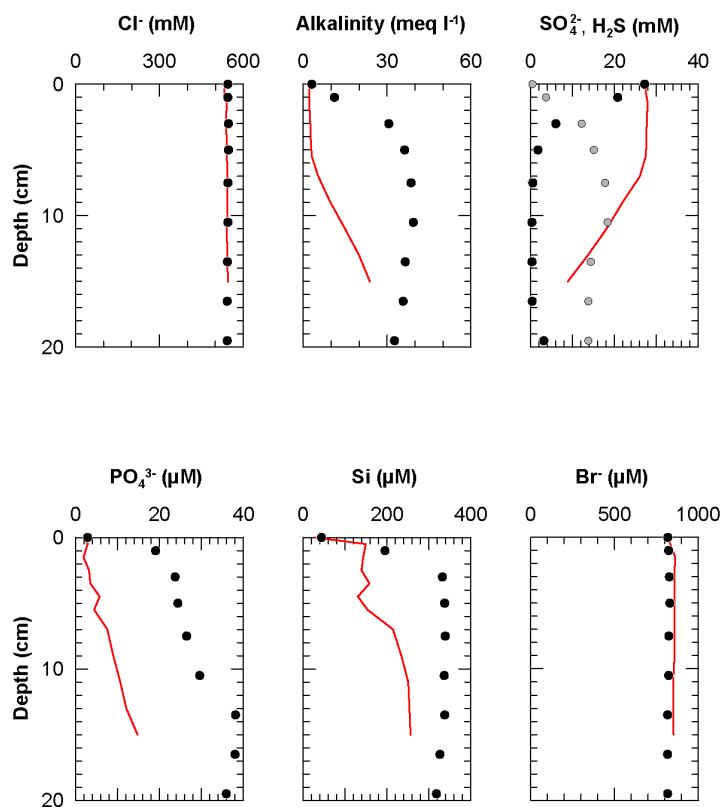
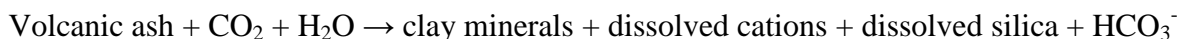


Fig. 6.10.3: Pore water profiles of chloride, alkalinity,  $\text{SO}_4^{2-}$  (black circle),  $\text{H}_2\text{S}$  (gray circle),  $\text{PO}_4^{3-}$ , Si and Br for 42-ROV05-PC05 from the Concepcion Methane Seepage Area (707 m WD). The red lines represent a reference core (54-MUC02) which was retrieved close by and which is not influenced by methane seepage.

#### *Pore water geochemistry of sediments on the accretionary prism*

Figure 6.10.4 shows pore water profiles of alkalinity, chloride and bromide for 2 GCs from the central accretionary prism. Both cores show downcore increasing concentrations of chloride and bromide, two parameters that behave largely conservative in shallow diagenetic environments (i.e. up to several meters depth). Moreover, the pore water profiles increase almost linearly with depth suggesting the presence of a deep-seated diagenetic process beyond the sampled depth interval. Possible mechanisms leading to an enrichment of chloride and bromide in pore water are the consumption of water through ash diagenesis or the addition of evaporated seawater (i.e. a primary brine) (Martin et al., 1995). The presence of primary brines has, to our knowledge, not been reported for sediments at the SE Pacific margins. The hypothesis of ash diagenesis, however, is further supported by the alkalinity profile of 81-GC21. The alkalinity in this core increases beyond the maximum value that may be produced through bacterial sulfate reduction ( $\sim > 60 \text{ meq l}^{-1}$ ). In a simplified manner, alteration of volcanic ash in a seawater environment may be expressed by the following equation:



It implies that ash is altered to clay minerals (mainly smectite), which is accompanied by the consumption of water and the conversion of  $\text{CO}_2$  to bicarbonate. These processes are clearly reflected in the pore water profiles 81-GC21 shown in Figure 6.10.4.



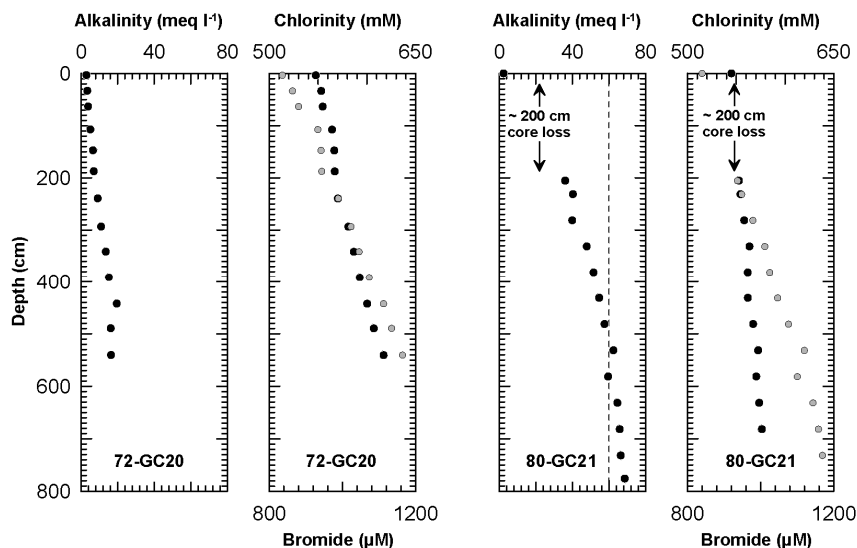


Fig. 6.10.4: Pore water profiles of alkalinity, chloride (black circle) and bromide (gray circle) for 72-GC20 and 80-GC21. The dashed line in the alkalinity profile of 80-GC21 represents the maximum value that may be produced through bacterial sulfate reduction.

#### *Pore water geochemistry of sediments from the Bio Bio Slide*

Bio Bio Slide is a landslide of unknown age located close to the submarine canyon of the Bio Bio river. One core from the glide plane has been subjected to pore water geochemical analyses. The resulting alkalinity profile is compared with a reference profile, corresponding to undisturbed sediments, in Figure 6.10.5. At the glide plane, two similar alkalinity profiles seem to be shifted above each other. This is also obvious from the core description revealing two light brown mud layers, one on top of the core and one at 96 to 99 cm depth. These superimposed sediment layers are most likely the result of a recent slide event. If the event had occurred longer time ago, the steep concentration-depth gradient at the transition would be equilibrated by molecular diffusion. This process and its effect on the pore water profile is indicated by the red line and black arrows in Figure 6.10.5. A possible trigger mechanism for the mass wasting event could be the February 27<sup>th</sup> 2010 earthquake whose epicenter was located close by.

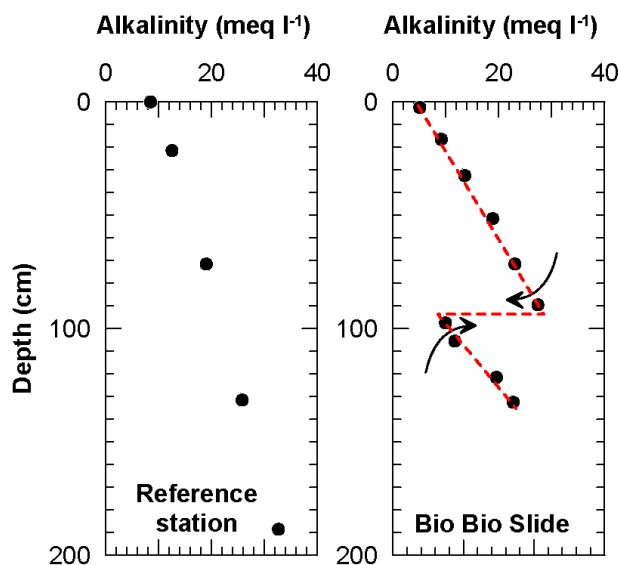


Fig. 6.10.5: Alkalinity profiles for 96-GC23 (2199 m WD) from a reference station and 39-1-GC11 (1448 m WD) from the glide plane of the Bio Bio Slide. See text for further explanation.

## 7 Acknowledgements

In the name of all cruise participants, we would like to thank Captain Lutz Mallon and his entire crew for the pleasant and professional co-operation and their support during the cruise. Erna Lange, Christine Utecht and the members of the Technology and Logistics Center at IFM-GEOMAR are acknowledged for their logistic support. Cruise SO210 with RV SONNE to the active continental margin off Chile was conducted by ship time exchange with RV METEOR. Funds for mobilizing the research team were provided by the German Science Foundation (DFG) in conjunction with the Collaborative Research Centre (SFB) 574 of the University of Kiel.

## 8 Data and Sample Storage and Availability

The raw data acquired during cruise SO210 were archived allowing for an immediate exchange of the data within the project group. Subsequent results may be added in the same context avoiding redundant metadata input. CTD data of the cruise are already uploaded to the server at IFM-GEOMAR (<https://portal.ifm-geomar.de>). DSHIP data of this cruise are available at the BSH (<http://dship.bsh.de>). The sample material will be stored in the IFM-GEOMAR Lithothek.

The metadata is already publicly accessible immediately. The associated scientific data will be made public in 2013. Published data and data out of moratorium will be submitted to World Data Centers (WDC) such as PANGAEA. The IFM-GEOMAR/University Kiel data management team will take care of the data transfers to long-term archives in order to ensure the data availability worldwide and for the far future.

## 9 References

- Angermann, D., J. Klotz, and C. Reigber (1999), Space-geodetic estimation of the Nazca-South America Euler vector, *Earth and Planetary Science Letters*, 171(3), 329-334.
- Bangs, N. L., and S. C. Cande (1997), Episodic development of a convergent margin inferred from structures and processes along the southern Chile margin, *Tectonics*, 16(3), 489-503.
- Berg, P., and M. Huettel (2008). Monitoring the seafloor using the noninvasive eddy correlation technique: Integrated benthic exchange dynamics. *Oceanogr.* 21:164-167.
- Berg, P., H. Røy, and P. L. Wiberg (2007). Eddy correlation flux measurements: The sediment surface area that contributes to the flux. *Limnol. Oceanogr.* 52:1672-1684.
- Berg, P., H. Røy, F. Janssen, V. Meyer, B. B. Jørgensen, M. Hüttl, and D. de Beer (2003). Oxygen uptake by aquatic sediments measured with a novel non-invasive eddy-correlation technique. *Mar. Ecol.-Prog. Ser.* 261:75-83.
- Berg, P., R. N. Glud, A. Hume, H. Stahl, K. Oguri, V. Meyer, and H. Kitazato (2009). Eddy correlation measurements of oxygen uptake in deep ocean sediments. *Limnol. Oceanogr. Methods* 7:576-584.
- Brand, A., D. F. McGinnis, B. Wehrli, and A. Wüest (2008). Intermittent oxygen flux from the interior into the bottom boundary of lakes as observed by eddy correlation. *Limnol. Oceanogr.* 53:1997-2006.
- Caress, D.W. and Chayes, D.N. (1996). Improved processing of Hydrosweep DS multibeam data on the R/V Maurice Ewing. *Marine Geophysical Researches*, 18(6): 631-650.
- Coffin, R., Gardner, J., Diaz, J., and Sellanes, J. 2006. Gas Hydrate Exploration, Mid Chilean Coast; Geochemical-Geophysical Survey. NRL/MR/6110-06-9006 Technical report. 61 pp. [Http://handle.dtic.mil/100.2/ADA461588](http://handle.dtic.mil/100.2/ADA461588)
- Diaz-Naveas, J. L. (1999), Sediment subduction and accretion at the Chilean convergent margin between 35° and 40°S, Ph.D. Thesis - University of Kiel, Kiel / Germany.
- Farías, M. et al., 2008. Late Miocene high and rapid surface uplift and its erosional response in the Andes of central Chile (33° - 35°S). *Tectonics*, 27(1): TC1005.

- Geersen, J., Behrmann, J.H., Völker, D., Krastel, S., Ranero, C.R., Diaz-Naveas, J. and Weinrebe, R.W. (2011-A) Active tectonics of the South Chilean marine forearc (35°S – 40°S). *Tectonics* 30, TC 3006.
- Geersen, J., Völker, D., Behrmann, J.H., Reichert, C. and Krastel, S. (2011-B) Pleistocene giant slope failures offshore Arauco Peninsula, Southern Chile. *Journal of the Geological Society* 168, 1237-1248
- Grasshoff K., Erhardt M. and Kremling K. (2002) *Methods of Seawater Analysis*. Wiley-VCH, Weinheim.
- Grevemeyer, I., N. Kaul, J.L. Diaz-Naveas (2006) geothermal evidence for fluid flow through the gas hydrate stability field off Central Chile – transient flow related to large subduction zone earthquakes? *Geophys. J. Int.* 166, 461-468.
- Keir R. S., Schmale O., Walter, M., Sültenfuß J., Seifert R., Rhein M. (2008), Flux and dispersion of gases from the "Drachenschlund" hydrothermal vent at 8°18'S, 13°30'W. *Earth and Planetary Science Letters*, 270: 338-348.
- Klaucke, I., Weinrebe, W., Linke, P., Kläschen, D., Bials, J. (in press): Sidescan sonar imagery of widespread fossil and active cold seeps along the Central Chilean Continental Margin. *Geo-Marine Letters*
- Kukowski, N., and O. Oncken (2006), Subduction Erosion – the "Normal" Mode of Fore-Arc Material Transfer along the Chilean Margin?, in *The Andes – active subduction orogeny*, edited by O. Oncken, G. Chong, G. Franz, P. Giese, H.-J. Götze, V. A. Ramos, M. R. Strecker and P. Wigger, pp. 217-236, Springer, Berlin.
- Kuwaie, T., K. Kamio, T. Inoue, E. Miyoshi, and Y. Uchiyama (2006). Oxygen exchange flux between sediment and water in an intertidal sandflat, measured in situ by the eddy-correlation method. *Mar. Ecol.-Prog. Ser.* 307:59-68.
- Lee, X., W. Massman, and B. Law (2004). *Handbook of Micrometeorology: A Guide for Surface Flux Measurement and Analysis*. Kluwer Academic Publishers.
- Levin L.A. (2005) Ecology of cold seep sediments: interactions of fauna with flow, chemistry and microbes. *Oceanography and Marine Biology Annual Review*, 43, 1–46
- Lomnitz, C. (1970), Major earthquakes and tsunamis in Chile during the period 1535 to 1955, *International Journal of Earth Sciences*, 59(3).
- Lomnitz, C. (2004), Major Earthquakes of Chile: A Historical Survey, 1535-1960, *Seismological Research Letters*, 75(3), 368-378.
- Lorrai, C., D. F. McGinnis, P. Berg, A. Brand, and A. Wüest (2010). Application of oxygen eddy correlation in aquatic systems. *J. Atmos. Oceanic Technol.* 27:1533-1546 [doi:10.1175/2010JTECH0723.1].
- Martin J.B., Kastner M. and Egeberg P.K. (1995) Origins of saline fluids at convergent margins. In: *Union Active margins and marginal basins of the western Pacific*, Geophysical Monograph 88, 219-239. American Geophysical Union.
- McGinnis, D. F., P. Berg, A. Brand, C. Lorrai, T. J. Edmonds, and A. Wüest (2008). Measurements of eddy correlation oxygen fluxes in shallow freshwaters: Towards routine applications and analysis. *Geophys. Res. Lett.* 35:L04403 [doi:10.1029/2007GL032747].
- McGinnis, D.F., S. Cherednichenko, S. Sommer, P. Berg, L. Rovelli, R. Schwarz, R.N. Glud, P. Linke (2011): Simple, robust eddy correlation amplifier for aquatic dissolved oxygen and hydrogen sulfide flux measurements, *Limnology and Oceanography: Methods*, 9 . pp. 340-347. DOI 10.4319/lom.2011.9.340
- Melnick, D., and H. P. Echtler (2006), Inversion of forearc basins in south-central Chile caused by rapid glacial age trench fill, *Geology*, 34(9), 709-712.
- Moreno, M., M. Rosenau, and O. Oncken (2010), 2010 Maule earthquake slip correlates with pre-seismic locking of Andean subduction zone, *Nature*, 467(7312), 198-202.
- Osborn, T. R., 1980. Estimates of the local rate of vertical diffusion from dissipation measurements. *Journal of Physical Oceanography* 10, 83-89.
- Ranero, C. R., R. von Huene, W. Weinrebe, and C. Reichert (2006), Tectonic Processes along the Chile Convergent Margin, in *The Andes – active subduction orogeny*, edited by O. Oncken, G. Chong, G. Franz, P. Giese, H.-J. Götze, V. A. Ramos, M. R. Strecker and P. Wigger, pp. 91-121, Springer, Berlin.
- Sellanes, J. & Krylova, E., 2005. A new species of Calyptogena (Bivalvia: Vesicomysidae) from a recently discovered methane seepage area off Concepción Bay, Chile (~ 36° S). *Journal of the Marine Biological Association of the United Kingdom*, 85: 969 – 976.

- Sellanes, J., Quiroga, E., & Gallardo V.A., 2004. First direct evidences of methane seepage and associated chemosynthetic communities in the bathyal zone off Chile. *Journal of the Marine Biological Association of the United Kingdom*, 84, 1065-1066.
- Sellanes, J., Quiroga, E., y C. Neira, 2008. Megafauna community structure and trophic relationships at the recently discovered Concepción Methane Seep Area, Chile, 36oS. *ICES Journal of Marine Science* 65(7), 1102-1111.
- Tebbens, S. F., and S. C. Cande (1997), Southeast Pacific tectonic evolution from early Oligocene to Present, *Journal of Geophysical Research*, 102(B6), 12061-12084.
- Ussler W., Paull, C. K., Boucher, J., Friederich, G. E., and Thomas, D. J. 2003. Submarine pockmarks: a case study from Belfast Bay, Maine. *Marine Geology*, 202: 175–192.
- Völker, D., M. Wiedicke, S. Ladage, C. Gaedicke, C. Reichert, K. Rauch, W. Kramer, and C. Heubeck (2006), Latitudinal Variation in Sedimentary Processes in the Peru-Chile Trench off Central Chile, in *The Andes – active subduction orogeny*, edited by O. Oncken, G. Chong, G. Franz, P. Giese, H.-J. Götze, V. A. Ramos, M. R. Strecker and P. Wigger, pp. 193-216, Springer, Berlin.
- Wessel, P. and Smith, W.H.F., 1998. New, improved version of the Generic Mapping Tools released. *EOS Trans. AGU*, 79: 579.

## Annex I: List of Stations

Station no	gear	gear_no	area	2010	Start (UTC)	s_lat "S"	s_long "W"	s_depth	Bottom (UTC)	d_lat "S"	d_long "W"	d_depth	End (UTC)	e_lat "S"	e_long "W"	e_depth
1	GC	1	Incoming Plate	26.09.	10:20	33°11.941	73°38.298	3790	11:31	33°11.979	73°34.280	3791	12:58	33°12.000	73°34.311	3792
2	GC	2	Incoming Plate	26.09.	17:00	33°48.957	73°49.487	4081	18:57	33°48.979	73°49.571	4069	20:55	33°48.78	73°49.36	4064
3	GC	3	Incoming Plate	27.09.	1:00	34°25.496	73°45.784	4663	2:51	34°25.496	73°45.792	4664	5:00	34°25	73°45	4665
4	CTD	1	Graben	27.09.	18:53	34°43.463	73°40.664	5172					21:17	34°43.463	73°40.664	5100
5	GC	4	Incoming Plate	28.09.	2:41	35°09.895	74°40.042	4308	4:09	35°10.004	74°39.994	4305	5:43	35°10.054	74°39.871	4311
6	GC	5	Reloca Toe	28.09.	10:34	35°33.150	73°54.689	5045	12:15	35°32.987	73°54.664	5044	14:50	35°32.98	73°54.73	5045
7	Posidonia Calibration- 1		slope	28.09.	16:41	35°43.705	73°38.170	2021					20:55	35°43.566	73°38.094	2100
8	OFOF	1	CMSA BOX 3	28.09.	22:59	35°58.401	73°38.479	1095	23:22	35°58.523	73°38.483	1055	4:09	35°59.744	73°38.386	936
9	CTD	2	CMSA BOX 3	29.09.	5:37	35°58.970	73°37.917	1050					7:21	35°59.388	73°38.178	1055
10	MB, PS	1	shelf	30.09.	8:14	36°04.908	72°56.028	185					18:25	35°54.174	73°0.198	250
11	OFOF	2	CMSA BOX 3	30.09.	21:45	35°58.192	73°37.752	1098	2:45	35°59.936	73°38.297	897	3:17	35°59.890	73°38.213	930
12	GC	6	Incoming Plate	01.10.	10:16	35°49.960	74°42.315	4389	11:48	35°50.000	74°42.305	4385	14:07	35°50.03	74°42.36	4413
13	GC	7	Incoming Plate	01.10.	19:25	36°29.985	75°09.992	4042	20:45	36°30.002	75°09.996	4046	22:25	36°30.12	75°10.11	4052
14.1	OFOF	3	CMSA BOX 2	02.10.	5:58	36°27.750	73°40.365	696	8:08	36°28.853	73°40.408	702	8:33	36°28.919	73°40.280	700
14.2	OFOF	4	CMSA BOX 2	02.10.	9:06	36°27.847	73°40.957	718	11:24	36°28.631	73°40.792	713	11:50	36°28.774	73°40.759	714
15	CTD	3	CMSA BOX 2	02.10.	12:53	36°28.210	73°40.720	698					15:10	36°28.227	73°40.220	700
16	TV-MUC	1	CMSA BOX 2	02.10.	15:15	36°28.217	73°40.729	699	16:06	36°28.244	73°40.735	700	16:30	36°28.28	73°40.71	700
17	CTD	4	CMSA BOX 2	02.10.	16:56	36°28.231	73°40.714	700					19:23	36°28.234	73°40.699	699
18	OFOF	5	CMSA BOX 1	02.10.	20:11	36°23.978	73°42.076	702	20:41	36°23.452	73°42.097	705	2:42	36°25.560	73°41.860	700
19	OFOF	6	CMSA BOX 4	03.10.	4:06	36°21.774	73°42.477	756	8:46	36°23.592	73°43.124	759	9:20	36°23.590	73°43.040	756
20	CTD	5	CMSA BOX 1	03.10.	9:54	36°24.646	73°42.201	688					12:57	36°24.670	73°42.214	682
21	ROV	1	CMSA BOX 1	03.10.	16:45	36°24.520	73°42.177	688	22:50	36°25.493	73°42.056	683	23:16	36°25.56	73°42.11	692
22	MS-	1 bis	CMSA BOX 1	04.10.	1:18	36°24.660	73°42.146	690					6:00	36°24.650	73°42.238	687



Station no	gear	gear_no	area	2010	Start (UTC)	s_lat "S"	s_long "W"	s_depth	Bottom (UTC)	d_lat "S"	d_long "W"	d_depth	End (UTC)	e_lat "S"	e_long "W"	e_depth
	CTD	3														
23	MS-CTD	4 bis 8	CMSA BOX 1	04.10.	6:18	36°24.466	73°42.380	701					9:15	36°22.696	73°42.322	
24	TVG	1	CMSA BOX 1	04.10.	10:40	36°25.174	73°42.064	671					13:35	36°25.370	73°42.157	673
25	ROV	2	CMSA BOX 4	04.10.	14:10	36°21.997	73°42.785	775	19:26	36°25.161	73°42.040	674	21:40	36°22.90	73°42.62	678
26	CTD	6	CMSA BOX 4	05.10.	0:20	36°22.868	73°42.757	685					3:45	36°22.855	73°42.762	685
27	MS-CTD	9 - 11	CMSA BOX 4	05.10.	5:00	36°22.856	73°42.760	693					6:32	36°22.862	73°42.784	690
28	CTD	7	CMSA BOX 1	05.10.	7:35	36°22.221	73°42.735	699					10:09	36°22.240	73°42.730	708
29	GC	8	CMSA BOX 2	05.10.	10:30	36°28.226	73°40.730	708	10:42	36°28.235	73°40.705	707	11:01	36°28.219	73°40.709	707
30	ROV	3	CMSA BOX 1	05.10.	13:00	36°25.265	73°42.038	675	19:15	36°25.152	73°42.024	671	20:00	36°25.140	73°42.042	672
31	TVG	2	CMSA BOX 1	05.10.	21:15	36°25.003	73°42.196	678	22:26	36°25.108	73°42.188	638	23:40	36°25.002	73°42.399	688
32	WOOD-Sample	1		06.10.					0:10	36°22.872	73°42.776	688				
33	GC	9	BioBio Slide	06.10.	1:36	36°42.972	73°42.595	1314	2:11	36°34.998	73°42.617	1315	2:39	36°34.999	73°42.619	1308
34	MS-CTD	12 - 15	CMSA BOX 2	06.10.	5:18	36°28.228	73°40.727	703					7:56	36°28.248	73°40.762	702
35	GC	10	Reference Core	06.10.	10:30	36°28.259	73°44.036	994	10:51	36°28.255	73°44.069	1008	11:40	36°28.255	73°44.064	1008
36	OCE	1	CMSA BOX 2	06.10.	13:32	36°28.194	73°40.697	699	14:06	36°28.222	73°40.714	699	14:35	36°28.206	73°40.678	699
37	ROV	4	CMSA BOX 2	06.10.	14:55	36°28.229	73°40.714	700					23:11	36°28.43	73°40.15	688
38	POZ	1	CMSA BOX 2	06.10.	23:55	36°28.227	73°40.690	700	0:30	36°28.242	73°40.737	698	0:52	36°28.970	73°40.700	701
39-1	GC	11	BioBio Slide	07.10.	2:06	36°36.390	73°43.039	1450	2:36	36°36.432	73°43.041	1448	3:40	36°36.403	73°43.044	1448
39-2, 40	GC	12	BioBio Slide	07.10.	3:45	36°36.394	73°43.048	1448	4:14	36°36.430	73°43.023	1449	4:51	36°36.430	73°43.010	1450
40	MS-CTD	1- 2	CMSA Box 2	07.10.	6:06	36°28.14	73°40.71	697					10:01	36°28.35	73°40.69	698
41	GC	13	CMSA BOX 4	07.10.	10:30	36°22.982	73°42.691	681	11:22	36°22.995	73°42.637	675		36°23.871	73°42.993	694
42	ROV	5	CMSA BOX 2	07.10.	12:55	36°28.207	73°40.728	707	13:00	36°28.382	74°40.147	703	20:42	36°28.21	73°40.75	703
43	GC	14	BioBio Slide	07.10.	22:35	36°38.001	73°45.750	1822	23:00	36°38.048	73°45.763	1824	0:20	36°38.104	73°45.944	1825

Station no	gear	gear_no	area	2010	Start (UTC)	s_lat "S"	s_long "W"	s_depth	Bottom (UTC)	d_lat "S"	d_long "W"	d_depth	End (UTC)	e_lat "S"	e_long "W"	e_depth
44	MB/PS	2	Arauco	08.10.	0:22	36°38.050	73°45.970	1847					9:25	37°47.930	74°11.880	1202
45	GC	15	Incoming Plate	08.10.	15:43	38°07.426	75°30.055	3953	16:59	38°07.666	75°30.723	3950	17:45	38°07.666	75°30.723	3950
46	GC	16	Incoming Plate	08.10.	23:50	37°16.238	75°25.267	4213	1:00	37°16.266	75°25.013	4213	3:20	37°16.266	75°25.013	4213
47	MB/PS	3	Isla Mocha	09.10.	11:50	38°06.760	74°15.520	539					0:32	38°22.640	74°06.520	196
48	CTD	8	Isla Mocha	10.10.	1:12	38°22.776	74°06.401	180					2:12	38°22.774	74°06.425	183
49	MB/PS	4	Isla Mocha	10.10.	2:42	38°22.990	74°06.850	383					11:10	38°14.730	74°02.990	89
50	CTD	9	Isla Mocha	10.10.	11:20	38°14.770	74°03.032	90					12:12	38°14.770	74°03.032	97
51	Abwettern / ROV reparatur		Isla Mocha	11.10.												
52	POZ	1	CMSA BOX 2	11.10.	7:14	36°27.851	73°40.297	692					7:31	36°27.851	73°40.297	692
53	OCE	1	CMSA BOX 2	13.10.	13:53	36°27.608	73°40.463	705					14:30	36°27.608	73°40.463	705
54	TV-MUC	2	CMSA BOX 2	13.10.	16:15	36°28.222	73°40.724	707	16:40	36°28.222	73°40.722	707	17:10	36°28.245	73°40.730	706
55	GC	17	CMSA BOX 6	13.10.	20:33	35°54.255	73°32.340	1417	20:58	35°54.230	73°32.370	1417	22:23	35°54.290	73°31.560	1344
56	OFOS	7	CMSA BOX 6	13.10.	22:49	35°54.257	73°31.613	1352	4:49	35°54.25	73°34.55	1370	4:52	35°54.272	73°34.512	1376
57	OFOS	8	CMSA BOX 6	14.10.	6:04	35°54.252	73°39.670	1848	10:20	35°54.246	73°41.147	2298	11:00	35°54.317	73°41.183	2310
58	PRFL	1	CMSA BOX 2	14.10.	15:36	36°28.194	73°40.792	706	16:07	36°28.228	73°40.718	705	16:23	36°28.227	73°40.718	705
59	CTD	10	CMSA BOX 2	14.10.	16:49	36°28.232	73°40.715	706					18:57	36°28.197	73°40.708	706
60	GC	18	CMSA BOX 4	14.10.	19:50	36°21.778	73°43.299	865	20:20	36°21.869	73°43.282	845	20:55	36°21.692	73°43.659	869
61	GC	19		14.10.					23:02	36°11.257	73°37.359	716	23:34	36°11.250	73°37.531	729
62	MB/PS	5	BioBio Slide	14.10.	2:21	36°33.819	73°43.924	1344					8:10	36°32.890	73°43.710	1259
63	TVG	3	CMSA BOX 3	15.10.	12:29	35°58.290	73°38.458	1113	14:10	35°58.549	73°38.410	1026	14:46	35°58.57	73°38.41	1026
64	TVG	4	CMSA BOX 3	15.10.	15:17	35°58.558	73°38.427	1034	16:00	35°58.558	73°38.388	1022	16:30	35°58.63	73°38.331	1004
65	CTD	11	CMSA BOX 3	15.10.	16:58	35°59.060	73°37.740	1045					20:16	35°59.120	73°37.770	1047
66	TV-MUC	3	CMSA BOX 4	15.10.	23:00	36°22.254	73°42.746	745	1:36	36°22.857	73°42.767	679	2:22	36°22.873	73°42.776	686

Station no	gear	gear_no	area	2010	Start (UTC)	s_lat "S"	s_long "W"	s_depth	Bottom (UTC)	d_lat "S"	d_long "W"	d_depth	End (UTC)	e_lat "S"	e_long "W"	e_depth
67	MB/PS	6	Isla Santa Maria	16.10.	5:53	36°52.871	73°46.486	1067					11:22	36°58.450	73°44.840	370
68	TV-MUC	4			14:00	36°28.195	73°44.032	998	14:37	36°28.242	73°44.071	1006	15:23	36°28.248	73°44.012	1000
69	TVG	5	CMSA BOX 1	16.10.	16:00	36°24.950	73°42.150	680	17:03	36°25.117	73°42.180	670	17:20	36°25.190	73°42.180	673
70	TVG	6	CMSA BOX 1	16.10.	17:37	36°25.212	73°42.154	672	20:10	36°25.457	73°41.975	678	20:35	36°25.463	73°41.990	666
71-1	OFOS	9	CMSA BOX 7	16.10.	23:16	36°02.308	73°41.483	1235	0:51	36°2.64	73°41.62	1254	1:25	36°2.67	73°41.62	1261
71-2	OFOS	10	CMSA BOX 7	17.10.	1:50	36°02.296	73°41.591	1265	3:19	36°02.611	73°41.744	1250	3:54	36°2.63	73°41.79	1292
72	GC	20		17.10.	10:04	36°20.509	74°03.097	3476	11:05	36°20.599	74°03.168	3544	12:54	36°20.516	74°02.516	3537
73	PRFL	1	CMSA BOX 2	17.10.	14:50	36°27.892	73°40.510	694	15:05	36°28.006	73°40.531	694	15:15	36°28.055	73°40.607	697
74	ROV	6	CMSA BOX 8	17.10.	15:50	36°26.489	73°41.359	706	16:28	36°26.418	73°41.323	700	22:06	36°26.63	73°41.35	697
75	BIGO	1	CMSA BOX 2	17.10.	22:50	36°28.184	73°40.739	705	23:32	36°28.213	73°40.708	706	23:33	36°28.216	73°40.706	699
76	CTD	12	CMSA BOX 8	18.10.	0:30	36°26.530	73°41.350	700					2:06	36°26.550	73°41.360	700
77	MB/PS	7	Arauco	18.10.	2:22	36°26.810	73°41.430	725					12:20	36°25.234	73°42.169	664
78	ROV	7	CMSA BOX 1	18.10.	12:20	36°25.234	73°42.169	664	12:44	36°25.161	73°42.113	673	21:50	36°25.53	73°42.27	685
79	PRFL	2	CMSA BOX 2	18.10.	23:08	36°28.195	73°40.740	720	23:48	36°28.233	73°40.705	700	23:48	36°28.233	73°40.705	700
80	GC	21	Accretionary Prism	19.10.	2:07	36°20.854	73°59.899	3193	3:05	36°20.834	73°59.961	3792	4:20	36°20.834	73°59.961	3792
81	GC	22	Accretionary Prism	19.10.	5:00	36°20.594	74°03.179	3528	6:11	36°20.604	74°03.171	3491	7:10	36°20.604	74°03.171	3491
82	BIGO	1	CMSA BOX 2	19.10.	11:00	36°28.184	73°40.380	697	11:02	36°28.189	73°40.389	697	11:35	36°28.239	73°40.674	700
83	OCE	2	CMSA BOX 4	19.10.	14:20	36°22.864	73°42.671	687	14:47	36°22.878	73°42.702	688	15:10	36°22.855	73°42.666	687
84	ROV	8	CMSA BOX 4	19.10.	15:40	36°22.870	73°42.687	687	16:18	36°22.868	73°42.606	682	21:27	36°22.96	73°42.84	686
85	POZ	2	CMSA BOX	19.10.	22:09	36°22.840	73°42.685	680	22:40	36°22.844	73°42.678	688	23:00	36°22.85	73°42.72	682
86	MB/PS	8	CMSA BOX 8	19.10.	23:46	36°23.030	73°42.820	716					10:38	36°25.410	73°42.990	793
87	CTD	13	CMSA BOX 4	20.10.	11:18	36°22.890	73°42.730	687					13:08	36°23.100	73°42.790	690
88	ROV	9	CMSA BOX 4	20.10.	14:00	36°22.960	73°42.135	700	15:05	36°23.225	73°42.328	687	22:47	36°22.83	73°42.91	689

Station no	gear	gear_no	area	2010	Start (UTC)	s_lat "S"	s_long "W"	s_depth	Bottom (UTC)	d_lat "S"	d_long "W"	d_depth	End (UTC)	e_lat "S"	e_long "W"	e_depth
89	OPOS	11	Accretionary Prism	21.10.	0:55	36°20.859	73°59.844	3202	7:00	36°20.38	74°01.64	3324	8:20	36°20.681	74°01.428	3197
90	PRFL	2	CMSA BOX 2	21.10.	11:28	36°28.036	73°41.259	714					12:04	36°28.139	73°41.150	709
91	TV-MUC	5		21.10.	13:36	36°28.140	73°40.749	706	14:25	36°28.222	73°40.719	705	14:26	36°28.222	73°40.717	705
92	MB/PS	9	Isla Santa Maria	21.10.	17:37	36°53.530	73°43.325	558					5:55	36°52.75	73°50.27	1097
93	OCE	2	CMSA BOX 4	22.10.	11:00	36°22.620	73°42.638	700					11:39	36°22.62	73°42.64	689
94	POZ	2	CMSA BOX 4	22.10.	11:41	36°22.588	73°42.544	700					12:10	36°22.737	73°42.634	700
95	ROV	10	CMSA BOX 1	22.10.	13:13	36°23.759	73°42.267	698	13:27	36°23.701	73°42.206	703	22:40	36°24.89	73°42.33	683
96	GC	23	Slope	23.10.	0:10	36°21.461	73°52.157	2202	0:52	36°21.952	73°52.144	2199	2:00	36°21.952	73°52.144	2199
97	GC	24	Accretionary Prism	23.10.	3:10	36°20.226	74°06.427	3850	4:37	36°20.22	74°06.445	3842	6:17	36°20.136	74°06.535	3833
98	ROV	11	CMSA BOX 3	23.10.	11:52	35°59.749	73°38.389	927	12:17	35°59.790	73°38.318	966	23:25	35°58.772	73°38.096	1001
99_1	GC	25	Valdez Slide	24.10.	2:20	35°31.411	73°22.807	1280	2:46	35°31.438	73°22.806	1295	3:25	35°31.444	73°22.823	1290
99_2	GC	26	Valdez Slide	24.10.	3:31	35°31.488	73°22.843	1241	3:56	35°31.489	73°22.837	1243	4:32	35°31.479	73°22.837	1280
100	GC	27	Valdez Slide	24.10.	4:56	35°30.429	73°22.419	1321	5:22	35°30.470	73°22.368	1315	5:58	35°30.520	73°22.371	1316
101	GC	28	Reloca Slide	24.10.	8:38	35°33.081	73°54.755	5047	10:29	35°33.182	73°54.801	5046	13:00	35°33.204	73°54.901	5056
102	GC	29	Trench	24.10.	13:41	35°39.779	73°57.105	5054	15:18	35°39.816	73°57.118	5054	17:39	35°40.361	73°57.273	5059
103	CTD	14	El Quisco	25.10.	11:02	33°23.400	71°52.800	340					12:03	33°23.400	71°52.100	338
104	TV-MUC	6	El Quisco	25.10.	12:26	33°23.355	71°52.737	337	12:52	33°23.388	71°52.788	338	13:11	33°23.388	71°52.774	340
105	CTD	15	El Quisco	25.10.	15:21	33°23.500	71°46.700	122					15:50	33°23.900	71°46.700	121
106	CTD	16	El Quisco	25.10.	16:30	33°23.400	71°05.700	549					17:15	33°23.100	71°54.600	550
107	TV-MUC	7	OMZ	25.10.	18:20	33°23.420	71°46.728	122	18:33	33°23.446	71°46.790	120	18:57	33°23.451	71°46.690	120
108	CTD	17	El Quisco	25.10.	19:45	33°23.400	71°53.500	410					20:37	33°23.400	71°53.500	415
109	PRFL	3	El Quisco	25.10.	21:05	33°23.402	71°52.745	337	21:31	33°23.402	71°52.748	337	21:44	33°23.395	71°52.834	342



Station no	gear	gear_no	area	2010	Start (UTC)	s_lat "S"	s_long "W"	s_depth	Bottom (UTC)	d_lat "S"	d_long "W"	d_depth	End (UTC)	e_lat "S"	e_long "W"	e_depth
110	GC	30	Taza Slide	25.10.	0:25	33°28.081	72°16.569	1771	1:00	33°28.083	72°16.560	1771	1:55	33°28.120	72°16.507	1763
111	MB/PS	10	Taza Slide	26.10.	2:00	33°28.140	72°16.490	1779					11:41	32°34.405	72°42.112	5973
112	ROV	12	Trench	26.10.	11:41	32°34.405	72°42.112	5973	14:56	32°34.377	72°42.101	5974	17:50	32°34.377	72°42.101	5974
113-1	TV-MUC	8	Quisco / OMZ	26.10.	23:20	33°23.350	71°51.913	227	23:32	33°23.980	71°51.499	120	23:52	33°23.980	71°51.499	120
113-2	TV-MUC	9	Quisco / OMZ	26.10.	23:53	33°23.388	71°51.989	232	0:07	33°23.416	71°52.009	235	0:22	33°23.418	71°52.006	235
114	CTD	18	El Quisco	27.10.	0:52	33°23.400	71°52.000	235					1:01	33°23.400	71°52.000	236
115	CTD	19	El Quisco	27.10.	1:39	33°23.400	71°53.800	441					2:27	33°23.400	71°53.800	443
116	CTD	20	El Quisco	27.10.	2:54	33°23.100	71°55.300	600					4:00	33°23.400	71°55.400	601
117	CTD	21	El Quisco	27.10.	4:30	33°23.400	71°57.600	826					6:06	33°23.200	71°57.600	820
118	ROV	13	El Quisco	27.10.	12:20	33°23.237	71°52.752	334	12:35	33°23.329	71°52.752	337	17:45	33°23.393	71°53.890	448
119	TV-MUC	10	Quisco / OMZ	27.10.	18:22	33°23.398	71°53.812	442	18:40	33°23.396	71°53.792	438	19:01	33°23.390	71°53.011	491
120	PRFL	3	El Quisco	27.10.	19:20	33°23.639	71°52.746	337					19:50			
121	TV-MUC	11	El Quisco	27.10.	21:37	33°23.390	71°55.241	599	22:00	33°23.390	71°55.250	599	22:27	35°23.399	71°55.247	596
122	GC	31	San Antonio Canyon	28.10.	9:05	33°04.560	72°21.985	3280	10:02	33°04.617	72°21.967	3246	11:17	33°04.633	72°21.957	3214
123	GC	32	San Antonio Canyon	28.10.	13:42	33°27'146	72°08.332	1787	14:15	33°27.169	72°08.350	1812	15:02	33°27.155	72°08.400	1813
124	TV-MUC	12	Quisco / OMZ	28.10.	16:40	33°23.425	71°51.010	165	16:50	33°23.415	71°51.018	165	17:06	33°23.425	71°51.009	165
125	TV-MUC	13	Quisco / OMZ	28.10.	17:39	33°23.441	71°54.252	490	17:58	33°23.421	71°54.208	486	18:21	33°23.412	71°54.201	485
126	MB/PS	11	Rio Mataquillo	28.10.	20:00	33°38.660	72°05.110	663					3:55	33°45.050	72°07.440	952

Abbreviations: BIGO: Biogeochemical Observatory, CTD: Conductivity, Temperature, Depth probe / rosette, GC: Gravity Corer, MB: Multi Beam, MS-CTD: Micro Structure CTD, OCE: Ocean Elevator, OFOS: Ocean Floor Observation system, PRFL: Profiler Lander, PS: ParaSound, ROV: Remotely Operated Vehicle, TV-MUC: Video-guided Multi Corer, TVG: Video-guided Grab, WOOD-Sample: Wood exposure experiment

## Annex II: Carbonate Sample Description

ROV carbonate and related bottom water sampling:

On cruise SO210 four different working areas were addressed by this technique, supported by TVG based sampling of oversized single blocks for detailed local depth profiles.

Stationno.	ROV_no. / VL prot. sub-pos.	area	Lat. "S"	Long. "W"	depth	figure no. & remarks
25	2 / 1	CMSA BOX 4	36.381	73.7128	692	Niskin bottle over bacteria
25	2 / 2	CMSA BOX 4	36.3813	73.7125	689	Niskin bottle over clam field
25	2 / 3	CMSA BOX 4	36.3813	73.7125	690	1, clam net catch
25	2 / 4	CMSA BOX 4	36.3813	73.7125	690	no pict., tubeworm on stone sampled, T.T.
25	2 / 5	CMSA BOX 4	36.3816	73.7121	684	2 a & b, 2 x carbonate sampled, distal rim around clam field
74	6 / 1	CMSA BOX 8	36.4428	73.6898	701	Niskin bottle (sb), bacterial mat (PC-13)
74	6 / 2	CMSA BOX 8	36.4428	73.6898	702	Niskin bottle (ps), bacterial mat (PC-18)
74	6 / 3	CMSA BOX 8	36.4428	73.6898	702	3, net scoop (2nd), active site (?), lowest level of structure, juvenile carbonate concretion (?)
74	6 / 4	CMSA BOX 8	36.4426	73.6894	702	4, top of carbonate structure, taken from solid nose incl. soft coral
78	7 / 1-1	CMSA BOX 1	36.4190	73.7020	678	Niskin bottle (sb), clams and tubeworms alive
78	7 / 1-2	CMSA BOX 1	36.4190	73.7020	678	5, 3 x Carbonate, broken from flat (plate-like) base (a lot living tube worms, some living clams)
78	7 / 2	CMSA BOX 1	36.4188	73.7023	675	6, saw cut, solitary block, some clams and tubeworms alive at base
78	7 / 3	CMSA BOX 1	36.4188	73.7024	674	Niskin bottle (ps), "flea site", above bacterial mat, (no chance for pc-penetration)
78	7 / 4	CMSA BOX 1	36.4187	73.7024	672	7, broken from tunnel-like structure, in tubeworm field (alive)
78	7 / 5	CMSA BOX 1	36.4187	73.7024	672	8, saw cut, 0.5 to 1m high vertical structure, upper left nose
78	7 / 6	CMSA BOX 1	36.4186	73.7025	668	9, white horizon in/on carbonate, (bacteria thiotr.,?), massive material, try of large brake-off failed, small fragments picked from seafloor (2 x)
78	7 / 7	CMSA BOX 1	36.4187	73.7031	667	10, massive laminated aragonite at white massive edge with bacteria, first triangle saw cut and tubeworm with bacteria recovered (T.T.) left from PC-site
78	7 / 9	CMSA BOX 1	36.4228	73.7018	660	11a & b, block on top of shallowest site, saw cut of nose incl. solitary coral ( <i>Bathycyathus chilensis</i> )
78	7 / 11	CMSA BOX 1	36.4243	73.7019	675	12, on downhill track, vertical structure at S-base, saw cut recovered in 2 pieces
95	10 / 1	CMSA BOX 1	36.3983	73.7047	697	13, flat structure on first top in muddy high Gorgonia density area
95	10 / 3	CMSA BOX 1	36.4047	73.6995	690	14, fragile porous block, saw cut of uppermost nose, recovered in 3 pieces, 1-3 big block base of nose, 2-3 picked potentially top, 3-3 un-fragmented left counter-side of cut broken from main block
95	10 / 5	CMSA BOX 1	36.4098	73.7032	685	15a & b, saw cut from big block middle nose, on track to next top of structure, recovered in 2 pieces, 1-2 upper part, 2-2 lower part
95	10 / 6-1	CMSA BOX 1	36.4102	73.7033	685	16, saw cut from block surrounded by enormous amount of living tube worms
95	10 / 6-2	CMSA BOX 1	36.4103	73.7032	685	Niskin (ps, yellow), high abundance of living tubeworms
95	10 / 7-1	CMSA BOX 1	36.4105	73.7035	685	17a & b, calcified focused fluid emanation site, with soft carbonate adjacent to hole, samples recovered in 3 fragments, 1-3 taken from hole-rim, saw cut into upper part, downward into massive hole bearing carbonate, 2-3 broken from main carbonate and 3-3 large piece of saw cut

Stationno.	ROV_no. / VL prot. sub-pos.	area	Lat. "S"	Long. "W"	depth	figure no. & remarks
95	10 / 7-2	CMSA BOX 1	36.4105	73.7035	685	18, clam shells close to emanation hole
95	10 / 7-3	CMSA BOX 1	36.4105	73.7035	685	Niskin (sb), direct above emanation hole
95	10 / 8	CMSA BOX 1	36.4113	73.7053	692	19, 2 x fragments of flat carbonate at W-base of last top on track, after passing large and steep field of carbonate bolders,
98	11 / 1	CMSA BOX 3	35.9956	73.6393	940	20, 3 fragments of outcropping layered basal carbonates
98	11 / 2	CMSA BOX 3	35.995	73.6399	905	21, 2 carbonates from bolder field (clams in cracks on top, outflow (?), whitish coated massive layer at base of porous block), 1-2 on first top of the track, 2-2 broken "nose" from block above
98	11 / 3	CMSA BOX 3	35.995	73.6403	901	22, flat carbonate block from the top above a crack, white "fluffy" stuff on surface, open vent hole, high abundance of clams on the way to the top
98	11 / 4	CMSA BOX 3	35.9859	73.6318	1008	23a & b, single block in valley-like structure, carbonate "nose" within outflow hole sampled, whitish soft coating, tubeworm and clams close by alive (T.T.: juvenile and big clams), bacterial mats, black and white patches, small carbonate plates and chips in net catch
98	11 / 5	CMSA BOX 3	35.9768	73.6336	974	24, 4 fragments of flat carbonate at base of a m-scaled vertical vein-like structure on top of TVG-4 hill site

Abbreviations: T.T.: Tina Treude, cruise participant hosting the sample, sb: starboard, ps: port side, PC site: Pushcorer sampling site, (?): still needs to be clarified, VL prot. sub-pos: Volker Liebetrau protocol, subsample position



Fig. 1: Box 4, 690 m; clam shell collection from dead clam field & Fig. 2a: Box 4, 684 m; adjacent carbonate rim (block left in this picture).



Fig 2b: Box 4, 684 m; carbonate block from clam field surrounding elevated rim. Reflecting disruption (fresh gray) from underlying main carbonate und multiple intercalated massive white layers.



Fig. 3: Box 8, 702 m; Soft carbonate concretion



Fig. 4: Box 8, 702 m; 2 fragments broken from a large



recovered by net scoop at potentially active seep site.



Fig. 5: Box 1, 678 m; carbonates from a site characterised by high abundance of living tube worms and clams.

bolder (incl. soft coral).



Fig. 6: Box 1, 675 m; saw cut from a solitary block displaying internal network, open pore system and solidified tube worm hole, the block was surrounded at its base by some living tubeworms and clams.



Fig. 7: Box 1, 672 m; flat carbonate broken from tunnel-like structure within field of living tubeworms.



Fig. 8: Box 1, 672 m; upper part of one of the rare but characteristic vertical structures, the saw cut is taken around 1m above the sea floor.



Fig. 9: Box 1, 668 m; carbonate on which white coating was observed, fragments broken from wide solid layer.



Fig. 10: Box 1, 667 m; 1<sup>st</sup> masterpiece of ROV diamond chain saw work; massive laminated aragonite at whitish coated edge of massive and wide carbonate bank covering the seafloor, with living tube worms & bacterial mats at base.



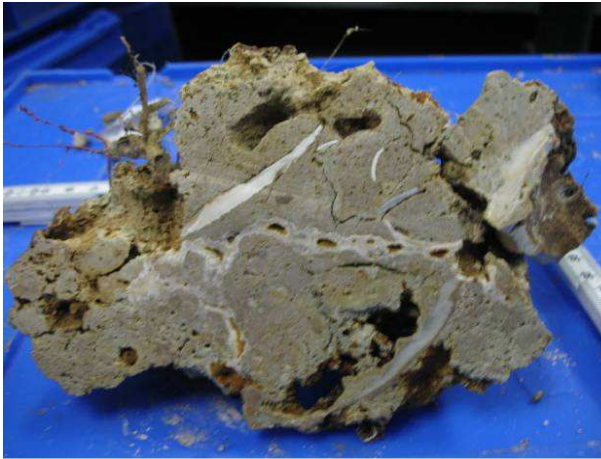


Fig. 11a: Box 1, 660 m; saw cut nose of solitary block on top of the shallowest site sampled for carbonates during the cruise. block on top of shallowest site, saw cut of nose incl. solitary coral (*Bathycyathus chilensis*)

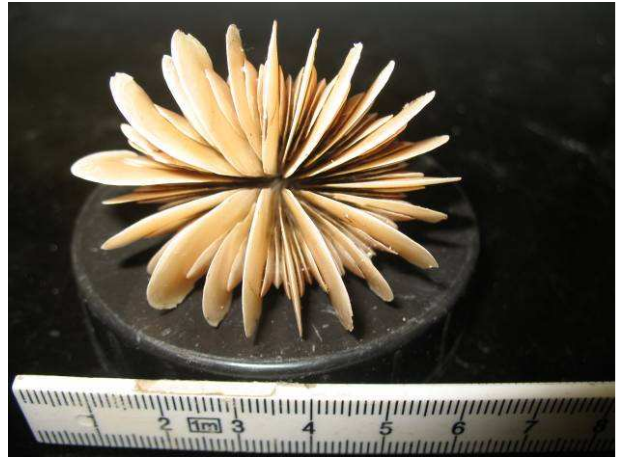


Fig. 11b: Box 1, 660 m; solitary cold water coral (*Bathycyathus chilensis*) recovered on saw cut of authigenic carbonate block (Fig. 11a)



Fig. 12: Box 1, 675 m; saw cut of upper part of vertical structure at S-base, dense material with some open pore space and white vein filling.



Fig. 13: Box 1, 697 m; flat structure with thin white layers surrounding dense detritus-rich material, sampled in muddy & high Gorgonia abundance area.



Fig. 14: Box 1, 690 m; fragile porous block, sampled by diamond chain saw at uppermost nose, recovered in 3 pieces, 3-3 displaying characteristic large open pore space.



Fig. 15a: Box 1, 685 m; saw cut from big block middle nose recovered in 2 pieces, sample 1-2 upper part sediment-rich and porous authigenic carbonate matrix.





Fig. 15b: Box 1, 685 m; lower part of saw cut (sample 2-2) reflects typical in-situ embedding of clams preserving original pore space. The lower one shows late stage collapse of shell.



Fig. 16: Box 1, 685; saw cut from block surrounded by enormous amount of living tube worms, showing white laminated filling of coarse pore space.



Fig. 17a: Box 1, 685 m; calcified focused fluid emanation site, with soft carbonate adjacent to the hole, samples recovered in 3 fragments, 1-3 displayed here was taken direct from hole-rim.



Fig. 17b: Box 1, 685 m; 2<sup>nd</sup> masterpiece of ROV chain saw application, calcified focused fluid emanation site, samples recovered in 3 fragments, the saw cut from the upper part downward into massive hole bearing carbonate (sample 2-3) shows the layered succession of authigenic carbonate.



Fig. 18: Box 1, 685 m; dead clam shells close to emanation hole and related carbonates shown in fig. 17.



Fig. 19: Box 1, 692; 2 x fragments of flat carbonate at W-base of last top on track, after passing large and steep field of carbonate bolder, displaying white vein and pore space filling.





Fig. 20: Box 3, 940 m; 3 fragments of outcropping layered basal carbonates.



Fig. 21: Box 3, 905 m; carbonates from bolder field on top of track, whitish coated massive layer on downside (not displ.).



Fig. 22: Box 3, 901 m; shallowest site sampled in Box 3, open vent hole in layered matrix, too wide for tube worm remnant, high abundance of clams observed during upward track.



Fig. 23a: Box 3, 1008 m; single block in valley-like structure, carbonate "nose" sampled directly out outflow structure, whitish soft coating, tubeworm and clams close by alive (T.T.: juvenile and big clams), bacterial mats, black and white patches, small carbonate plates and chips in net catch.



Fig. 23b: Box 3, 1008 m; downside close-up of fragment of solitary block in valley-like structure, showing whitish soft to slate-like coating as potentially juvenile cold seep driven authigenic carbonate precipitation, deepest site sampled for carbonates accompanied by living cold seep fauna during the cruise.



Fig. 24: Box 3, 974 m; 4 fragments of flat carbonate at base of an extended several m-scaled vertical vein-like structure on top of TVG-4 hill site.

**Annex III: List of Core Stations**

Station #	GC #	Date	Time (UTC)	Lat °S	Long °W	Water depth	Area	Remarks
1	1	26.09.10	10:20	33°11.941	73°38.298	3790	Incoming Plate	12m / 10.08m recovery / description in CR
2	2	26.09.10	17:00	33°48.957	73°49.487	4081	Incoming Plate	12m / 7.45m recovery / description in CR
3	3	27.09.10	1:00	34°25.496	73°45.784	4663	Incoming Plate	12m / 11.00m recovery / description in CR
5	4	28.09.10	2:41	35°09.895	74°40.042	4308	Incoming Plate	12m / 11.50m recovery / description in CR
6	5	28.09.10	10:34	35°33.150	73°54.689	5045	Reloca Toe	12m / no recovery
12	6	01.10.10	10:16	35°49.960	74°42.315	4389	Incoming Plate	12m / 8.85m recovery / description in CR
13	7	01.10.10	19:25	36°29.985	75°09.992	4042	Incoming Plate	12m / 8.00m recovery / description in CR
29	8	05.10.10	10:30	36°28.226	73°40.730	708	CMSA BOX 2	3m / 3.00m recovery / description in CR
33	9	06.10.10	1:36	36°42.972	73°42.595	1314	BioBio Slide	6m / 5.64m recovery / core not opened yet
35	10	06.10.10	10:30	36°28.259	73°44.036	994	Reference Core	6m / 5.88m recovery / description in CR
39-1	11	07.10.10	2:06	36°36.390	73°43.039	1450	BioBio Slide	3m / 1.37m recovery / description in CR
39-2	12	07.10.10	3:45	36°36.394	73°43.048	1448	BioBio Slide	6m / 4.60m recovery / core not opened yet
41	13	07.10.10	10:30	36°22.982	73°42.691	681	CMSA BOX 4	3m / 1.04m recovery / description in CR
43	14	07.10.10	22:35	36°38.001	73°45.750	1822	BioBio Slide	6m / 5.77m recovery / description in CR
45	15	08.10.10	15:43	38°07.426	75°30.055	3953	Incoming Plate	12m / 7.80m recovery / description in CR
46	16	08.10.10	23:50	37°16.238	75°25.267	4213	Incoming Plate	12m / 10.10m recovery / description in CR
55	17	13.10.10	20:33	35°54.255	73°32.340	1417	CMSA BOX 6	6m / 5.60 m recovery / sampled on deck (gas samples), no description
60	18	14.10.10	19:50	36°21.778	73°43.299	865	CMSA BOX 4	6m / 5.80m recovery / sampled on deck (gas samples), no description
61	19	14.10.10	23:02	36°11.257	73°37.359	716	CMSA	6m / 4.90m recovery / sampled on deck (gas samples), no description
72	20	17.10.10	10:04	36°20.509	74°03.097	3476	Accretionary Prism	6m / 5.70m recovery / description in CR
80	21	19.10.10	2:07	36°20.854	73°59.899	3193	Accretionary Prism	6m / 5.83m recovery / description in CR
81	22	19.10.10	5:00	36°20.594	74°03.179	3528	Accretionary Prism	6m / 4.38m recovery / sampled on deck (gas samples), no description
96	23	23.10.10	0:10	36°21.461	73°52.157	2202	Slope	6m / 5.70m recovery / description in CR
97	24	23.10.10	3:10	36°20.226	74°06.427	3850	Accretionary Prism	6m / 5.73m recovery / description in CR
99-1	25	24.10.10	2:20	35°31.411	73°22.807	1280	Valdez Slide	3m / 0.45m recovery / core not opened yet
99-2	26	24.10.10	3:31	35°31.488	73°22.843	1241	Valdez Slide	3m / 0.42m recovery / core not opened yet
100	27	24.10.10	4:56	35°30.429	73°22.419	1321	Valdez Slide	3m / 0.42m recovery / core not opened yet
101	28	24.10.10	8:38	35°33.081	73°54.755	5047	Reloca Slide	6m / 3.37m recovery / core not opened yet
102	29	24.10.10	13:41	35°39.779	73°57.105	5054	Trench	6m / 5.70m recovery / description in CR
110	30	25.10.10	0:25	33°28.081	72°16.569	1771	Taza Slide	6m / no recovery
122	31	28.10.10	9:05	33°04.560	72°21.985	3280	San Antonio Canyon	6m / no recovery
123	32	28.10.10	13:42	33°27°146	72°08.332	1787	San Antonio Canyon	6m / 0.20m recovery in core catcher (gravel), no description

Meiofauna samples SO-210			
	Station	Replicate	Cut sediment (cm)
MUC 1	16	1	0-1 ; 1-2 ; 2-3 ; 3-5 ; 5 -10
MUC 2	54	1	0-1 ; 1-2 ; 2-3 ; 3-5
MUC 2	54	2	0-1 ; 1-2 ; 2-3 ; 3-5 ; 5 -10
MUC 4	68	1	0-1 ; 1-2 ; 2-3 ; 3-5 ; 5 -10
MUC 5	91	1	0-1 ; 1-2 ; 2-3 ; 3-5 ; 5 -10
MUC 5	91	2	0-1 ; 1-2 ; 2-3 ; 3-5 ; 5 -10
MUC 5	91	3	0-1 ; 1-2 ; 2-3 ; 3-5 ; 5 -10
ROV 4	37	1	0-1 ; 1-2 ; 2-3 ; 3-5 ; 5 -10
ROV 4	37	2	0-1 ; 1-2 ; 2-3 ; 3-5 ; 5 -10
ROV 6	74	1	0-1 ; 1-2 ; 2-3 ; 3-5

[illegible]

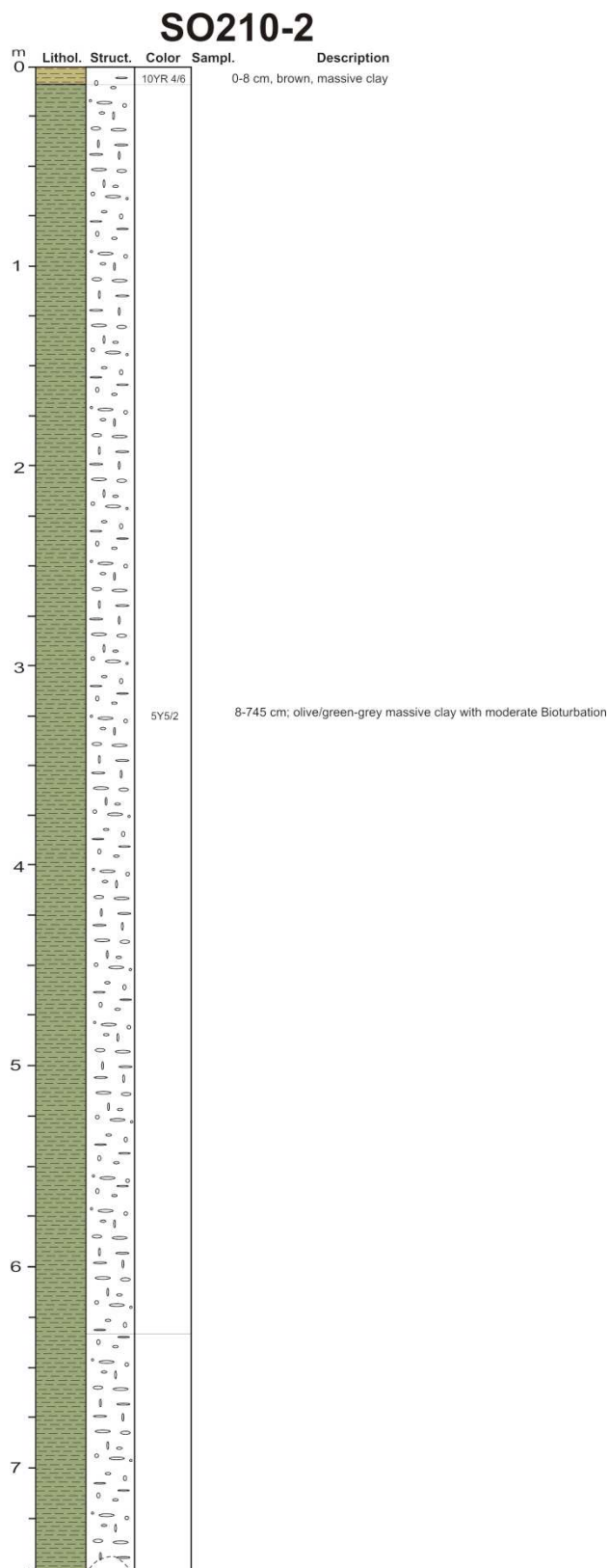
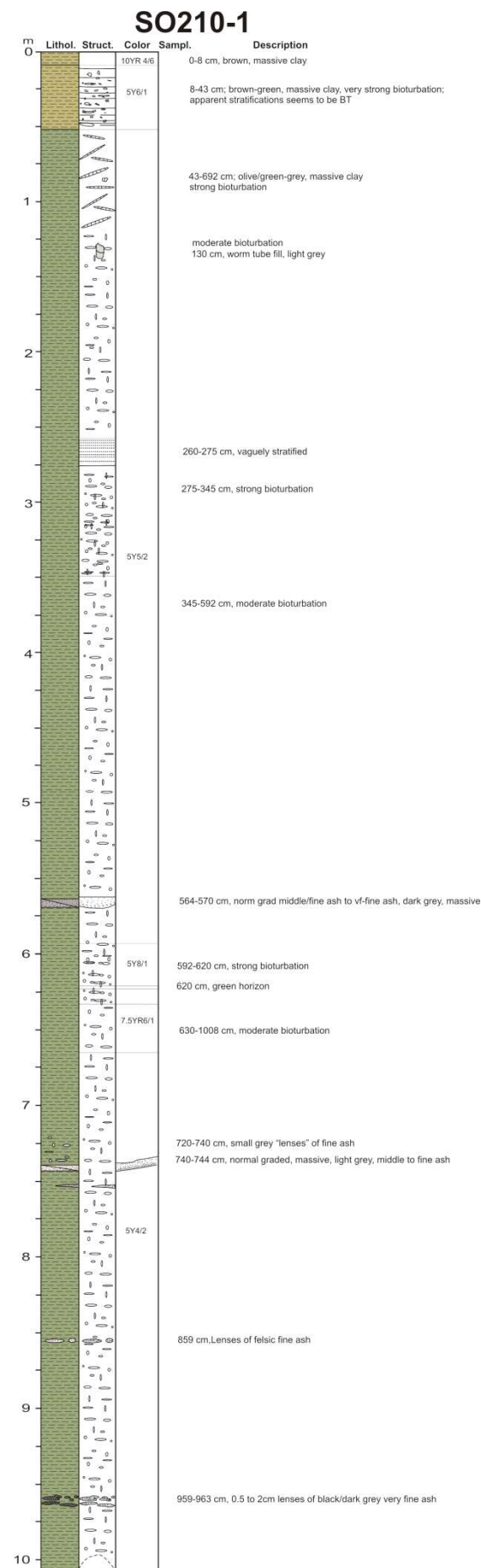




Taxa	Station													total
	16	25	42	54	64	69	74	78	84	88	91	95	98	
Polychaeta sp. 4					1									1
Mollusca														
<i>Acharax</i> sp.							1							1
<i>Adipicola</i> sp.		6												6
<i>Archivesica</i> sp.													6	6
<i>Calliostoma crustulum</i>									1					1
<i>Calyptogena gallardoi</i>	5	5		12			4		28					54
<i>Lepidozona</i> sp.					4	4								8
<i>Leptochiton americanus</i>					1							1		2
<i>Lothia</i> sp.						2								
<i>Margarites huloti</i>						2						1		3
<i>Propeleda longicaudata</i>							1							1
<i>Provanna</i> sp.		32							1					33
<i>Pyropelta</i> sp.		4							4				6	14
Scaphopoda sp.		1							2					3
Turridae sp.									1					1
Veneridae sp. 1	3			1			2				1			7
<i>Zetella alphonsini</i>		1												1
Gastropoda sp. 1					3									3
Arthropoda														
<i>Aega</i> sp.						3						1		4
Cirripedia sp. 1					16							3		19
<i>Munida propinqua</i>						1								1
<i>Scalpellum</i> sp.									1			1		2
Amphipoda sp. 1				1										1
Amphipoda sp. 2					1									1
Echinodermata														
<i>Astrodia tenuispina</i>								2						2
<i>Astrostoma agassizi</i>								1						1

[illegible]

## Annex V: Core Descriptions





## SO210-3

m	Lithol.	Struct.	Color	Sampl.	Description
0					
			5Y4/2		massive clay moderate bioturbation
					From 60 cm small black pyrite spots
1					100-140 strong bioturbation
					140-11087 cm moderate bioturbation
2					205 cm Lenses of silty clay
					234 + 250 cm, black, large pyrite concretion
3					295-295.5 cm, black, very fine ash
					328 + 385 cm, black, large pyrite concretion
4					425 cm, thin double layer of fine sand
					455 cm, thin bed of fine sand
5					483 cm, lenses of very fine ash
					small pyrite lenses and rare radiolarite-lenses
6			10YR4/3		
					rare radiolarite-lenses
7			5YR4/2		680 cm, lenses of fine sand
					700 cm, large pyrite concretion
					720-740 cm, small grey "lenses" of fine ash
					740-744 cm, normal graded, massive, light grey, middle to fine ash
8			5Y4/2		
					875 cm, Pyrite concretions
9					rare radiolarite-lenses
10					1080 cm, black, very fine ash

## SO210-5

m	Lithol.	Struct.	Color	Sampl.	Description
0					0-40 cm disturbed (fell from tube)
			5Y4/2		0-78 cm massive clay, strong bioturbation
1					78-285 cm massive clay, moderate bioturbation
2					2 mm dark grey layer
3			5Y4/2		285-400 cm massive clay, strong bioturbation
					2 layers each ~1 cm darkgrey very fine ash black spot= very fine ash
					375 cm very smooth clay layer
4			5Y4/2		400-465 cm massive clay, moderate bioturbation
					434-436 cm white ash 445 cm lense with shards
			5Y4/2		465 cm fine black line, no ash, no bioturbation
			5Y4/2		475 cm 3mm ash, very fine- fine ash
5					475-550 cm massive clay, strong bioturbation
					501 cm and 502 cm each < 2mm ash, abundant shards
			5Y4/2		550-575 cm massive clay, moderate bioturbation
6			5Y4/2		575-705 cm massive clay, strong bioturbation
7					675 cm dark line, no ash
			5Y4/2		705-806 cm massive clay, moderate bioturbation
8			5Y4/3		806-850 cm massive clay, strong bioturbation gn bioturbation lenses
			5Y4/2		850-906 cm massive clay, moderate bioturbation
9			5Y4/2		906-950 cm massive clay, strong bioturbation green bioturbation lenses
			5Y4/2		950-1157 cm massive clay, moderate bioturbation 965 cm 1mm layer w. terrestrial components no ash
10					1005 cm dark lense with terrestrial particles, no ash
					~ 1mm discontinuous layer of black very fine ash

## SO210-12

m	Lithol.	Struct.	Color	Sampl.	Description
0					
			5Y3/2		0-145 cm: massive clay moderate bioturbation
1					
			2.5Y3/2		145-159 cm: darker colour, silty clay, massive little bioturbation at 155cm: 1mm dark very-fine-ash-layer
2					
					159-200cm: massive clay little bioturbation at 184cm: black clay lense
					200-229cm: massive clay moderate bioturbation, with abundant black bi-tracks
					229-279cm: massive clay strong bioturbation
					279-431cm: massive clay moderate bioturbation
3					
4					
					431-490cm: compacted massive clay strong bioturbation abundant black bioturbation streaks at 440cm: 1cm black very-fine-ash at 450cm: unconformity or bioturbation? at 462cm: 3mm dark grey-green fine-ash
5			5Y4/2		490-834cm: compacted massive clay moderate bioturbation
					572-574 normal graded black ash
6					at 598cm black very-fine-ash
7					
					at 772cm: dark grey clay layer
8					834-870cm: compacted massive clay with fine black bioturbation streaks strong bioturbation

## SO210-13

m	Lithol.	Struct.	Color	Sampl.	Description
0			5Y3/2		0-129 cm massive clay, moderate bioturbation 21-22 cm brown stripe, clay
					65-66 cm ~1cm f-sand
1					97 cm darker layer, fine-sand 108 cm green f-sand dark green sandy lenses
			5Y3/2		129-140cm darker clay, strong bioturbation
			5Y3/2		144 cm silty layer 148cm, 151 cm, 153 cm green fine sand 154 cm dark green fine sand
			5Y4/2		155-342 cm massive clay, little bioturbation
2					
3			5Y3/2		342-470 cm massive clay, moderate bioturbation
					371cm, 375 cm ~1cm sandy layer 392 cm layer/lenses of very fine ash
4			5Y4/2		
			5Y3/2		470-543 cm massive clay, little bioturbation
5			5Y4/2		
			5Y3/2		543-573 cm massive clay, moderate bioturbation
			5Y4/2		573-580 cm very strong bioturbation 580-643 cm massive clay, little bioturbation
6					643-673 cm massive clay, moderate bioturbation
					673-700 cm massive clay, strong bioturbation 673 cm dark grey bioturbation lense 688 cm dark grey green bioturbation lense
7			5Y4/2		700-947 cm massive clay, very little bioturbation 710 cm dark grey lense
8			5Y4/2		838 cm thin zone with ash 844 cm lenses with ash
					886-890 cm small pods with ash&minerals
9			5Y4/2		947-992 cm massive clay, little bioturbation 964-967 cm lenses with ash

SO210-29

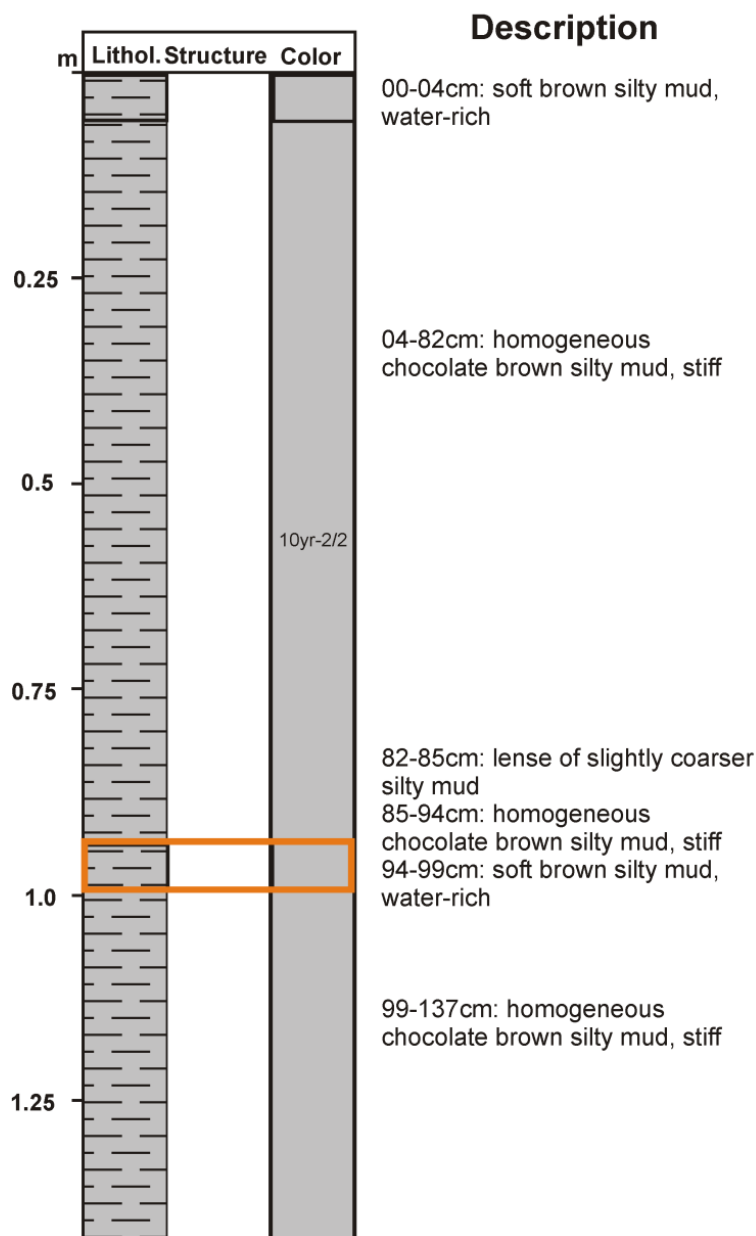
m	Lithol.	Struct.	Color	Sampl.	Description
0				Gley 1 5/10Y	ca. 50 cm of top is missing
				Gley 1 4/10Y	11-20 cm carbonate clast, mudstone (clay carboniferous cemented); carboniferous clay
					20-35 cm normal background sediment: structurless green clay with carbonate cement)
					25 cm lense of dark clay (gley 1- 3/56Y)
					30-35 cm horizon with carbonated clay (carbonate clasts), mudstone slightly consolidated
					40-62 cm degassing structures in sediment
					layer of dark clay (less carbonate in matrix)
					54 cm 3mm horizon with the dark clay
					62 cm dark lense of less carboniferous clay (~2 cm)
					0-302 cm no bioturbation
1				Gley 1 5/10Y	103-106 cm lighter, stronger consolidated (cement!)
				Gley 1 4/10Y	106 cm more carboniferous clay. At the base hardened clasts
					background sediment is structureless, slightly consolidated, slightly carboniferous clay
					some "Schlieren" of lighter stronger carboniferous zones between 109-112 cm
					129-140cm darker clay, strong bioturbation
				#1	137-147 cm horizon with mixture of background sedimentation and lenses of
				#2	lighter, stronger consolidated, more carboniferous clay. Within lighter parts clasts
				#1	154-160 cm layer clasts of hardened carbonate (mudstone)
				#2	167-173 cm layers of hardened carbonate (mudstone)
				#1	
				#2	
2					starting from 205 cm some black small lenses (~1mm)
				Gley 1- 5/56Y	same as #2 but lighter in color, structureless, less carbonate, consolidated like #2
3					

# SO210-35

m	Lithol.	Struct.	Color	Sampl.	Description
0					
			2.4Y 2/3		5-50 cm structureless clay, moderate bioturbation in the lower half strongly bioturbation -> hemipelagic 24 cm small basaltic clast or sandstone 36-38 cm lenses of continental detritus with minerals+glass+glaukonite
			5Y3/2		50-52 cm lenses like at 36-38 cm 50-65 cm strong bioturbation 65-99 cm decreasing bioturbation 50-99 cm structureless clay mixed with clay from above by bioturbation
1					hardened clay clast ~4mm 99-200 cm structureless clay with same hardened clasts and sulfid needles 120 cm clay clast ~4 mm
2					183 cm bioturbation traces 187 cm shale claystone clasts until 215 cm 200-300 cm structureless clay, low bioturbation
3					bioturbation 300-400 cm structureless clay with some sulfide needles
4			Gley 1 4/10Y		400-465 cm structureless clay
5			5Y3/2		"Schlieren" at the transition into new colour horizon with enriched sulfide needles 500-588 cm structureless clay, no bioturbation 530 cm some traces of mussels
			5Y4/2		



# SO210-39-1

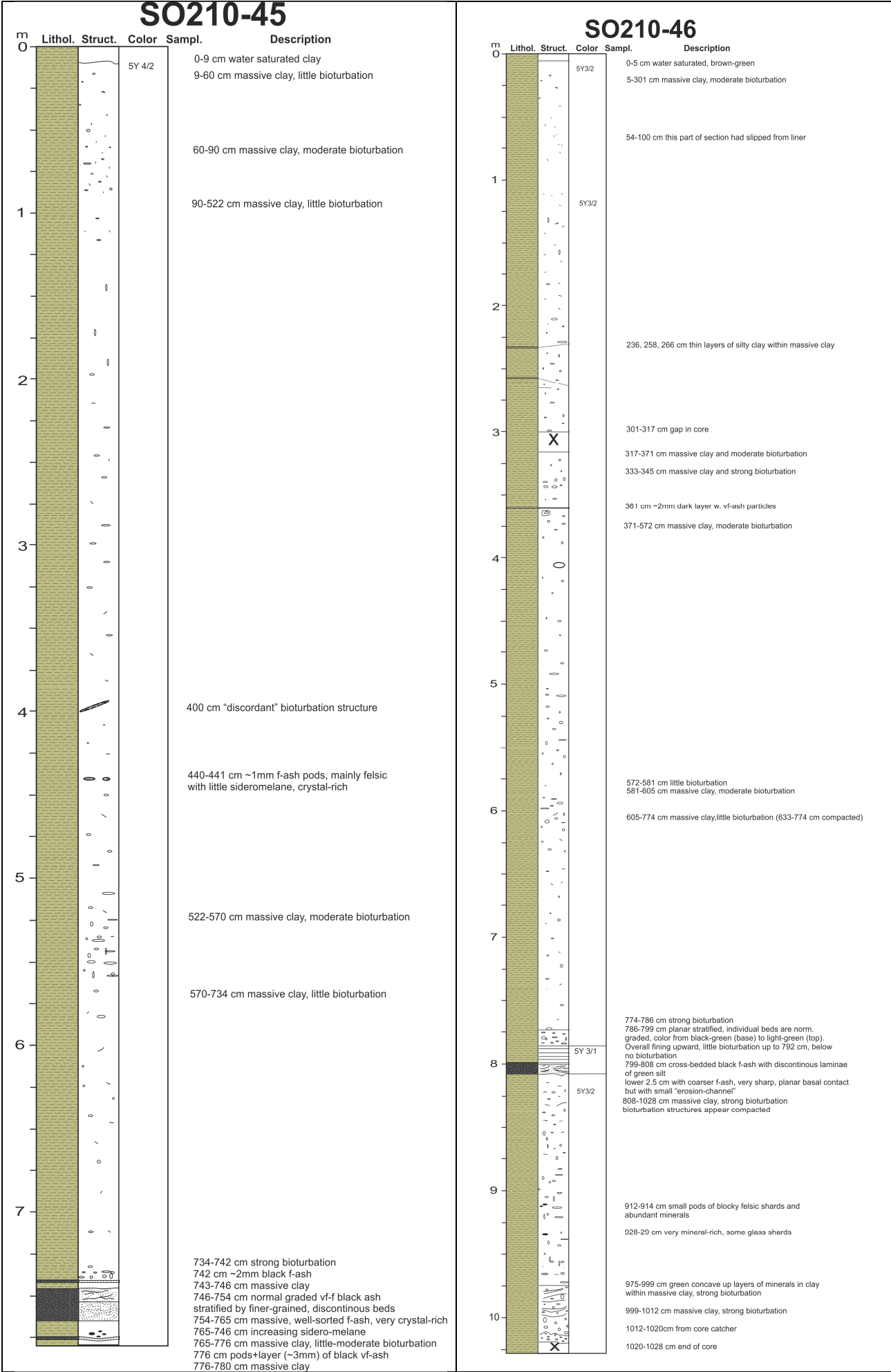


# SO210-41

m	Lithol.	Struct.	Color	Sampl.	Description
0		X	Gley 1 4/10Y		carbonate matrix of clay darker green parts, slightly carboniferous lighter green parts stronger carboniferous matrix strongly hardened and very dry
			Gley 1 5/10Y		
			Gley 1 4/10Y		
			mixture of both		from 44 to 96 cm increasing in hardness and compactation more carbonate in matrix
1					In general no visible carbonate clasts

# SO210-43

m	Lithol.	Struct.	Color	Sampl.	Description
0					0-5 cm oversaturated and blackish
		----		Gley 1	5-22 cm silty clay, moderate bioturbated
		----		2.5/10GY	22-25 cm silty clay, silt lenses
		.....		5Y-3	25-42 cm clayey silt, moderate bioturbated
				5Y 3/2	42-70 cm clayey silt, bioturbated, pyrite needles
				5Y 3/2	52 cm lenses of fine sand (minerals, rock fragments, glass cherts)
		~ ~ ~		5Y 3/2	70-80 cm bioturbation
		~ ~ ~		5Y-3	80 cm color contrast
1					99-111 cm silty clay, bioturbated
					114-119 cm fine sand with zircon
					119-159 cm silty clay, internal deformation, more consolidated light lenses, minerals, no HCl-reaction
					159/174-199 cm angular clasts of clay and silty clay, stiff clast supported matrix, matrix silty clay, roughly inversely graded
2				5Y 2.5/2	199-257/261 cm silty clay- clay homogenous, structureless
					257/261-299 cm angular clasts, same as 174-200 cm clast rather rounded, degassing pocks
				5Y 3/2 Gley 6/N	275 cm internal shear
3					293 cm sheared clast
					298-324/333 cm black mottles
					324/333-365 cm huge clasts of silty clay-clay sheared matrix and clasts huge clast from 336-356 cm
					365-399 cm matrix slightly laminated, silty clay
4				5Y 3/2	399-477 cm rounded, sheared clasts, silt lenses in matrix, silty lenses contain carboniferous needles
				5Y3/2	477-500/512 cm large rounded-angular clasts (clay- silty clay) in homogenous matrix
5					539 cm clusters of carbonate
					540-555 cm blackish Schlieren
					577 cm end of core




# SO210-72

m	Lithol.	Struct.	Color	Sampl.	Description
0			5Y 4/3		0-17 cm silty clay-clay, soft many voids
					17-60 cm silty clay, firm
					from ~60 cm on down, clasts of coarse sand -> dark grey ash particles 60cm, 62 cm, 67 cm, 74 cm, 82 cm ~ up to 5 mm
1					95 cm silty clay-clay ash-clasts at 110 cm, 115 cm, 117 cm
			5Y 4/1		131-136 cm Volc. Ash Layer
			5Y 4/3		coarse san particles, dark and lght grey downward termination sharp, upward less sharp 136-196 cm silty clay- clay homogenous
					ash clasts, dark grey ash clasts, white
2					196-296 cm silty clay 216 cm ash clast ~5 mm
					230 cm ash clast ~5 mm
					257 cm ash clast ~5 mm 260-270 cm bioturbation
3			5Y 3/1		298-302 cm ash lens, dark grey
			5Y 4/2		302-311 cm silty clay, greenish brown
			5Y 5/3		311-314 cm silty clay, lighter greenish grey
			5Y 4/2		314-333 cm silty clay, greenish brown
			5Y 2.5/1		333 cm ash lens, extreme coarse
			5Y 4/2		334-342 cm siltstones of ~1 cm, fining upward?, color gradient 342-350 cm silty clay matrix, ash clasts, silt stones 350-355 cm ash lens, coarse, siltstones of ~5 mm
					366-368 cm ash lens, sand 368-444 cm silty clay, homogenous, slight bioturbation
4					
			5Y 3/1		436 cm ash layer/lens 444-450 cm drak grey ash layer, intersected by clay layer
			5Y 4/2		claystones of ~2-5 mm 450-570 cm silty clay matrix 462, 465 cm siltstone clasts
5					490,492 cm siltstone clasts 495 cm bioturbation, more colorful 509 cm ash clast
			5Y 4/1		530 cm-end (~570 cm) degassing bubbles 535 cm ash clast
			5Y 4/2		544-548 cm distinct color change at sharp boundary



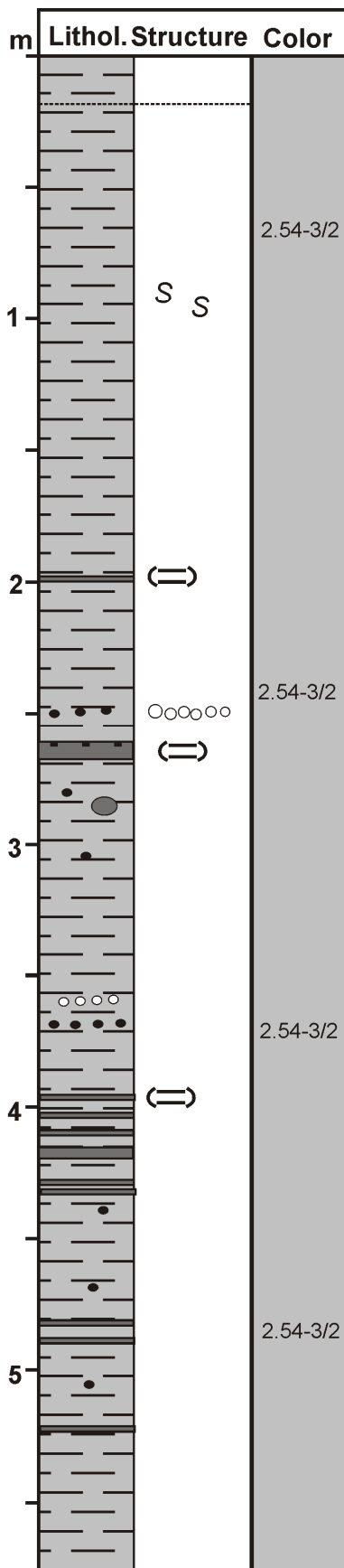
SO210-80

m	Lithol.	Struct.	Color	Sampl.	Description
0			2.5Y 3/2		0-74 cm silty clay, brown, homogenous
					74-80 cm clay, same color
					80-209 cm homogenous silty clay, brown
1					bioturbation
					ash clasts, dark grey ash clasts, white
2					209-244 cm silty clay, homogenous
					244-250 cm clay 250-330 cm silty clay, degassing
3					330-340 cm clay
					340-388 cm silty clay
4					388-392 cm clay 392-400 cm silty clay 400-408 cm clay 408-458 cm matrix silty clay, homogenous
					429 cm color change
					458-470 cm more clayey
					487-491 cm clay
5					505-513 cm clay 513-583 cm silty clay, homogenous, brown

# SO210-96

m	Lithol. Structure Color		Description
	S S		00-60cm: silty clay, bioturbation
		2.5y-3/3	60-65cm & 93-96cm: clay
1			
			96-248cm: homogeneous silty clay
2			
	(=)		248-250cm: fine sand layer
		2.5y-3/1	280-364cm: silty clay with black streaks, mottles and spots
3		5y-3/2	
			364-367cm: lighter coloured clay body
			386 cm: fine sand layer
4		5y-3/2	387-487cm: brown silty clay with black mottles
	(=)	5y-3/1	487-490cm: well-defined clay layer
5			490-576cm: brown silty clay with black mottles

# SO210-97



## Description

0-15cm: silty clay-clay, soft, water-rich

15cm-198cm: homog. silty clay, stiff

30-80cm: small white fragments

75-100cm: bioturbation

100-198cm: silty clay, homogeneous

170-190cm: white ash clasts

198cm: thin fine sand layer

200-250cm: silty clay, homogeneous

250-258cm: large (5mm) clasts of reworked dark siltstone

265-270cm: graded sand layer, darker hue

280cm: dark spot, 20mm

282cm, 299cm: siltstone clasts

273cm, 280cm, 292cm: white clasts (ash?)

305cm: dark clast, 5mm

300-389cm: silty clay matrix

361cm: whitish ash clast

370cm: dark ash clast

389cm: layer of dark ash clasts

404-406cm: fine sand layer, dark

408-409cm: fine sand layer, dark

413-414cm: fine sand layer, dark

425cm, 428-429cm: fine sand layer, dark

440cm: large (7mm) siltstone clast

467cm: siltstone clast

482, 488cm: fine sand layer, dark

505cm: dark single clast

522cm: sand-sized ash layer

Matrix: silty clay with black streaks

565cm: blackish horizon

# SO210-102

m	Lithol. Structure	Color	Description
	S		00-17cm: silty clay, brown
	S		17cm: fine sand layer
	S		17-110cm: silty clay, brown, dark mottles, bioturbation
	S		Silty clay matrix with fine sand layers, grading upward at:
	S		110-112cm; 119-120cm; 127-128cm
	S		136-137cm; 141cm; 143cm; 153cm
	S		155-158cm, possibly two sand layers
	S		166-168cm
	S		170-173cm
	S		177cm
	S		180 cm
	(=)		192-200cm interfingering Bouma sequences, 4-6 distal turbidites
	S		brown silty clay with thin, sandy layers (distal turbidites) at:
	S		216cm; 222cm; 230cm; 234cm
	S		260-263cm: Thick, fine sand layer, sharp transition at top & bottom, no visible grading. Ash layer?
	ash?		thin fine sand layers at:
	S		276-277cm; 284-285cm; 293cm
	S		307-308cm
	S		328-330 cm: thin double fine sand layer
	S		337-338cm: thin fine sand layer
	S		347-348: thin fine sand layer, sharp lower bound
	S		388-389: thin fine sand layer, sharp lower bound
	S		398cm: fine sand layer
	S		fine sand layers at:
	S		401-402cm; 411-412cm; 417cm;
	S		422cm; 435-436cm; 444-445cm;
	S		472cm
	S		fine sand layers at:
	S		502cm; 506cm;
	S		512cm; 526cm
	S		530-538cm: multiple fine sand layer
	S		brown silty clay with thin, sandy layers (distal turbidites) at:
	S		543cm; 553-555cm; 559-560cm;
	S		562-563cm
	S		
	S		
	S		
	S		
	S		
	S		
	S		
	S		
	S		
	S		
	S		
	S		
	S		
	S		
	S		



<b>No.</b>	<b>Title</b>
11	FS Sonne / Fahrtbericht / Cruise Report SO 192-1: MANGO: Marine Geoscientific Investigations on the Input and Output of the Kermadec Subduction Zone, 24.03. - 22.04.2007, Ernst Flüh & Heidrun Kopp, 127 pp. In English
12	FS Maria S. Merian / Fahrtbericht / Cruise Report MSM 04-2: Seismic Wide-Angle Profiles, Fort-de-France – Fort-de-France, 03.01. - 19.01.2007, Ed.: Ernst Flüh, 45 pp. In English
13	FS Sonne / Fahrtbericht / Cruise Report SO 193: MANIHIKI Temporal, Spatial, and Tectonic Evolution of Oceanic Plateaus, Suva/Fiji – Apia/Samoa 19.05. - 30.06.2007, Eds.: Reinhard Werner and Folkmar Hauff, 201 pp. In English
14	FS Sonne / Fahrtbericht / Cruise Report SO195: TOTAL Tonga Thrust earthquake Asperity at Louisville Ridge, Suva/Fiji – Suva/Fiji 07.01. - 16.02.2008, Eds.: Ingo Grevemeyer & Ernst R. Flüh, 106 pp. In English
15	RV Poseidon Fahrtbericht / Cruise Report P362-2: West Nile Delta Mud Volcanoes, Piräus – Heraklion 09.02. - 25.02.2008, Ed.: Thomas Feseker, 63 pp. In English
16	RV Poseidon Fahrtbericht / Cruise Report P347: Mauritanian Upwelling and Mixing Process Study (MUMP), Las-Palmas - Las Palmas, 18.01. - 05.02.2007, Ed.: Marcus Dengler et al., 34 pp. In English
17	FS Maria S. Merian Fahrtbericht / Cruise Report MSM 04-1: Meridional Overturning Variability Experiment (MOVE 2006), Fort de France – Fort de France, 02.12. - 21.12.2006, Ed.: Thomas J. Müller, 41 pp. In English
18	FS Poseidon Fahrtbericht /Cruise Report P348: SOPRAN: Mauritanian Upwelling Study 2007, Las Palmas - Las Palmas, 08.02. - 26.02.2007, Ed.: Hermann W. Bange, 42 pp. In English
19	R/V L'ATALANTE Fahrtbericht / Cruise Report IFM-GEOMAR-4: Circulation and Oxygen Distribution in the Tropical Atlantic, Mindelo/Cape Verde - Mindelo/Cape Verde, 23.02. - 15. 03.2008, Ed.: Peter Brandt, 65 pp. In English
20	RRS JAMES COOK Fahrtbericht / Cruise Report JC23-A & B: CHILE-MARGIN-SURVEY, OFEG Barter Cruise with SFB 574, 03.03.-25.03. 2008 Valparaiso – Valparaiso, 26.03.-18.04.2008 Valparaiso - Valparaiso, Eds.: Ernst Flüh & Jörg Bialas, 242 pp. In English
21	FS Poseidon Fahrtbericht / Cruise Report P340 – TYMAS "Tyrrhenische Massivsulfide", Messina – Messina, 06.07.-17.07.2006, Eds.: Sven Petersen and Thomas Monecke, 77 pp. In English

<b>No.</b>	<b>Title</b>
22	RV Atalante Fahrtbericht / Cruise Report HYDROMAR V (replacement of cruise MSM06/2), Toulon, France - Recife, Brazil, 04.12.2007 - 02.01.2008, Ed.: Sven Petersen, 103 pp. In English
23	RV Atalante Fahrtbericht / Cruise Report MARSUED IV (replacement of MSM06/3), Recife, Brazil - Dakar, Senegal, 07.01. - 31.01.2008, Ed.: Colin Devey, 126 pp. In English
24	RV Poseidon Fahrtbericht / Cruise Report P376 ABYSS Test, Las Palmas - Las Palmas, 10.11. - 03.12.2008, Eds.: Colin Devey and Sven Petersen, 36 pp, In English
25	RV SONNE Fahrtbericht / Cruise Report SO 199 CHRISP Christmas Island Seamount Province and the Investigator Ridge: Age and Causes of Intraplate Volcanism and Geodynamic Evolution of the south-eastern Indian Ocean, Merak/Indonesia – Singapore, 02.08.2008 - 22.09.2008, Eds.: Reinhard Werner, Folkmar Hauff and Kaj Hoernle, 210 pp. In English
26	RV POSEIDON Fahrtbericht / Cruise Report P350: Internal wave and mixing processes studied by contemporaneous hydrographic, current, and seismic measurements, Funchal – Lissabon, 26.04.-10.05.2007 Ed.: Gerd Krahnemann, 32 pp. In English
27	RV PELAGIA Fahrtbericht / Cruise Report Cruise 64PE298: West Nile Delta Project Cruise - WND-3, Heraklion - Port Said, 07.11.-25.11.2008, Eds.: Jörg Bialas & Warner Brueckmann, 64 pp. In English
28	FS POSEIDON Fahrtbericht / Cruise Report P379/1: Vulkanismus im Karibik-Kanaren-Korridor (ViKKi), Las Palmas – Mindelo, 25.01.-12.02.2009, Ed.: Svend Duggen, 74 pp. In English
29	FS POSEIDON Fahrtbericht / Cruise Report P379/2: Mid-Atlantic-Researcher Ridge Volcanism (MARRVi), Mindelo- Fort-de-France, 15.02.-08.03.2009, Ed.: Svend Duggen, 80 pp. In English
30	FS METEOR Fahrtbericht / Cruise Report M73/2: Shallow drilling of hydrothermal sites in the Tyrrhenian Sea (PALINDRILL), Genoa – Heraklion, 14.08.2007 – 30.08.2007, Eds.: Sven Petersen & Thomas Monecke, 235 pp. In English
31	FS POSEIDON Fahrtbericht / Cruise Report P388: West Nile Delta Project - WND-4, Valetta – Valetta, 13.07. - 04.08.2009, Eds.: Jörg Bialas & Warner Brückmann, 65 pp. In English
32	FS SONNE Fahrtbericht / Cruise Report SO201-1b: KALMAR (Kurile-Kamchatka and Aleutian MARGinal Sea-Island Arc Systems): Geodynamic and Climate Interaction in Space and Time, Yokohama, Japan - Tomakomai, Japan, 10.06. - 06.07.2009, Eds.: Reinhard Werner & Folkmar Hauff, 105 pp. In English
33	FS SONNE Fahrtbericht / Cruise Report SO203: WOODLARK Magma genesis, tectonics and hydrothermalism in the Woodlark Basin, Townsville, Australia - Auckland, New Zealand 27.10. - 06.12.2009, Ed.: Colin Devey, 177 pp. In English

<b>No.</b>	<b>Title</b>
34	FS MARIA S. MERIAN Fahrtbericht / Cruise Report MSM 03-2: HYDROMAR IV: The 3rd dimension of the Logatchev hydrothermal field, Fort-de-France - Fort-de-France, 08.11. - 30.11.2006, Ed.: Sven Petersen, 98 pp. In English
35	FS SONNE Fahrtbericht / Cruise Report SO201-2 <b>KALMAR: Kurile-Kamchatka and <b>AL</b>eutian <b>MAR</b>ginal Sea-Island Arc Systems: Geodynamic and Climate Interaction in Space and Time</b> Busan/Korea - Tomakomai/Japan, 30.08. - 08.10.2009, Eds.: Wolf-Christian Dullo, Boris Baranov, and Christel van den Bogaard, 233 pp. In English
36	RV CELTIC EXPLORER Fahrtbericht / Cruise Report CE0913: Fluid and gas seepage in the North Sea, Bremerhaven - Bremerhaven, 26.07. - 14.08.2009, Eds.: Peter Linke, Mark Schmidt, CE0913 cruise participants, 90 pp. In English
37	FS SONNE Fahrtbericht / Cruise Report: TransBrom SONNE, Tomakomai, Japan - Townsville, Australia, 09.10. - 24.10.2009, Eds.: Birgit Quack & Kirstin Krüger, 84 pp. In English
38	FS POSEIDON Fahrtbericht / Cruise Report POS403, Ponta Delgada (Azores) - Ponta Delgada (Azores), 14.08. - 30.08.2010, Eds.: Torsten Kanzow, Andreas Thurnherr, Klas Lackschewitz, Marcel Rothenbeck, Uwe Koy, Christopher Zappa, Jan Sticklus, Nico Augustin, 66 pp. In English
39	FS SONNE Fahrtbericht/Cruise Report SO208 Leg 1 & 2 Propagation of Galápagos Plume Material in the Equatorial East Pacific (PLUMEFLUX), Caldera/Costa Rica - Guayaquil/Ecuador 15.07. - 29.08.2010, Eds.: Reinhard Werner, Folkmar Hauff and Kaj Hoernle, 230 pp, In English
40	Expedition Report "Glider fleet", Mindelo (São Vicente), Republic of Cape Verde, 05. - 19.03.2010, Ed.: Torsten Kanzow, 26 pp, In English
41	FS SONNE Fahrtbericht / Cruise Report SO206, Caldera, Costa Rica - Caldera, Costa Rica, 30.05. - 19.06.2010, Ed.: Christian Hensen, 95 pp, In English
42	FS SONNE Fahrtbericht / Cruise Report SO212, Talcahuano, Chile - Valparaiso, Chile, 22.12. - 26.12.2010, Ed.: Ernst Flüh, 47 pp, in English
43	RV Chakratong Tongyai Fahrtbericht / Cruise Report MASS-III, Morphodynamics and Slope Stability of the Andaman Sea Shelf Break (Thailand), Phuket - Phuket (Thailand), 11.01. - 24.01.2011, Ed.: Sebastian Krastel, 42 pp, in English.
44	FS SONNE Fahrtbericht / Cruise Report SO-210, Identification and investigation of fluid flux, mass wasting and sediments in the forearc of the central Chilean subduction zone (ChiFlux), Valparaiso - Valparaiso, 23.09. - 01.11.2010, Ed.: Peter Linke, 112 pp, in English.





Das Leibniz-Institut für Meereswissenschaften  
ist ein Institut der Wissenschaftsgemeinschaft  
Gottfried Wilhelm Leibniz (WGL)

The Leibniz-Institute of Marine Sciences is a  
member of the Leibniz Association  
(Wissenschaftsgemeinschaft Gottfried  
Wilhelm Leibniz).

**Leibniz-Institut für Meereswissenschaften / Leibniz-Institute of Marine Sciences**

IFM-GEOMAR  
Dienstgebäude Westufer / West Shore Building  
Düsternbrooker Weg 20  
D-24105 Kiel  
Germany

**Leibniz-Institut für Meereswissenschaften / Leibniz-Institute of Marine Sciences**

IFM-GEOMAR  
Dienstgebäude Ostufer / East Shore Building  
Wischhofstr. 1-3  
D-24148 Kiel  
Germany

Tel.: ++49 431 600-0  
Fax: ++49 431 600-2805  
[www.ifm-geomar.de](http://www.ifm-geomar.de)